Nanoporous Layered Silicate Heterostructures Formed By Intra-Gallery Assemblies of Organic Surfactants

by

Anis Fakhruddin Barodawalla

A DISSERTATION

Submitted to
Michigan State University
in partial fulfillment of the requirements
for the degree of

DOCTOR OF PHILOSOPHY

Department of Chemistry
1997

Abstract

Nanoporous Layered Silicate Heterostructures Formed By Intra-Gallery Assemblies of Organic Surfactants

by

Anis Fakhruddin Barodawalla

A new templating mechanism which we recently reported[1] allows us to expand the use of lamellar compounds for the design of nanoporous materials. By appropriate choice of a reaction medium and combinations of neutral and ionic co-surfactants, new intercalated structures containing large channels similar to those formed in mesoporous molecular sieves (MCM-41)[2,3] can be synthesized. Here we present the gallery-templated synthesis using clays as layered hosts and affording what we call porous clay heterostructures (PCHs). Our approach is based on the use of intercalated quaternary ammonium cations (noted Q^+) and neutral amines into ionic lamellar solids. Into these swollen galleries is added a neutral inorganic precursor (for example, tetraethylorthosilicate (TEOS)) which forces the co-surfactants to order in a rod-shaped array of mixed quaternary ammonium cations and neutral amines. The inorganic structure self-assembles around this array leading to one-dimensional channels. Removal of the surfactants by calcination affords mesoporous solids with surface areas in the range 470-750 m^2/g and pore widths in the range 14-

23 Å depending on the quaternary ammonium/neutral amine chain length used. These new porous structures are more stable than large pore molecular sieves because of the pore structure being confined between 2d lattices. PCHs provide unique opportunities to improve the chemical and physical properties of surface active lamellar structures by enhancing the diffusion in such layered materials. In addition, owing to the complementary chemical functionalities of the layered and gallery-templated components, PCHs offer new design strategies for heterogeneous catalyst systems.

1 Galarneau, A; Barodawalla, A. and Pinnavaia, T. J., *Nature* , **374**, 529-531 **(1995)**.

2 Kresge, C. T.; Leonowicz, M. E.; Roth, W. J.; Vartulli, J. C.; Beck, J. S., *Nature* **359**, 710-712 **(1992)**.

3 Beck, J.S.; Vartulli, J. C.; Roth, W. J.; Leonowicz, M. E.; Kresge, C. T.; Schmitt, K. D.; Chu, C. T-W.; Olson, D. H.; Sheppard, E. W.; McCullen, S. B.; Higgins, J. B.; Schlenker, J. L., *J. Am. chem. Soc.* **114**, 10834-10843 **(1992)**.

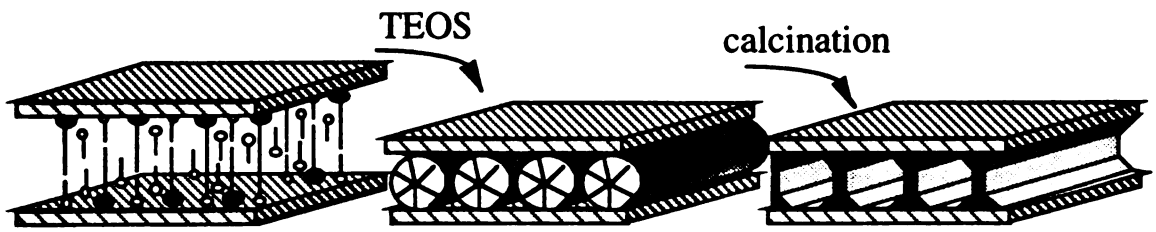

ACKNOWLEDGEMENTS

I would like to thank my research advisor Professor Thomas J. Pinnavaia for supplying patient guidance and support during this course of study. Special thanks go to Professor Harry A. Eick for his helpful comments as a second reader and Prof Baker and Prof Blanchard for being on my committee. I would also like to thank my deepest gratitude and heart-felt thanks to all the Pinnavaia group members past and present, who made graduate school an enjoyable learning experience. Prof. Wang, Dr. M. Chibwe, Wouter Ijdo, Dr. S. Bagshaw deserves special thanks for their encouragement and friendship they have given me over the years. A special thanks goes to Dr. A. Galarneau for collaborating on this project, and also making it an enjoyable experience.

Financial support given by the Department of Chemistry Michigan State University, the National Science Foundation is gratefully acknowledged and appreciated.

To my family I extend my love and thanks for being so supportive. I especially want to thank my father, mother, brother, sister, Grandparents, Aunts and Uncles who have stood behind me always and who have an unending affection and gratitude.

Most importantly I am grateful to my wife Rumu for all the love and understanding she has given me over this past year. Her friendship and patience during this time were instrumental to the completion of this dissertation.

TABLE OF CONTENTS

Chapter **pages**

Chapter IV. Physico-chemical properties of PCH materials

LIST OF TABLES

Table **Page**

LIST OF FIGURES

Figure **Page**

Figure **Page**

Figure **Page**

LIST OF THE ABBREVIATIONS

IUPAC - International Union of Pure and Applied Chemistry.
TEOS - tetraethyl orthosilicate : $Si(OC_2H_5)_4$.
TEOT - tetraethyl orthotitanate : $Ti(OC_2H_5)_4$.
TIPOT - teraisopropyl orthotitanate : $Ti[OCH(CH_3)_2]_4$.
TMAOH - tetramethylammonium hydroxide : $(CH_3)_4NOH$.
$DDDMA^+$ - didecyldimethylammonium : $(C_{10}H_{21})_2N(CH_3)_2^+$.
$DODDMA^+$ - dioctadecyldimethylammonium : $(C_{18}H_{37})_2N(CH_3)_2^+$
DA^+ - decylammonium : $(C_{10}H_{21})NH_3^+$.
$DTMA^+$ - decyltrimethylammonium : $(C_{10}H_{21})N(CH_3)_3^+$.
DDA^+ - dodecylammonium : $(C_{12}H_{25})NH_3^+$.
$DDTMA^+$ - dodecyltrimethylammonium : $(C_{12}H_{25})N(CH_3)_3^+$.
HDA - hexadecylammonium : $(C_{16}H_{33})NH_3^+$.
$HDTMA^+$ - hexadecyltrimethylammonium : $(C_{16}H_{33})N(CH_3)_3^+$.
Q^+-Clay - organo clays
Q_n^+-FH - Quaternary ammonium exchanged fluorohectorite.
P_n^+-FH - primary ammonium exchanged fluorohectorite.
PCH - porous clay heterostructure.
EPMES - equipotential periodic minimal energy surfaces.
XRD - X-ray diffraction.
TEM - transmission electron microscopy.
SEM - scanning electron microscopy.
TGA - thermogravimetric analysis.
NMR - nuclear magnetic resonance.
S_{BET} - specific surface area in m^2/g obtained from the linear part of the Brunauer - Emmett - Teller equation.
BET - Brunauer - Emmett - Teller.
P/P_0 - relative pressure. P is the equilibrium pressure of the adsorbate and P_0 is the saturation pressure of the adsorbate at the temperature of the adsorbent, volume adsorbed is at standard temperature and pressure.
H-K - Horvath - Kawazoe pore size distribution.
AlPO - aluminophosphate molecular sieves.
VAPO - vanadium phosphate molecular sieves.
M41S - broad family of mesoporus silica - based molecular sieves with lamellar, hexagonal or cubic structures.
MCM-41 - Mobil Composition of Matter number 41 possessing long range hexagonal order (a member of the M41S family)
MCM-48 - Mobil Composition of Matter number 48 possessing cubic

symmetry (a member of the M41S family)
HMS - hexagonal mesoporous molecular sieves.
FID - flame ionization detector.
TS-1 - microporous titanium - substituted silica molecular sieve with MFI topology (analogous to ZSM-5)
TS-2 - microporus titanium - substituted silica molecular sieve with MEL topology (analogous to ZSM-11)
Al-MCM-41 - aluminum - substituted analog of MCM-41.
Ti-MCM-41 - titanium - substituted analog of MCM-41.
Ti-PCH - titanium substituted analog of PCH.

Chapter I

"Advances in the design of nanoporous molecular sieves".

A. Introduction

1. Introduction to nanochemistry.

As stated by Geoffrey Ozin[1], nanochemistry, as opposed to nanophysics, is an emerging sub-discipline of solid-state chemistry that emphasizes the synthesis rather than the engineering aspects of preparing little pieces of matter with nanometer sizes in one, two or three dimensions. Currently there is considerable interest in nanoscale objects, since they exhibit novel material properties largely as a consequence of their finite small size. The nanochemist can be considered to work towards this goal from the atom "up", whereas the nanophysicist tends to operate from the bulk "down". Building and organizing nanoscale objects under mild and controlled conditions "one atom at a time " instead of "manipulating" the bulk, should in principle provide a reproducible method of producing materials that are perfect in size and shape at the atomic level. A cartoon illustration of this comparison is shown in Figure I.1 These little objects can be made of organic, inorganic and/or organometallic components. Their structure property relationships are designed to yield new materials with novel electronic, optical, magnetic, transport, photochemical, electrochemical, catalytic and mechanical behavior. Areas of application that can be foreseen to benefit from the small size and organization of nanoscale objects include quantum electronics, nonlinear optics, photonics, chemoselective sensing, and information storage and processing.

The chemist prides himself on being able to synthesize perfect objects having nanometer dimensions. To be able to make nanostructures

that are useful in electronic, optical and information processing systems, chemists

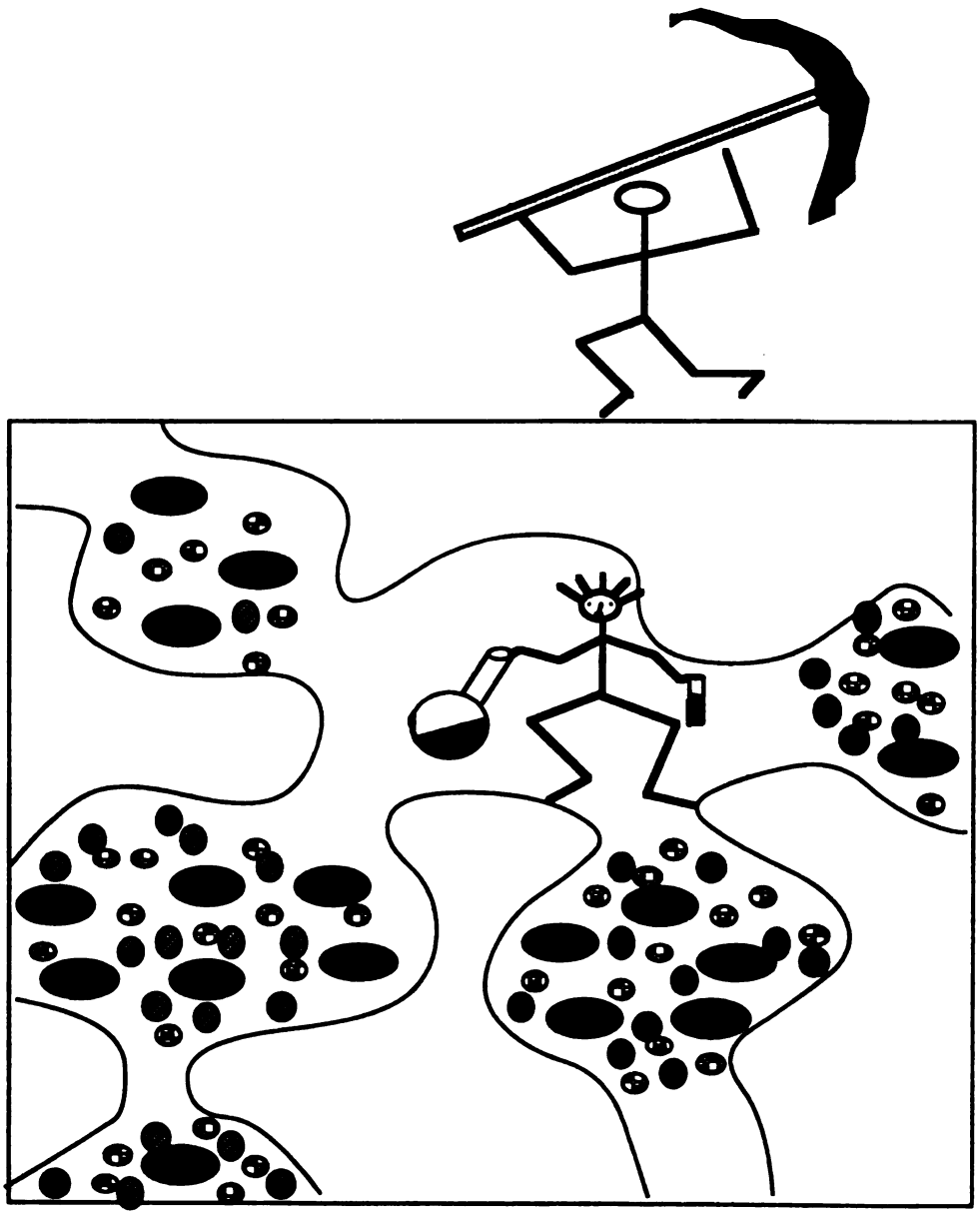

Figure I.1 : Nanochemistry as compared to nanophysics[1].

also have to develop synthetic methods that have the ability to position these tiny objects in appropriately connected organized arrays. The chemical alternatives for meeting this challenge and building such nanoscale devices from scratch involve patterning and templating methods. Nanolithography is used to spatially define chemically active foundation sites, usually on planar substrates, upon which subsequent site specific chemical synthesis allows the growth of nanoscale objects. Templating methods exploit the perfectly periodic, single size and shape channel, layer and cavity spaces of crystalline nanoporous host structures for performing host-guest inclusion chemistry. Both approaches benefit from the principle of synthesis and self organization in preexisting regions of a planar substrate or a porous solid, both with restricted dimensions on the nanoscale.

With respect to the template based preparation, organization and stabilization of nanoscale objects, the nanochemist generally dreams up chemical synthesis inside the void spaces of nanoporous host materials. The strategy requires the judicious selection of the host materials in addition to suitable precursors to the desired guest(s). There now exists a huge range of hosts[2]. They can be of an inorganic, organic or organometallic compositional type, with one dimensional (1-D) tunnel, 2-D layer and 3-D framework structures. Hosts may be of the insulating, semiconducting, metallic or superconducting type, or may attain these properties following inclusion of the chosen guest[3]. On surveying known host structures, one finds that channel, interlamellar and cavity dimensions vary widely in size, separation and perfection, spanning the size range from barely being able to accommodate the smallest ionic or molecular guests all the way to channel dimensions of about 5-10000 Å, interlamellar spaces of 3-50 Å and cavity diameters of 6-10000 Å.

2. Classification of porous materials

In general terms, nanoporous materials are solids with an accessible open space in the 1.0 - 10.0 nm range. In describing porous materials, the IUPAC has defined three size domain : micropores, <2 nm; mesopores, 2-50 nm; and macropores, 50 nm[4](see Figure I.2). Thus, the nanoporous regime spans the traditional midmicropores to lower-mesopore size range. Inorganic macroporous solids are well known as porous gels[5] or porous glasses[6]; these substances generally possess relatively broad pore size distributions due to their amorphous structures. Their typical applications are in the field of separation processes, for example in chromatography or as catalyst supports. Meso and macropores usually are associated with materials that are either finely divided or structurally highly disordered (amorphous). That is, meso and macro porosity often are consequences of the texture of a material. Microporous solids are exemplified by zeolites and their related compounds. Zeolites are aluminosilicates with a periodic three-dimensional framework structure containing voids; related compounds possess similar structures but differ in chemical composition of the frame work (e.g., aluminophosphates). Due to the periodicity of the structure of these crystalline solids, they exhibit an extremely narrow pore size distribution. This is important for their size-specific application in absorption, molecular sieving and shape selective catalysis[7-9]. More recently, non classical uses of the host-guest chemistry of zeolites have been envisaged[10-21]. The open frame work structures are used as nano-sized reaction vessels[11-13] or as hosts for the controlled construction of assemblies of metal and semiconductor clusters[14,15], of organic molecules[16-18] or for

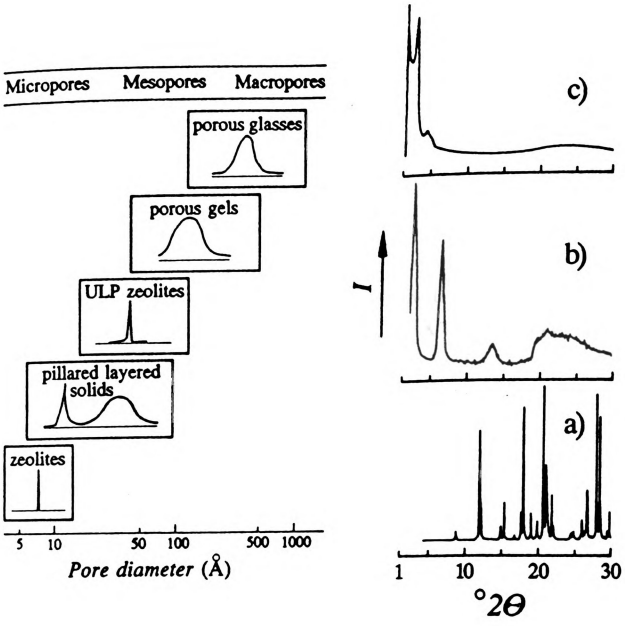

Figure I.2 : (a) Defination of micro-, meso-, and macropores together with the representative materials and their pore size distributions. (b) Schematic X-ray diffractograms of a zeolite, pillared solid and a ultr-large pore molecular sieve[100].

polymerization reactions leading possibly to molecular wires in the case of conducting polymers[15-19]. Exciting applications have been proposed for these nanocomposite materials, for example in nonlinear optics[20], as devices in electronic and optical computing and image processing[21] or as pigments.

The outstanding properties of zeolites and related compounds have made these materials one of the most important subjects of research in solid state chemistry in the last two decades. The major drawback for their use has been their limited pore size, which excludes larger molecular entities from the size specific processes occurring in the voids of these materials. Since the first applications of zeolites have been established, an urgent need has been developed for solids with well-defined pore sizes larger than the ~7Å diameter window occurring in X/Y zeolites. Typical extensions of current uses of zeolites include :

•The catalytic cracking of heavy oil fractions : Aluminosilicate zeolite Y is currently being used with an enormous impact in the oil-refining industry as a cracking catalyst for the "middle distillates" in order to convert these to gasoline. However the restricted pore size of zeolites excludes the larger hydrocarbon molecules of the "heavy end of the barrel" from highly selective intra-pore cracking processes.

•Zeolite-like compounds with a pure silicate framework ("zeosils"), for example silicate, exhibit a high efficiency in selectively sorbing organic hydrophobic pollutants from waste waters. Increased pore sizes might extend the use of pure silicate frameworks to larger molecules, for example to the adsorption of toxic polychlorinated biphenyl's from chemical products or of traces of herbicide and pesticide molecules from drinking water.

•More recently, metal porphyrin complexes have been incorporated into zeolite void structures, and molecular microstructures consisting of several redox-active organic and inorganic species have been generated on zeolite host systems[11], providing immobilized enzyme mimics[22] or models of biochemical electron transfer chains[11,23]. Again, larger pores would allow a much better fine-tuning of such structures, for example by the possibility of using bulkier ligands.

The fact that most of the envisaged uses of mesoporous solids are extensions of applications of zeolites means that the mesoporous regime of most interest is located at the lower end (pore sizes of 20Å to >200 Å) of the IUPAC definition. Compared to the chemistry of microporous solids, that of mesoporous solids is at a less elaborate stage. Two major paths of the synthesis of mesoporous solids have developed over the years. Firstly, there have been numerous attempts to extend the hydrothermal synthesis procedures used to prepare microporous zeolite-type structures to the mesoporous regime. Until recently, however, success was very limited, so that in the meantime other routes to mesopores solids with narrow pore size distribution had been investigated. The most important of these is the "pillaring" of layered solids, i.e. the controlled intercalation of spacers between the layers of clay minerals

B. Enlarging the Pore Sizes of Zeolites and Related Compounds

The most obvious approach[1] to obtaining controlled mesoporosity is the extension of zeolite-like three dimensional framework structures to

larger pore sizes. The early work on hydrothermal zeolite synthesis by Barrer and co-workers[24] showed that the inorganic and oganic cations present in an aluminosilicate gel that is subjected to hydrothermal treatment play a decisive role in determining the type of three-dimensional framework formed. Even nowadays, this "template effect" is not understood completely. Templating agents change the chemistry of the gels and are occluded in the growing zeolite crystals during hydrothermal synthesis. Larger organic molecules are thus supposed to act also as "void fillers" that inhibit the crystallization of thermodynamically more stable nonporous phases. Quite naturally, it was anticipated that the use of larger templating agents, especially of larger organic molecules and cations, would lead to larger pore sizes — from the micro to the mesoporous regime. Other attempts were directed at changes in the gel chemistry, with one or both of the components Al and Si being substituted by main-group elements Be, Ga, Ge, P, and As or by transition metals such as Ti, Fe and Co.

For a longtime, however, these attempts failed to enlarge the pore sizes of zeolite-like solids. Zeolites X/Y, naturally occurring as the mineral faujasite and synthesized for the first time in the 1950's, with their ~12Å diameter cavity and their ~7Å diameter windows, maintained their position as the largest pore materials in the class of zeolites and related materials for a long time.

After roughly four decades of zeolite and molecular sieve synthesis, it appeared that the experimental accessible range of pore sizes had an intrinsic upper stability limit of the 12 T-atom ring, with a diameter of about 7-8 Å[25]. (T refers to apex linked tetrahedral TO_4 building units, where T is most commonly Si, Al, P). However, a dramatic turn of events

occured in 1988 with the discovery by Davis and co-workers[26] of an extra-large pore molecular sieve based on aluminophosphate, denoted VPI-5, having an essentially circular 18 T atom ring uni-dimensional channel structure, with a diameter of about 12-13 Å. This breakthrough shattered the "psychological" 12 T atom ring barrier, and had the effect of revitalizing synthetic efforts aimed towards extra-large-pore and even ultralarge-pore materials. Not long after this amazing breakthrough, a method was discovered in 1990 for the controlled phase transformation of VPI-5 to a related yet smaller pore 14 T atom ring material, denoted AlPO-8 [27]. In 1991, Estermann and co-workers[28] announced another spectacular discovery with the synthesis and structure determination of an extra-large-pore gallophosphate molecular sieve called cloverite. This novel material contains a 20 T atom cloverleaf-shaped entrance window leading into an impressive 29-30 Å diameter supercage. The overall structure of the cubic unit cell is based on two non-intersecting, three dimensional, 8 T atom and 20 T atom channel systems. An intriguing feature of cloverite is the existence of P(OH)OGa(OH) terminal hydroxyl groups completely covering the inside surface of the supercage and protruding into the cloverleaf-shaped pore openings. Zeolite and molecular sieve frameworks normally contain TO_4 (T= Si, Al, P) tetrahedral building units connected by T-O-T bonds, with only a low level of terminal T(OH) defect groups, whereas cloverite contains large numbers of terminal T(OH) groups as an integral part of the structure and is referred to as having "interrupted framework". The thermal stability and chemical reactivity of cloverite is under intense investigation, as the properties of the interrupted framework will probably determine the use of the material for the

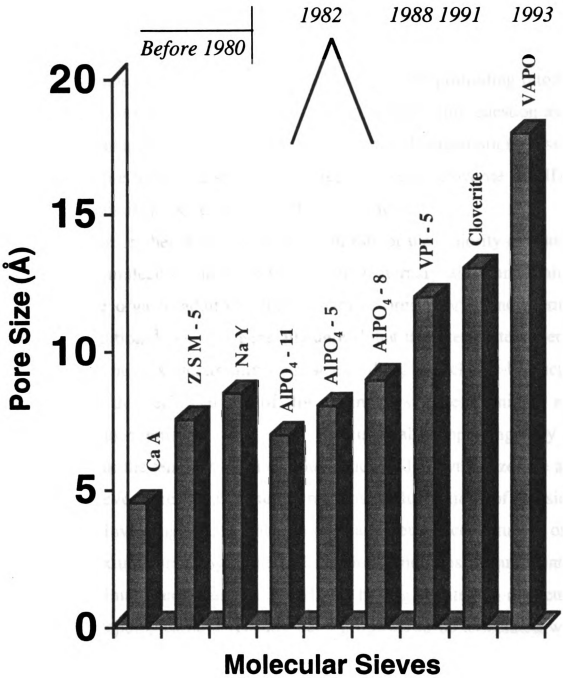

Figure I.3 : Pore size of microporus zeolites and other recently developed molecular sieves[99].

catalytic, adsorption and advanced materials applications. Shortly after Estermann and co-workers discovered cloverite, Xu and co-workers[29] disclosed the synthesis of JDF-20, an aluminophosphate molecular sieve with an elliptically shaped 20 T atom ring unidimensional channel structure. Curiously, JDF-20 also contains terminal hydroxyl groups lining the inside surface of the 20 T atom channel and protruding into the pore opening, just like cloverite. This raises the interesting question as to whether interrupted frameworks are an intrinsic characteristics of such extra-large-pore molecular sieves, so far represented by cloverite and JDF-20, and are possibly a kind of extended "giant defect".

A common theme pervading the synthesis of the majority of known zeolites and molecular sieves is the use of quaternary alkyl ammonium and/or amine organic additives under hydro or organo or amino thermal reaction conditions[30,31]. It is generally agreed that these template moieties serve one or more structure-directing, space filling and charge-balancing functions in the self-assembly of, for example, silicate aluminate and phosphate basic building units. One scientifically appealing way of thinking about the template-mediated nucleation and growth of zeolite and molecular sieve materials is in terms of density fluctuations of transient local order, involving the cationic, anionic and neutral constituents of a synthesis mixtures under hydrothermal reaction conditions. Equipotential periodic minimal energy surfaces (EPMESs) having zeolite and molecular sieves type topologies have recently been proposed to be associated with these fleeting structure domains in the liquid and/or gel phases[32]. Proper use of template on the loci of these EPMESs, the basic building units are imagined to undergo a spatially constrained condensation polymerization to form the seed that is responsible for the nucleation of a particular zeolite

or molecular sieve structure type. The surfaces of the crystal nuclei themselves bear their own characteristic EPMESs, which are viewed as being responsible for the continued growth and crystallization of the product material.

With this in mind, it is interesting to note that some zeolites and molecular sieves synthesized to date, based on monomeric, oligomeric and even polymeric quaternary alkyl ammonium and/or amine templates, appear to display framework topologies that bear a resemblance to the shape of the template. Thus spherically shaped templates may lead to cavity type structures and rod shaped ones, may result in channel type structures. However, the pore sizes, channel and cavity spaces have been generally restricted roughly to the molecular diameter of individual spherically shaped templates or the width of the rod-shaped ones, resulting in the current pore size maximum of the 20 T atom rings found in cloverite and JDF-20.(Adapted from an article by Ozin)[1].

C. Propping Layered Materials — Pores by Pillaring.

1. Lamellar Solids.

Solids with layered structures possess basal planes of atoms that are tightly bonded within the planes but relatively weakly bonded in the direction perpendicular to the planes. The asymmetric bonding interactions translate into greatly different physical properties for the material in the in-plane and out-of-plane directions. The weakly interacting region between the stacked units is usually referred to as the

"interlayer" or "gallery" region. When the layers are electrically neutral, as in graphite or FeOCl, the galleries are empty and the basal planes of the adjacent layers are in van der Waals contact. Neutral guest molecules often can be incorporated between the host layers to form regularly intercalated derivatives. The incorporation of neutral species into the van der Waals gap typically is accompanied by electron-transfer reaction between the molecular guest and the layered host[33]. The free energy change associated with the electron transfer step provides much of the driving force for the intercalation reaction.

In several classes of lamellar solids, the layered units carry a net electrical charge[34]. These include smectite clays, layered double hydroxides, and Group 4 metal phosphates. To achieve an electrically neutral structure, counterions, usually solvated by water or other polar molecules, occupy the gallery region between the layers. Thus, ionic lamellar solids qualitatively resemble the conventional intercalation compounds formed by electron-transfer reactions between neutral guest and layered host precursors. The difference, however, is that in ionic lamellar solids, charge separation between gallery ions and the layers is complete, whereas in conventional intercalates the extent of charge transfer between guest and layered host is seldom complete. Consequently, ionic lamellar compounds can justifiably be described as intercalation compounds, although in practice they are not formed by electron-transfer reactions. Instead they simply crystallize, complete charge separation between the gallery species and the host layers being a distinguishing feature of their structure.

Owing to their nanoscale periodicity, ionic lamellar solids give rise to very large intracrystalline surface areas of several hundred square

meters per gram or more. However, in most cases the gallery surface area is accessible only to water and other small polar molecules that are capable of solvating the gallery counterions and the charged layer surfaces. Removing the solvating molecules by outgassing at elevated temperatures results in the recollapse of the galleries, especially if the intercalated counterions are small relative to interstices occupied by the ions on the gallery surfaces. If the counterions are relatively large, they can function as molecular props or "pillars" and thereby prevent the galleries from collapsing completely when the solvating medium is removed[35,36]. The gallery space might then be accessible to other small molecules the size of H_2O, for example, N_2, CO, or NH_3. But simply facilitating the adsorption of small molecules is relatively uninteresting. Ideally, one would like to tailor the gallery structure on a length scale that would allow the accommodation of organic and inorganic molecules for molecular assembly and, perhaps, catalytic chemical conversions. Pillaring reactions of a lamellar host are an important route to achieving these desired structural modifications.(adapted from an article by Pinnavaia)[98]

Compared to the hydrothermal synthesis of zeolite-like compounds, where the aggregation of matter to a porous material has to start from a "zero point", i.e., from a solution or gel, the preformation of layers in the precursor compounds of pillared materials[37] should facilitate the process of formation of large pores. In a simplified box of bricks picture,(see Figure I.3 a) it is only necessary to choose the right length of the props and distribute them in an ordered manner between the layers. Real chemistry is not that simple, of course. There are currently three main types of layered materials that are used for pillaring, namely smectite clays, layered double hydroxides, and phosphates and phosphonates of tetravalent metals.

Clays are naturally occurring three-layer sheet silicates. The sheets are formed of two layers with tetrahedrally coordinated atoms surrounding a layer with octahedrally coordinated atoms. The whole structure carries a net negative charge resulting from substitutions in either the tetrahedral (Al^{+3}, Fe^{+3} for Si^{+4}) or the octahedral (Fe^{+2}, Mg^{+2} for Al^{+3}, Li^{+} for Mg^{+2}) layer. This negative charge is compensated by interlayer cations, which in natural smectite clays are alkali or alkali earth ions. In the case of smectite clays, the net negative charge of the layer is rather small; the clay can then easily swell in water. After swelling, the interlayer cations may be exchanged for larger oligomeric cations, for example the Keggin ion $[Al_{13}O_4(OH)_{24}(H_2O)_{12}]^{+7}$ ("Al_{13}")[38] or the zirconyl cation $[Zr(OH)_2(H_2O)_4]_4^{+8}$. These cations are present in solutions of the metal ions under appropriate conditions of pH, concentration and temperature. Subsequent calcination of the exchanged clay at elevated temperatures, e.g. 500°C, dehydrates the pillars and establishes stable links between them and the layers. Due to the fact that the ion exchange capacity, i.e. the number of cations necessary for charge compensation, is small, aporous material with space left between pillars is obtained (see Figure I.4 a).

Pore size distributions derived from sorption data of materials prepared in this way shows that the majority of pores are in the microporous range <10Å, as may be expected due to the rather small pillars. However, these compounds also exhibit mesopores with a rather broad size distribution between 20 and 200Å. The mesoporosity in these compounds may be traced back to a disordered arrangement as depicted schematically in figure I.4 b : During swelling and ion exchange the clay delaminates to form small layer packages or single layers. On drying after the pillaring reaction these layer packages arrange themselves as shown in

figure I.3 b and are stabilized in this configuration by calcination. This

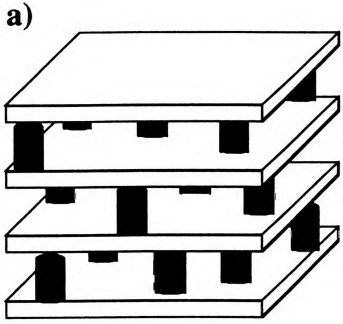

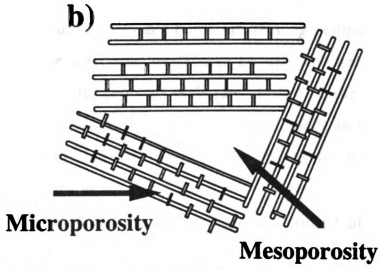

Figure I.4 : The approach to mesoporosity via pillaring of layered solids:(a) In most pillared solids, the interlayer regions contain only micropores. (b) Mesoporosity is usually connected with a disordered arrangement of layer packages[100].

leaves open spaces — mesopores —between them. Another possibility for the formation of mesopores is bending of the layers. Both types of mesoporosity, however, are generated in an uncontrolled process and there is no simple way of designing pore shapes or sharpening the pore size distribution.

The aim of obtaining controlled interlayer mesoporosity by pillaring has been tackled by the use of larger pillars[39-41]. These attempts include the DIMOS route, i.e., the direct intercalation of metal oxides sols. Enlarged interlayer distances were indeed observed in the pillared clays. However, sol particles are usually spherical (or nearly so), so that, as they enlarge the height of the interlayer galleries, they also fill up the additional interlayer space. Large elongated ("slim") pillars tend to incline with respect to the layer surfaces(Figure I.5 a). It may be possible to overcome this problem by the post-intercalation of suitable organic molecules. Their space requirement might serve to keep the pillars upright (Figure I.5.b). During calcination, when stable links are being established between the layers and the pillars, the organic burns off, leaving behind a pillared solid with increased interlayer spacing (Figure I.5 c). Another way to achieve interlayer mesoporosity requires elaborate control of the shape of pillar, which is equipped with "bases" so that it cannot adopt an inclined position (Figure I.5 d). So far, this approach seems to be feasible only for zirconium phosphonates.

Another important class of layered solids consist of layered double hydroxide(LDHs). The structure of these compounds is based on that of $Mg(OH)_2$, brucite. In brucite, magnesium ions occupy the octahedral sites between each second layer of a close-packing of hydroxide ions, thus giving rise to a layer sequence OH-Mg-OH-OH-Mg-OH in the direction

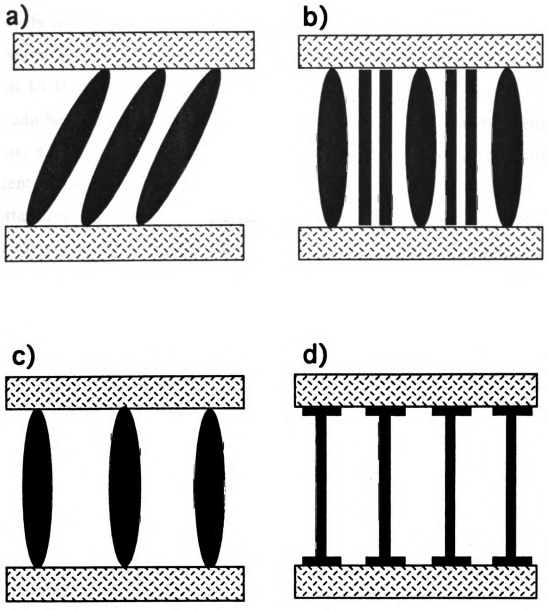

Figure I.5 : Approaches to mesoporosity via pillaring of layered solids : (a) Attempts to use large elongated ("slim") pillars to create interlayer mesoporosity may fail because the pillars are inclined w.r.t the layers. (b) This failure may be prevented by post-intercalating organic substances that (c) can be burnt off during calcination when stable links between pillars and the layers are formed. (d) Another possibility is the intercalation of pillars with bases[100].

perpendicular to the layers. $Mg(OH)_2$ layers are neutral but substituting some of the divalent Mg^{+2} ions by trivalent ions, e.g. Al^{+3}, gives rise to positively charged layers. The interlayer gaps are filled by charge compensating anions (often carbonate and/or hydroxide) and water. A typical LDH is the mineral hydrotalcite, $[Mg_6Al_2(OH)_{16}]CO_3 \cdot 4H_2O$. LDH can be prepared with many different combination of di and trivalent cations, e.g., Fe^{+2}, Ni^{2+}, Zn^{+2}, Cr^{+3}, Fe^{+3}, and the ratio of divalent to trivalent metal ions can vary in a broad compositional range. The most important property of LDHs is the fact that they are anion exchangers, and these compounds have been termed anionic clays[42]. Most of the inorganic ion exchange active compounds such as zeolites, clays and others are cation exchangers[43], and thus LDHs play an outstanding role in that regime. Besides that, they have (potential) applications in catalysis, as sorbents and as pharmaceuticals, e.g. as antacids. Although the possibility of pillaring LDHs has been demonstrated[44], this chemistry is still in its infancy. The fact that among the oligomeric oxo/hydroxo ions many more anions than cations are known makes the extension of the pillaring approach from clays to LDHs very promising. The thermal stability of the hydroxides, however, is reduced in comparison to that of aluminosilicate clays. This shows up, for example, in the fact that calcining an LDH under conditions where clays are stable leads to an amorphous solid; astonishingly enough, the double hydroxide layer is restored after intercalation of an organic compound.

The third important class of pillared layered solids is based on the expansion of the interlayer space of the phosphates $Me(HPO_4)_2 \cdot nH_2O$ of tetravalent metals (Me) such as Ti, Zr and Sn[45,46]. In these compounds the metal ions are octahedrally coordinated by oxygen atoms of the phosphate

ions; metal and phosphate ions together the layers of the structure. The protons of the $[HPO_4]^{2-}$ group project into the interlayer region, which is filled with water. Typical substances capable of intercalating into the acidic interlayer regions of the layered phosphates are organic amines. Pillaring agents such as the Keggin ion Al_{13} do not intercalate directly but enter the gaps only when the layers have been spread apart by pre-intercalation with amines[47]. This procedure leads to porous materials with a 10-30Å range. Direct intercalation of pillars is also possible if the pillars are combined with organic amino functions, as is the case for octa(aminopropyl)silsesquioxanes $(H_2NCH_2CH_2CH_2)_8[Si_8O_{12}]$. Although this species fills up the interlayer region, the organic part of the intercalate can be burned off, thus generating interlayer porosity[48].

Another type of pillaring is possible by using organic disphosphonic acids (HO_3P-R-PO_3H), which contain two phosphonates groups bonded to an organic residue[46]. Pillared layered zirconium phosphonates can be prepared directly by hydrolysis of zirconium fluorocomplexes in the presence of the diphosphonic acid. Zirconium phosphonates $Zr[O_3P$-R-$PO_3]$ are formed with $Zr(PO_3)_2$ layers similar to those occurring in the phosphate, but with the R group protruding into the interlamellar region and keeping the layers apart. By using this approach, the interlayer space is filled by the organic residue due to the fact that there is a 1:1 ratio of Zr atoms in the layer and the residues "R". Partial replacement of the pillars "R" by smaller residues R' such as H or CH_3, however, should lead to the formation of pores in the mixed phosphonates $Zr(O_3P$-R-$PO_3)_{1-x}(R'PO_3)_{2x}$. Then the length of the residue "R" determines the height of the pores, and the ratio of the residues R:R', their width. Due to the ability of the organic chemist to construct a large variety of diphosphonic acids

with different residues "R", this approach seems especially promising with regard to the aim of a fully controlled design of not only pore size and shape but also, by introducing special functional groups on the pillars, intrapore reactivity[46,49,50]. The construction of pillars, with bases, to prevent them from being inclined with respect to the layers, also seems to be feasible. The disadvantage of this class of compounds lies in the reduced thermal stability of the organic residues, restricting their use to temperatures below 250°C. Higher thermal stability would be provided by inorganic pillars. If in the future it becomes possible to influence the chemistry of inorganic oligomeric species as deliberately as that of organic molecules, a similar approach could yield thermally stable "tailor-made" porous materials.

Recently a novel pillaring procedure (Figure I.6) to convert dense, layered metal oxides and silicates into high surface area molecular sieves with large interlayer separations was developed by Landis, et al[51]. This procedure is applicable to a wide variety of layered phases and allows for the engineering of microporous materials with diverse composition and physical properties.

The pillaring procedure developed for smectite clays are not generally applicable to the wide variety of laminar metal oxides that do not spontaneously delaminate in water. This new approach has been effective to tailor-make materials with varied but controllable pore sizes from metal oxides with unique chemistries, It was found that pillaring could be facilitated by utilizing a pre swelling step in which the interlayer is exposed to organoammonium ions. According to procedures developed earlier, layered metal oxides[52] and silicates[53] were intercalated with an aqueous solution of long-chain organoammonium salt or amine. An organic pillar

precursor such as tetraethyl orthosilicate (TEOS) was then absorbed into the organophilic interlayer region, where it was converted to a metal oxide pillar. Typically, the organoammonium ion exchanged product was stirred with excess TEOS for 1-3 days at 25-80°C, filtered and dried. The final microporous material was produced by calcination for several hours in air at 538°C, which removes the water, the pre swelling organoammonium ion, and the organic byproduct from TEOS hydrolysis, affording a silica-pillared product. This procedure has allowed preparation of porous products from a wide variety of layered oxides, including alkali titanates, alkali metal-substituted titanates $A_x[MTi]_2O_4$ [54] and layered silicates such as magadiite, $Na_2Si_7O_{15}$, and kenyaite, $K_2Si_{14}O_{29}$.

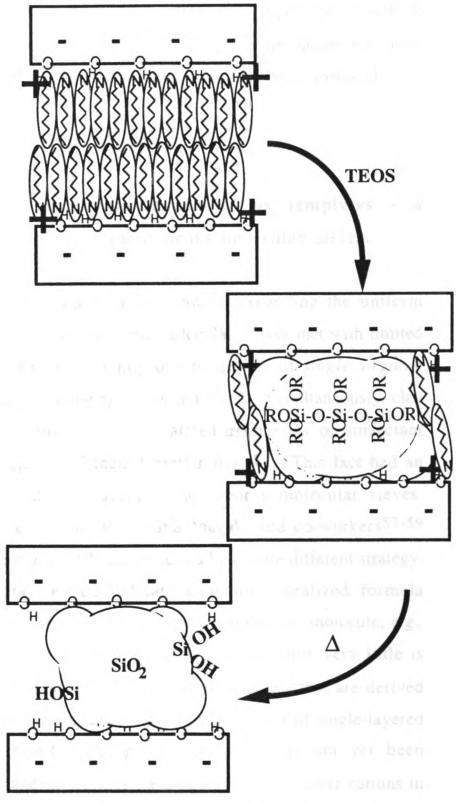

Figure I.6 : Schematic representation for the intercalation and pillaring of alkylammonium solvated magadiite[101].

The ability to controllably modify chemical composition as well as pore size provides the flexibility to tailor catalysts for specialized end uses, and the catalytic potential of these materials is actively being explored.

D. Mesoprous Molecular Sieves.

1. Assemblies of surfactant molecules as templates - a milestone to the synthesis of mesoporous molecular sieves.

The considerable synthetic effort toward expanding the uniform micropore size available in zeolites and molecular sieves met with limited success until 1992. This was mainly due to the use of *single organic molecules* as structure directing agents or templates. Simultaneously, clay scientists studied the behavior of intercalated *assemblies* of surfactant molecules in the galleries of their lamellar hosts[55]. This fact had an important impact on the discovery of mesoporus molecular sieves. Independently, Yanagisawa et al [56]. and Inagaki and co-workers[57-59] prepared mesoporous silicates/aluminosilicates by a quite different strategy, i.e., by using the layered polysilicate kanemite (idealized formula $NaHSi_2O_5.3H_2O$) and a quaternary ammonium surfactant molecule, e.g., $C_{16}TMACl$, as starting reactants materials. At this time very little is known about the formation of the mesoporous materials that are derived from kanemite. Although the layers of kanemite consist of single-layered sheets of SiO_4 tetrahedra, the precise structure has not yet been determined. Lagaly and co-workers have shown that interlayer cations in layered silicates and other materials, e.g. Na^+ in kanemite, can be exchanged by organic cations with

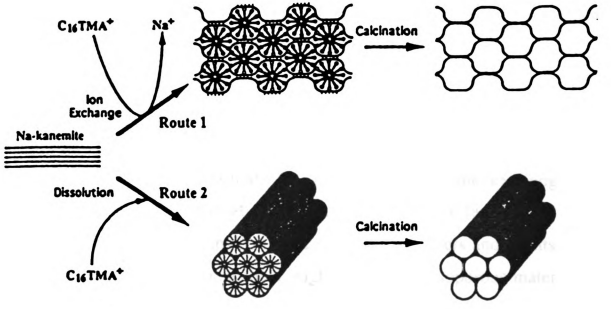

Figure I.7 : Synthesis mechanism for mesoporous materials derived from kanemite as proposed by inagaki et al[77].

long alkyl chains such as $C_{16}TMA^+$. Because of the hydrophobic/hydrophilic properties of these long chain organic cations, their positively charged head groups interact with the negatively charged inorganic layers resulting in the formation of bimolecular packings of organic cations between the silicate layers. It is postulated that the long-chain cations in the organic bilayers are arranged in the so-called "kink-block" and/or "gauche-block" structures. The "kink" conformation originates from regular sequences of trans and gauche bonds of the long alkyl groups. Inagaki et al., [57-59] proposed that mesoporous materials are formed from kanemite and surfactant molecules by route 1 schematically illustrated in fig *. First, the surfactant molecules pillar the kanemite layers (may be similar to procedure described by Beneke and Lagaly,[53]) after which the flexible silicate layers wind around the exchanged $C_{16}TMA^+$ ions. The curvature of the silicate layers facilitates the condensation of silanol groups on the adjacent silicate layers and results in the formation of a three dimensional, highly ordered mesoporous material with an hexagonal arrangement of uniformly sized channels, as confirmed by ^{29}Si MAS NMR and TEM. The silicate-organic complexes were converted by calcination, to micro- and mesoporous materials with uniform pore size distribution. The specific surface areas of the calcined products are 900 m^2/g and the pore size can be altered by varying the chain length of the alkyltrimethylammonium ions used. This route represents an entirely new way to prepare mesoporous, and possibly microporous, materials, i.e., by the transformation of a two-dimensional silicate structure into a three-dimensional network.

2. Mobils Ordered Mesoporous M41S Materials-A leap into the ultralarge-pore size molecular sieves.

A giant stride forward into the ultralarge pore size range of 15-100Å has very recently been disclosed[60] by Mobil researchers in the patent and open literature, with the creative use of surfactant liquid crystal templates. These consist of hexagonal or cubic close packed aggregates of cylindrically shaped micelles, the latter being composed of surfactant molecules containing hydrophobic alkane chains, hydrophilic alkylammonium cationic head groups and proximal charge balancing hydroxyl and/or halide anions. It is believed that under the hydrothermal conditions of a zeolite or a molecular sieve type synthesis, silicate aluminate and/or phosphate building units undergo a spatially constrained condensation-polymerization reaction on a cylindrically shaped EPMAS associated with the close packed array of cylindrically shaped micelles. The latter effectively serves as "massive templates" for the creation of ultralarge cylindrically shaped pore, zeolite and molecular sieve-like structures. By judiciously selecting the alkyl chain lengths of the surfactant, the solution chemistry, and the use of auxiliary organic molecule fillers, the effective diameter of the cylindrical micellar aggregates can be adjusted to yield ultralarge-pore zeolite like structure with diameters in the range of 15-100 Å.

Members of this family of Mobil materials designated MCM-41, were first observed in electron micrographs of products from hydrothermal reactions of aluminosilicate gels in the presence of quaternary ammonium surfactants. A typical mobil preparation of MCM-41 involves an aqueous solution of cationic surfactant, such as

observed in the low angle 2θ region can be indexed on a hexagonal unit cell with a = 45 Å ($2d_{100}/\sqrt{3}$). Generally, both electron and X-ray diffraction pattern show only a few low order members of the hk0 subset of hexagonal reflections. The BET surface area of the preparation is >1000 m^2/gm with exceptionally high sorption capacities of ≥ 50 wt% cyclohexane at 40 torr, 49 wt% n-hexane at 40 torr, and 67 wt% benzene at 50 torr. The pore volume of this sample is 0.79 cm^3/gm. The range of pore volumes for MCM-41 samples is 0.7-1.2 cm^3/gm*. Figure ?? shows the N_2 adsorption isotherms for this material and for an amorphous mesoporous silica. The morphology of MCM-41 depends on the synthesis conditions, but it is possible to obtain relatively large (2μm) hexagonal prisms of MCM-41. The nature of the ordering in the walls of MCM-41 - that is, the degree to which the atoms are precisely ordered is not fully understood. The C/N molar ratio for as-synthesized C_{16}-based MCM-41 is 19, which is consistent with the surfactant remaining intact. Another way of altering the pore diameter of MCM-41 is to add auxiliary hydrocarbons such as alkylated benzene (for example 1, 3, 5 trimethylbenzene), to the synthesis mixture[61]. The incremental addition of 1, 3, 5 trimethylbenzene results in the concomitant increase of d_{100} and the pore diameter. Hexagonal phases with pore diameter up to 100 Å have been characterized.

The microscopy and diffraction results presented above are strikingly similar to those obtained from lyotropic liquid crystal phases[62-64] which are ordered arrays of surfactant aggregates that occur at specific amphiphile concentrations[65-66]. One such phase, the middle or "H1" phase, produces TEM images[67] analogous to those of MCM-41 . The H1 phase is a hexagonal array of cylindrical micelles in which the hydrophobic hydrocarbon chains are gathered in the center and the polar groups are

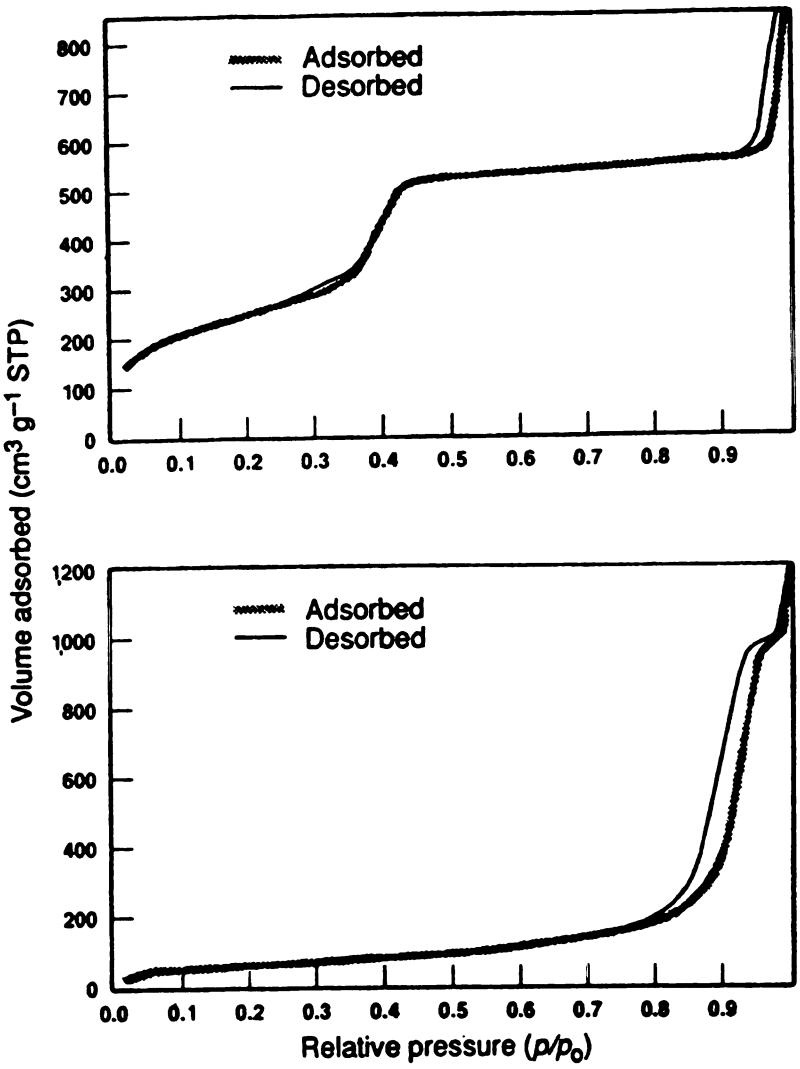

Figure I.9 : Nitrogen adsorption isotherm for MCM-41 (above) and amorphous silica -BET surface area 306 m^2/g (below)[60].

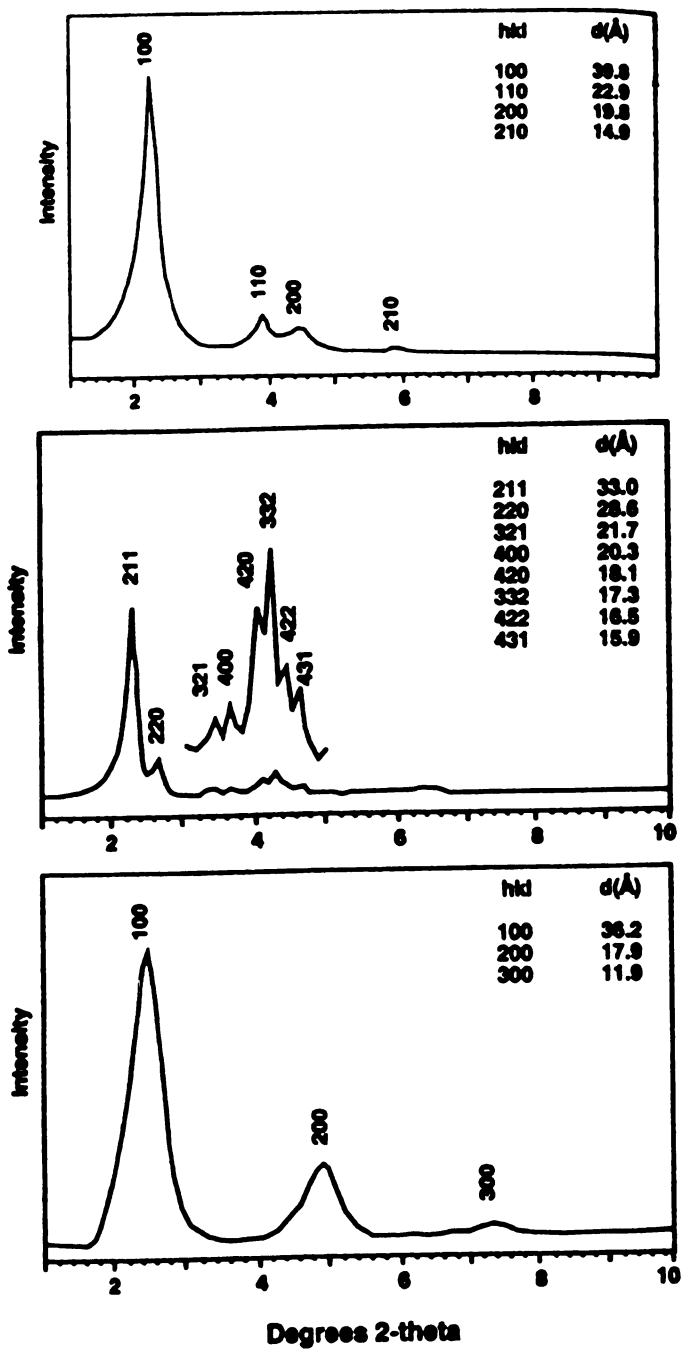

Figure I.10 : Representative XRD patterns of calcined MCM-41 (above), calcined cubic MCM-48 (middle) and as-synthesized unstable lamellar material (below)[60].

arrayed on the surface, in contact with a continuous region of water surrounding the micelles. The repeat dimensions of the MCM-41 prepared as described above are consistent with those determined for hexadecyltrimethylammonium based liquid crystals, where a cylinder to cylinder repeat distance of 40 Å is observed[65].

The observed dependence on alkyl chain length and the influence of auxiliary organic molecules on the resultant inorganic product are also consistent with two phenomena observed for liquid crystals. The diameter of hexagonal liquid-crystal phases prepared with anionic surfactants depends on the alkyl chain lengths of the surfactant *. Organic species may be solubilized inside the hydrophobic regions of micelles, causing an increase in micelle diameter. Reagents soluble in micellar solutions can increase the porosity of amorphous adsorbents.

These similarities suggest that these mesoporous molecular sieves are formed by a liquid-crystal templating mechanism. In this mechanism *, inorganic material occupies the continuous solvent (water) region to create inorganic walls between the surfactant cylinders. It may be that encapsulation occurs because anionic aluminosilicate species enter the solvent region to balance the cationic hydrophillic surfaces of the micelles. Alternatively, it may be the introduction of the aluminosilicate species themselves that mediates the hexagonal ordering. Once an ordered array is established, subsequent thermal processing is used to remove the organic material and produce a stable molecular sieve. Details of the precise shape of the pores (e.g. hexagonal, cylindrical) are under intense investigation[60].

From the standpoint of a range of basic scientific issues and technological applications, this discovery of ultra large-pore silicates, aluminosilicates and aluminophosphates must be considered a landmark in

the history of the synthesis of zeolite and molecular sieve type materials. Presumably one can tune the pore sizes and even dimensionality further by the appropriate choice of "secondary" chemistry involving the aluminum sites and / or the surface hydroxyl groups on the inside of the walls of the cylindrical channels, following removal of the micellar template. These ultra large-pore materials have tremendous potential for very large molecule size and shape selective catalysis, gas adsorption and separation, as well as advanced materials for future nanoscale device applications.

The 6-13 Å pore size barrier of known zeolite and molecular sieve type materials has been dramatically broken by the discovery of the ultra large-pore materials. The 6-100Å range of window and channel spaces now available enormously expands the kinds of host-guest inclusion chemistry accessible to the nanochemist. This provides an unprecedented opportunity to make interesting and significant contributions to the world of small perfect and organized nanomaterials for various kinds of nanoscale device applications. The future of the newly emerging field of nanochemistry, based on these kinds of ultra large-pore materials, looks extraordinarily bright.

Many results in this research area have been reported, such as various synthesis and formation mechanisms for the M41S family (MCM-41, MCM-48, and MCM-50)[68-79]. Other examples includes the synthesis of silica and alumina mesoporous materials with non-ionic polyethene oxide surfactants[80-81], of high aluminum MCM-41 [82-84], of mesoporous materials by using a layered silicate (kanemite)[69], layered mesophase formation[85], grafting metallocene complexes[86], ion exchange and thermal stability of MCM-41 [87], the synthesis and catalysis of Ti-MCM-41 [88,89], V-MCM-41 [90], B-MCM-41 [91,92], Fe-MCM-41 [93], Mn-MCM-41, Mn-MCM-

48 [94], V-MCM-48 [95] and Ti-MCM-48 [96]. Some mesostructured transition element and other main group element oxides have been described. A generalized synthesis method has been developed for a wide range of transition and main group element oxide mesostructured materials with cationic and anionic surfactants, by using acidic and basic media (e.g. SBA-1, SBA-2, and SBA-3), low concentrations of surfactants, and low reaction temperatures.

We very recently,[97] reported a new route to obtain mesoporous molecular sieves, through the use of intercalated surfactants for the templated synthesis of structures within the interlayer spaces (galleries) of clays. We designated our material as porous clay heterostructures (PCHs). Our approach to designing porous clay heterostructures is based on the use of intercalated quaternary ammonium cations and neutral amines as co-surfactants to direct the interlamellar hydrolysis and condensation polymerization of neutral inorganic precursor (for example tetraethylorthosilicate, TEOS) within the galleries of an ionic lamellar solid. (see figure **). As illustrated in typical syntheses that follow, Li^+-fluorohectorite (Li^+-FH) was converted to a quaternary ammonium exchanged form (Q^+-FH) by ion exchange with a two fold excess of aqueous $[C_{16}H_{33}N(CH_3)_3]^+Cl^-$. The intercalate was then washed free of excess surfactant, and air dried. Mixtures of the hydrated Q^+-FH (~ 7 H_2O per O_{20} F_4 unit cell), neutral amines and TEOS at different stoichiometric ratios were allowed to react for 4 h at ambient temperature. Under these stoichiometric conditions the galleries are swollen by the co-templating amine and are readily accessible to TEOS. Also, the extra gallery water concentration is low, as judged by the water content of the amines (~0.4 wt%). Thus the base catalysed hydrolysis of TEOS is much faster in the

clay galleries than in solution, minimizing the formation of extra gallery silica. The resulting intercalates were centrifuged, dried in air to further promote intragallery TEOS hydrolysis and then calcined at 600°C to remove the templating surfactants. Two or more orders of (001) X-ray reflections, indicating layered structures, were observed for all products. Because of the complementary chemical functionality of the layered and gallery-templated components and stable pore size distributions, porous clay heterostructures formed by gallery-templated reactions of layered silicate clays offer new opportunities for the rational design of heterogeneous catalyst systems.

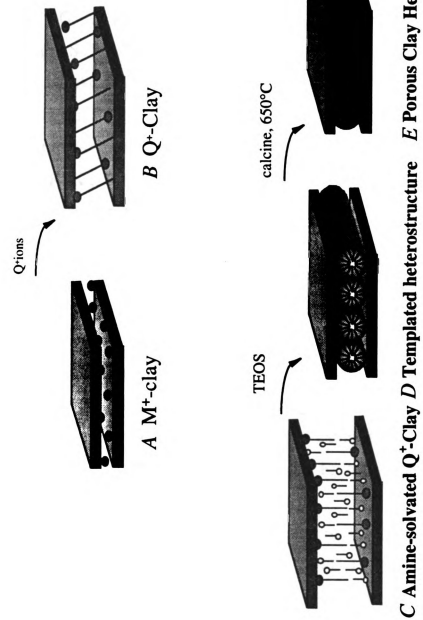

Figure I.11 : Schematics of Porous Clay Heterostructure Formation [97].

References :

1. Ozin, G. A., *Adv. Mater.* **1995**, 4, 612.
2. Farrington, G.; Shriver, F.; *Chem. Eng. News.* **1985**, 63, 42, and references therein.
3. Ozin, G. A.; Kuperman, S.; Nadimi, S., unpublished.
4. Gregg, S. J.; Sing, K. S. W. *Adsorption, Surface Area, and Porosity,* 2nd ed; Academic Press, Inc: London **(1983)**.
5. Janowski, F.; Heyer, W.; *Porose Glaser*, VEB Deutscher Verlag fur Grundstoffindustrie, Leipzig **1982**.
6. Iler, R. K.; *The Chemistry of Silica*, Wiley, New York **1979**.
7. For an excelent review of the state-of-the-art classical zeolite science as of 1990 see H. van Bekkum, Flanigen, E. M.; Jansen, J. C.(Eds), Introduction to Zeolite, Science and Practice, Vol. 58 of *Studies in Surface Science and Catalysis,* Elsevier, Amsterdam **1991**.
8. For the various aspects of the use of zeolite A as ion exchanger in *detergents* see P. Christophliemk, Gerike, P.; Potokar, M.; in *Detergents* (ed: N.T. de Oude), Springer, Berlin **1992**.
9. An Overview of the potential of zeolite catalysts in organic synthesis is provided by Holderich, W. F.; Hesse, F.; Naumann, F.; *Angew. Chem. Int. Ed. Engl.*, **1988**, 100, 232.
10. Bein, T.; (Ed), *Supramolecular Architecture, ACS .Symp. Ser.* **1992**, 499., Ozin, G.A; *Adv. Mater.* **1992**, 4, 612.
11. Ozin, G.A.; Gil, C.; *Chem. Rev.* **1989**, 89, 1749.
12. Herron, N.; in *Inclusion Compounds*, Vol. 5 (Eds.: J.L.Atwood, J.E.D. Davies, D.D. MacNicol), Oxford University Press Oxford **1991**, p. 90.

13. Ozin, G. A.; Ozkar, S.; Pastore, H. O.; Poe, A. J.; Vichi, J. S.; *ACS Symp. Ser.* **1992**, 499, 314.

14. Ozin, G. A., *Adv. Mater.* **1989**, 1, 69.

15. Bein, T.; *ACS Symp. Ser.* **1992**, 499, 274.

16. Cox, S. D.; Gier, T. E.; Stucky, G. D.; *Chem. Mater.* **1990**, 2, 609.

17. Werner, J.; Caro, J.; Finger, G.; Karnatowski, J; *Zeolites* **1992**, 12, 658.

18. Hoppe, R.; Schulz-Ekloff, G.; Wohrle, D.; Ehrl, M.; Brauchle, C.; in *Zeolite Chemistry and Catalysis* (Eds. : Jacobs, P. A.; Jaeger, N. I.; Kubelkova, L.; Wichterlova, B.), Vol. 73 of Studies in Surface Science and Catalysis, El-sevier, Amsterdam **1991**, p. 199.

19. Bein, T.; Enzel, P.; *Angew. Chem. Int. Ed. Engl.* **1989**, 28, 1692, Enzel, P.; Bein, T.; *J. Phys. Chem.* **1989**, 93, 6720.

20. Stucky, G. D.; *Mater. Res. Soc. Symp. Proc.* **1991**, 206, 507.

21. Stein, A.; Ozin, G. A.; Stucky, G. D.; *J. Soc. Photogr. Sci. Technol. Jpn.* **1990**, 53, 322.

22. Herron, N.; *CHEMTECH* **1989**, 542.

23. Li, Z.; Wang, C. M.; Persuad, L.; Mallouk, T.E.; *J. Phys. Chem.* **1988**, 92, 2592.

24. Barrer, R. M.; *Hydrothermal Chemistry of Zeolites*, Academic, London **1982**.

25. Davis, M. E.; Saldarrige, C.; Montes, C.; Garces, J.; Crowder, C.; *Nature*, **1988**, 331, 698.

26. Breck, D. W.; *Zeolite Molecular Sieves*, Kieger, Malabar, **1984**.

27. Vogt, E. T. C.; Richardson, J. W.; *J. Solid State Chem* **1990**, 87, 469.

28. Estermann, M.; McCuster, L. B.; Berlocher, C.; Merrouche, A.;

Kessler, H.; *Nature*, **1991**, 352, 320.

29. Huo, Q.; Xu, R.; Li, S.; Ma, Z.; Thomas, J. M.; Jones, R. H.; Chippindale, A. M.; *J. Chem. Soc. Chem. Commun.* **1992**. 875.
30. Davis, M. E.; Saldarrige, C.; Montes, C.; Garces, J.; Crowder, C.; *Nature*, **1988**, 331, 698.
31. Barrer, R. H.; *Hydrothermal Chemistry of Zeolites*, Academic, New York **1972**. b) Szostak, R.; *Molecular Sieves, Principles of Synthesis and Identification.* Van Nostrand Reinhold, New York. **1989**.
32. Anderson, S.; Hyde, S. T.; Larsson, K.; Lidin, S.; *Chem. Rev.* **1988**, 88, 221.
33. Intercalation Chemistry; Whittingham, M. S.; Jacobson, A. J.; Eds.; Academic: New York, **1982**.
34. Lagaly, G.; *Solid State Ionics* **1986**, 22, 43.
35. Pinnavaia, T. J.; *Science* (Washington, D.C.) **1983**, 220, 365.
36. Vaughan, D. E. W.; In Prespectives in Molecular Sieve Science; Flank, W. H.; Whyte, T. E.; Jr.; Eds.; *ACS. Symp. Ser.* 368, Amer. Chem. Soc. Washington D.C., **1988**, 308.
37. Chang, A. C.; Pfeiffer, W. F.; Guillaume, B.; Baral, S.; Fendler, J. H.; *J. Phys. Chem.* **1990**, 94, 4284. b) Fendler, J. H.; *Chem. Rev.* **1987**, 87, 877.
38. Iijima, S.; *Nature* **1991**, 354, 56.
39. Kratschmer, W.; Lamb, L. D.; Fostiropoulos, K.; Huffman, D. R.; *Nature*, **1990**, 347, 354.
40. Curl, R. F.; Smalley, R. E.; *Sci. Am.* **1991** Oct., 54.
41. See, e.g., Kroto, H. W.; Allot, A. W.; Balm, S. P.; *Chem. Rev.* **1991**, 91, 1213.
42. Iqbal, Z.; Baughman, R. H.; Ramakrishna, B. L.; Khare, S.; Murthy,

N. S.; Bornemann, H. J.; Morris, D. E.; *Science*, **1991**, 254, 826.

43. Iijima, S.; *J. Cryst. Growth* **1980**, 50, 675.
44. Kroto, H.; *Science*, **1988**, 242, 1139.
45. Ebbesen, T. W.; Ajayan, P. M.; *Nature*, **1992**, 358, 220.
46. Enzel, P.; Bein, T.; *J. Phys. Chem.* **1989**, 93, 6270.; *J. Chem. Soc. Chem Commun.* **1989**, 1326.; *Angew. Int. Ed. Engl.* **1989**, 28, 1692.; *Mol. Cryst. Liq. Cryst.* **1990**, 181, 315.; *J. Am. Chem. Soc.*; in press. *Chem. Mater.* **1992**, 4, 819.
47. (a)Terasaki, O.; Yamazaki, K.; Thomas, J. M.; Ohsuna, T.; Watanabe, D.; Sanders, J. V.; Barry, J. C.; *Nature*, **1987**, 330, 58. (b)Bogomolov, V. N.; Kholodkevich, S. V.; Romanov, S. G.; Agroskin, L. S.; *Solid State Commun.* **1983**, 47, 181. c) Tamura, K.; Hosokawa, S.; Endo, H.; Yamasaki, S.; Oyanogi, H.; *J. Phys. Soc. Jpn.* **1986**, 55, 528. d) Parise, J. B.; MacDougall, J. E.; Herron, N.; Farlee, R.; Sleight, A. W.; Wang, Y.; Bein, T.; Moller, K.; Moroney, L. M.; *Inorg. Chem.* **1988**, 27, 221.
48. Nozne, Y.; Kodaira, T.; Terrasaki, O.; Yamazaki, K.; Goto, T.; Watanabe, D.; Thomas, J. M.; *J. Phys.: Condens. Matter*, in press.
49. Terasaki, O.; *Acta. Chem. Scand.* **1991**, 45, 785.
50. Davis, M. E.; Saldarrige, C.; Montes, C.; Garces, J.; Crowder, C.; *Nature*, **1988**, 331, 698.
51. Landis, M. E.; Aufdembrink, B. A.; Chu, P.; Johnson, I. D.; Kirker, G. W. & Rubin, M. K. *J. Am. Chem. Soc.* , **1991**, *113*, 3189.
52. Weiss, A.; Angew. Chem. **1960**, 413.
53. (a) Lagaly, G.; Beneke, K.; Weiss, A.; *Am. Miner.* **1975**, 60, 650. (b) Beneke, K.; Lagaly, G.; Am. Miner. **1983**, 68, 818.
54. Reid, A. F.; Mumme, W. G.; Wadsley, A. D.; Acta. Crystallogr.

1968, B24, 1228. Groult, D.; Mercey, C.; Raveau, B.; *J. Solid. State. Chem.* **1980**, 32, 289, 55

56. Yanagisawa, T.; Shimuzu, T.; Kuroda, K.; Kato, C.; *Bull. Chem. Soc. Jpn.* 63, **1990**, 988.
57. Inagaki, S.; Fukushima, Y.; Okada, A.; Kurauchi, T.; Kuroda, K.; Kato, C.; *Proceedings of the 8th International Conference on Zeolites*, Montreal, **1992**, Butterworth-Heinmann, Boston, MA, **1992**, p.305.
58. Inagaki, S.; Fukushima, Y.; Kuroda, K., *J. Chem. Soc. Chem . Commun.*, **1993**, 680.
59. Inagaki, S.; Fukushima, Y.; Kuroda, K., *Zeolites and Related Microporous Materials: State of the Art,* **1994**.
60. Kresge, C. T.; Leonowicz, M. E.; Roth, W. J.; Vartuli, J. C.; Beck, J. S.; Schmitt, K. D.; Olson, D. H.; Sheppard, E. W.; McCullen, S. B.; Higgens, J. B.; Chu, C. T.; Schlenker, J. L.; *Proc. 9th. Int. Zeolte Assoc. Conf.*, Montreal, 07/**1992**; *Nature* in press.
61. Beck, J. S.; *U.S. Patent No.* 5,5057,298, **1991**.
62. Ekwall, P.; *Advances in Liquid Crystals*, Vol. 1, **1971**.
63. Ekwall, P.; Mandell, L.; Fontell, K., *Liquid Crystals*, 325-334, **1969**.
64. Luzzati, V.; *Biological Membranes*, 71-123, **1968**.
65. Tiddy, G. J. T.; *Phys. Rep.*, 57, No. 1, 1-46, **1980**.
66. Winsor, P. A.; *Chem. Rev.*; 68, no. 1-40, **1968**.
67. Goodman, J. F.; Clunie, J. S.; *Electron Microscopy of Liquid Crystals*, Vol. 2, 1-23, **1974**.
68. Vartuli, J. C.; Kresge, C. T.; Leonowicz, M. E.; Roth, W. J.; Vartuli, J. C.; Beck, J. S.; Schmitt, K. D.; Olson, D. H.; Sheppard, E.

W.; McCullen, S. B.; Higgens, J. B.; Chu, C. T.; Schlenker, J. L. *J. Am. Chem. Soc.* **1992**, 114, 10834.

69. Vartuli, J. C.; Schmitt, K. D.; Kresge, C. T.; Roth, W. J.; Chu, C. T.; McCullen, A. S.; Johnson, I. D.; Sheppard, E. W., *Chem. Mater.* **1994**, 6, 2070.
70. Beck, J. S.; Vartuli, J. C.; Kennedy, G. J.; Kresge, C. T.; Roth, W. J.; Schramm, S. E.; *Chem. Mater.*, **1994,** 6, 1816.
71. Huo, Q.; Margolese, D. I.; Ciesla, U.; Feng, P.; Gier, T. E.; Sieger, P.; Leon, R.; Petroff, P. M.; Schmuth, F.; Stucky, G. D.; *Nature*, **1994**, 368, 317.
72. Huo, Q.; Margolese, D. I.; Ciesla, U.; Demuth, D. G.; Feng, P.; Gier, T. E.; Sieger, P.; Leon, R.; Chmelka, B. F.; Schmuth, F.; Stucky, G. D. *Chem. Mater.* **1994**, 6, 1176.
73. Tanev, P. T.; Pinnavaia, T. J. *Science*, **1995**, 267, 865.
74. Firouzi, A.; Kumar, D.; Bull, L. M.; Besier, T.; Sieger, P. Huo, Q.; Walker, S. A.; Zasadzinski, J. A.; Glinka, C.; Nicol. J.; Margolese, D.; Stucky, G. D.; Chmelka, B. F. *Science*, **1995**, 267, 1138.
75. Monnier, A.; Schuth, F.; Huo, Q.; Kumar, D.; Margolese, D.; Maxwell, R. S.; Stucky, G. D.; Krishnamurthy, M.; Petroff, P. M.; Firouzi, A.; Janicke, M.; Chmelka, B. F. *Science*, **1993**, 261, 1299.
76. Stucky, G. D.; Monnier, A.; Schuth, F.; Huo, Q.; Margolese, D.; Kumar, D.; Krishnamurthy, M.; Petroff, P. M.; Firouzi, A.; Janicke, M.; Chmelka, B. F. *Mol. Cryst. Liq. Cryst.* **1994**, 240, 187.
77. Chen, C. Y.; Burkett, S. L.; Li, H-X and Davis, M. E., *Micro. Mater.*, **1993**, *2*, 27-34.
78. Chen, C. Y.; Burkett, S. L.; Li, H-X and Davis, M. E., *Micro. Mater.*, **1993**, *2*, 17.

79. Cheng, C. F.; Luan, Z.; Klinowski, J.; *Langmuir*, **1995**, 11, 2815.

80. Bagshaw, S. A.; Prouzet, E.; Pinnavaia, T. J.; *Science*, **1995**, 269, 1242.

81. Attard, G. S.; Glyde, J. C.; Golner, C. G.; *Nature*, **1995**, 378, 366.

82. Luan, Z. H.; Cheng, C. F.; Zhou, W. Z.; Klinowski, J., *J. Phys. Chem.* **1995**, 99, 1018.

83. Janicke, M.; Kumar, D.; Stucky, G. D.; Chmelka, B. F. *Zeolites and Related Microporous Materials : State of the Art* **1994**,.

84. Schmidt, R.; Akporiaye, D.; Stocker, M.; Ellestad, O. H.; *J. Chem. Soc. Chem. Commun.* **1994**, 1493.

85. Bull, L. M.; Janicke, M.; Kumar, D.; Miller, S. P.; Besier, T.; Stucky, G. D.; Chmelka, B. F. *Zeolites and Related Microporous Materials : State of the Art* **1994**,.

86. Maschmeyer, T.; Rey, F.; Sankar, G.; Thomas, J. M.; *Nature*, **1995**, 378, 159.

87. Kim, J. M.; Kwak, J. H.; Jun, S.; Ryoo, R., *J. Phys. Chem.* **1995**, 99, 16742.

88. Corma, A.; Marvarro, M. T.; Perez-Pariente, T. J., *J. Chem. Soc. Chem. Commun.* **1994**, 147.

89. Franke, O.; Rathousky, J.; Schulz-Ekloff, G.; Starek, J.; Zukal, A.; *Zeolites and Related Microporous Materials : State of the Art* **1994**,.

90. Reddy, K. M.; Moudrakovski, I.; Sayari, A., *J. Chem. Soc. Chem. Commun.* **1994**, 147.

91. Sayari, A.; Danumah, C.; Moudrakovski, I. L.; *Chem. Mater.* **1995**, 7, 813.

92. Sayari, A., *J. Phys. Chem.* **1995**, 99, 16373.

93. Yuan, Z. Y.; Liu, S. Q.; Chen, T. H.; Wang, J. Z.; Li, H. X., *J.*

Chem. Soc. Chem. Commun. **1995**, 973.

94. Morey, M.; Davidson, A.; Eckert, H.; Stucky, G. D.; *Chem. Mater.* **1996**, 8, 486.
95. Morey, M.; Davidson, A.; Stucky, G. D., *Micropor. Mater.* **1996**, 6, 99.
96. Antonelli, D. M.; Ying, J. Y.; *Angew. Chem. Int. Ed. Engl.* **1995.**, 34, 2014.
97. Galarneau, A.; Barodawalla, A. and Pinnavaia, T.J., *Nature*, **1995**, *374*, 529-531.
98. Pinnavaia, T. J.; *ACS Adv. Chem. Ser.* 245, 283, **1995**.
99. Davis, M. E.; *Acc. Chem. Res.*, 26, 11, **1993**.
100. Behrens, P.; Adv. Mater., 5, No 2, 127, **1993**.
101. Dailey, J. S.; Pinnavaia, T. J. *Chem. Mater.*, 4, 855-863, **1992**.

Chapter II

"A New synthetic strategy for forming nanoporous molecular sieves via intra-gallery templating of a lamellar host."

Abstract

The recent discovery by Mobil researchers[1, 2] of surfactant-templated M41S mesoporous molecular sieves has stimulated interest in large pore structures for selective catalysis[3-5] and other materials applications[6]. Many of the same ionic surfactants used for mesostructure synthesis [7, 8] can be intercalated into a variety of layered structures[9, 10]. The assembled nature of the intercalated surfactants raises the possibility of conducting a templated synthesis of an open framework structure within the constrained gallery regions of the layered host. The present work reports the gallery - templated synthesis of a new family of porous clay heterostructures, denoted PCHs, wherein the layered and gallery components are regularly stacked on a nanometer length scale. PCH synthesis is based on the use of intercalated quaternary ammonium cations and neutral amine surfactants to direct the interlamellar hydrolysis and condensation polymerization reactions of tetraethylorthosilicate. PCHs complement conventional zeolites, pillared clays and templated mesostructures, in part, by exhibiting pore sizes in the supermicropore to small mesopore range (14 - 22 Å). Since the layered and gallery - templated components of a layered heterostructure can differ in chemical functionality, PCHs offer new opportunities for the rational design of heterogeneous catalysts.

A Introduction.

In some respects, our approach of porous clay heterostructure is similar to conventional pillaring reactions of lamellar solids. But, whereas pillared clays are formed by the insertion of dense, nanoscale aggregates into the galleries of the layered host, our new intra-gallery templating process involves in situ assembly of surfactant inorganic precursor nanostructures, the morphology of which is determined by the collective energetics of the inorganic and organic species as they assemble together 11.

Our approach design strategy for porous clay heterostructures (PCHs) is based on the use of intercalated quaternary ammonium cations and neutral amines as co-surfactants to direct the interlamellar hydrolysis and condensation polymerization of neutral inorganic precursor (for example, tetraethylorthosilicate, TEOS) within the galleries of 2:1 layered silicates. High charge density 2:1 smectite clays are well suited layered hosts.

1. 2 : 1 Layered Silicate Clays

The hydrous layer silicates commonly known as clay minerals are part of a larger family called phyllosilicates. The layer silicates considered in this work contain a continuous two dimensional tetrahedral sheets of composition M_2O_5 (M=tetrahedral cation, generally Si, Al, Fe^{+3}) in which individual tetrahedra are linked with neighboring tetrahedra by sharing three corners each (the basal oxygens) to form a hexagonal mesh pattern (Figure II.1 a). The fourth tetrahedral corner (the apical oxygen) points in a direction normal to the sheet and at the same time forms a part of an immediately adjacent octahedral sheet in which individual octahedra are

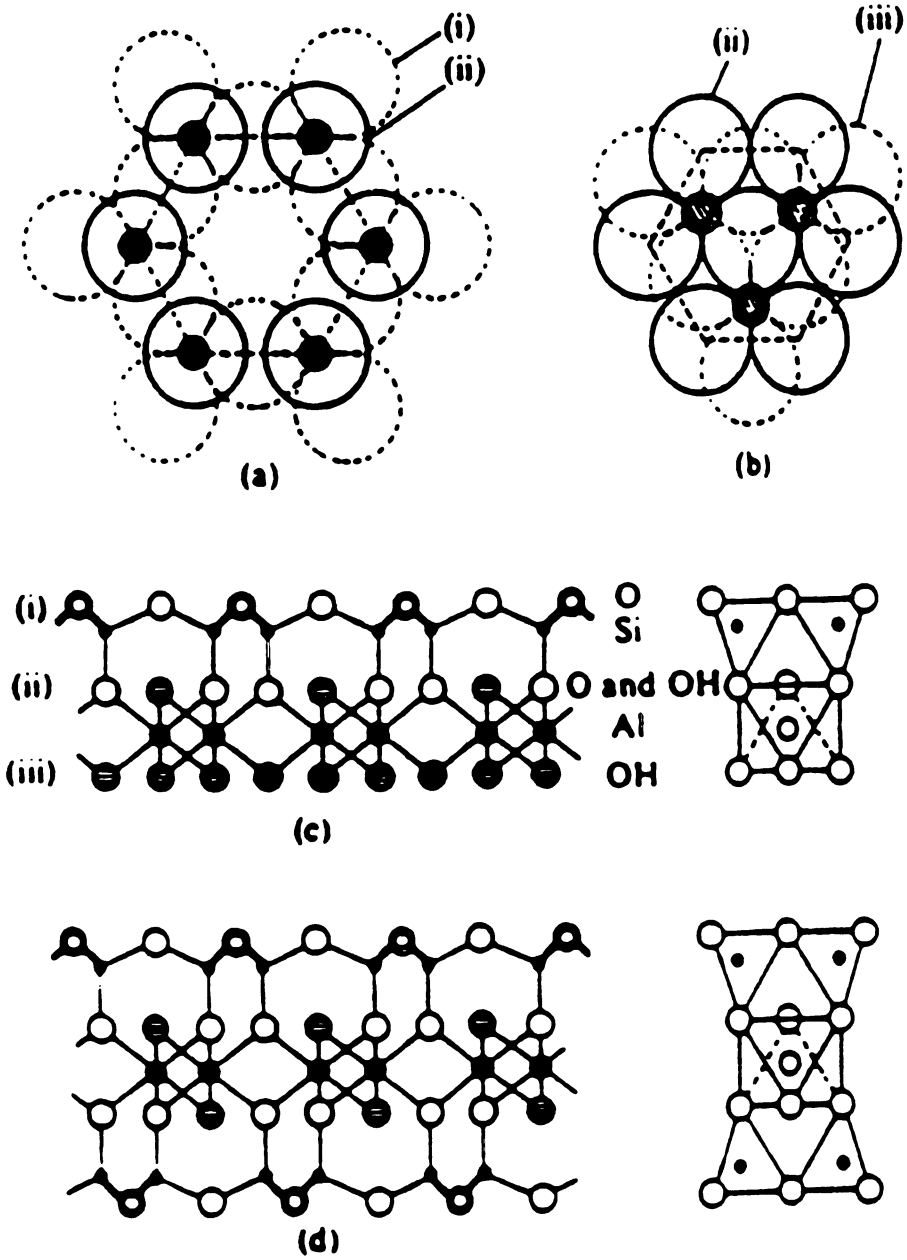

Figure II.1 : The formation of composite aluminum oxygen or silicon-magnesium oxygen layers[18].

linked laterally by sharing octahedral edges (fig II.1 b). The common plane of junction between the tetrahedral and the octahedral sheets consists of the shared apical oxygen and unshared OH groups that lie at the center of each tetrahedral six-fold ring at the same z-level as the apical oxygen. Fluorine may substitute for OH in some species. The octahedral cations normally are Mg^{+2}, Al^{+3}, Fe^{+2}, and Fe^{+3}. The assemblage formed by linking one tetrahedral sheet with one octahedral sheet is known as a 1:1 layer. In such layers the uppermost, unshared plane of anions in the octahedral sheet consists entirely of OH groups. A 2:1 layer links two tetrahedral sheets with one octahedral sheet. In order to accomplish this linkage, the upper tetrahedral sheet must be inverted so that its apical oxygen points down and can be shared with the octahedral sheet below (fig II.1 c, d)) [12, 13, 14].

The idealized oxygen framework of a 2:1 clay is shown in figure II.2. In a unit cell formed from twenty oxygen and four hydroxyl groups, there are eight tetrahedral sites and six octahedral sites along with four cavities surrounded by a six-membered oxygen ring on the surface. When two thirds of the octahedral sites are occupied by cations, the mineral is classified as a dioctahedral 2:1 phyllosilicate. A trioctahedral 2:1 phyllosilicate has all the octahedral sites filled with cations. Based on the magnitude of the layer charge per unit cell, 2:1 phyllosilicates are divided into five groups; talc-pyrophillite, smectite, vermiculite, mica and brittle mica (table II.1)[13, 15]. The members of each group are distinguished by the type and location of cations in the oxygen framework.

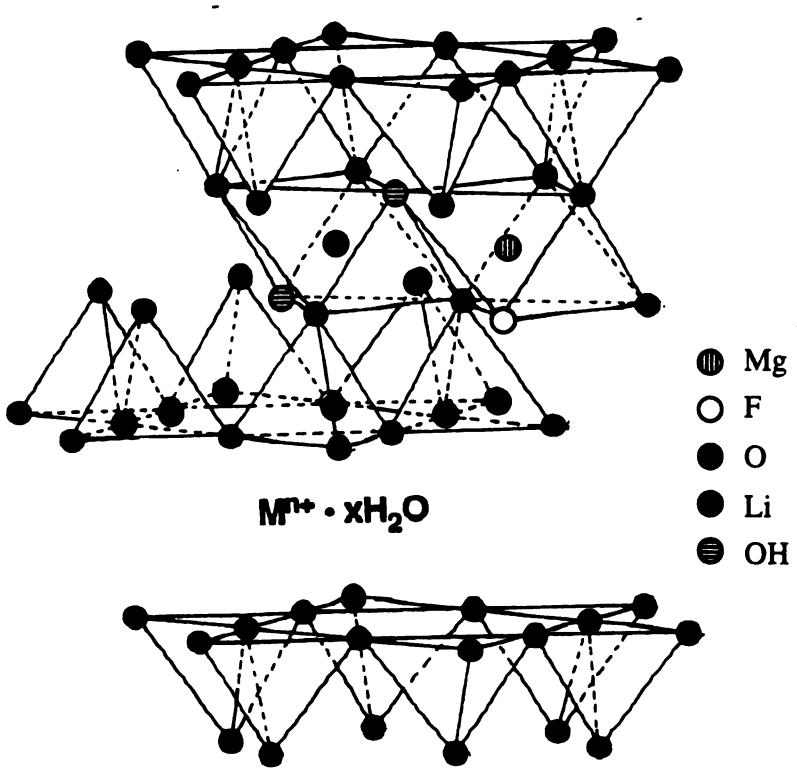

Figure II.2 : Idealized oxygen framework of clay minerals.

In talc, all the terahedral and octahedral sites are filled by Si^{+4} and Mg^{+2} respectively, and the layers are electrically neutral. In pyrophyllite two thirds of the octahedral sites are occupied by Al^{+3} ions leaving a neutral aluminosilicate layer. Therefore, in crystals of these minerals the

layers are coupled through relatively weak dipolar and van der Waals forces[16]. In contrast to talc and pyrophyllite, the layers in muscovite and phlogopite bear a net charge of $2e^-$ per Si_8O_{20} unit due to a positive charge deficiency which results from the substitution of Si^{+4} by Al^{+3} in tetrahedral positions. The charge deficiency is balanced by interlayer potassium ions which are coordinated to the hexagonal arrays of oxygen atoms at the layer surface[13]. Among the 2:1 layered phyllosilicates, the brittle mica group has the highest layer charge, $4e^-$ per Si_8O_{20} unit cell. the layer charge in vermiculite arises from the substitution of Al^{+3} for Si^{+4} in the tetrahedral layer. Vermiculite has a varying layer charge depending on the amount of substitution, 1.2-1.8 e^- per Si_8O_{20} unit.

The charge on the layers of smectite is intermediate between 0.4-1.2 e^- per Si_8O_{20} unit[17]. To balance the layer charge, layers of hydrated cations are intercalated between the clay layers. The moderate layer charge in smectite clays gives physical and chemical properties that are not found in the end members. In montmorillonite, the most familiar and common member of the smectite group, the layer charge originates from the substitution of octahedral Al^{+3} by Mg^{+2}. Hectorite is also negatively charged with Li^+ substituting for Mg^{+2} in the octahedral sheet. Nontronite is a negatively charged smectite with Al^{+3} replacing Si^{+4} in the tetrahedral sheet and Fe^{+3} replacing Al^{+3} in the octahedral sheet. Laponite and fluorohectorite are synthetic hectorites and they represent two extremes in particle size and layer charge within the smectite group. Fluorohectorite has

Table II.1 : Idealized structural formula for representative 2:1 phyllosilicates. In each formula the parentheses and bracket define metal ions in tetrahedral and octahedral sites respectively.

Mineral group	Dioctahedral	Trioctahedral
Pyrophyllite-Talc	Pyrophyllite	Talc
	$[Al_4](Si_8)O_{20}(OH)_4$	$[Mg_6](Si_8)O_{20}(OH)_4$
Smectite	Montmorillonite	Hectorite
(x = 0.4 - 1.2)	$x/nM^{n+}yH_2O[Al_{4-x}Mg_x](Si_8)O_{20}(OH)_4$	$x/nM^{n+}yH_2O[Mg_{6x}Li_x](Si_8)O_{20}(OH)_4$

Table II.1 : **Contd.**

Beidellite	Saponite
$x/nM^{n+}yH_2O[Al_4](Si_{8-x}Al_x)O_{20}(OH)_4$	$x/nM^{n+}yH_2O[Mg_6](Si_{8-x}Al_x)O_{20}(OH)_4$
Nontronite	Laponite
$x/nM^{n+}yH_2O[Fe_4](Si_8)O_{20}(OH)_4$	$x/nM^{n+}yH_2O[Mg_{6-x}Li_x](Si_8)O_{20}(OH)_4$
	Fluorohectorite
	$x/nM^{n+}yH_2O[Mg_{6-x}](Si_8)O_{20}(F_4)$

Table II.1 : **Contd.**

Vermiculite	-	Vermiculite
(x = 1.2 - 1.8)		$x/nM^{n+}yH_2O[Mg_6](Si_{8-x}Al_x)O_{20}(OH)_4$
Mica	Muscovite	Phlogopite
	$K_2[Al_4](Si_6Al_2)O_{20}(OH)_4$	$K_2[Mg_6](Si_6Al_2)O_{20}(OH)_4$
Brittle Mica	Margarite	Clintonite
	$Ca_2[Al_4](Si_4Al_4)O_{20}(OH)_4$	$Ca_2[Mg_4Al_2](Si_2Al_6)O_{20}(OH)_4$

Table? II.1 : Contd.

Trioctahedral types only

Sepiolite-palygoskite	Palygoskite
(x = variable)	$[Mg_{5-y-z}R_y^{+3}{}_z](Si_{8-x}R_x^{+3})O_{20}(OH)_2(OH_2)_4R^{+2}{}_{(x-y+2z)/2} \cdot 4H_2O$
	Sepiolite
	$[Mg_{8-y-z}R_y^{+3}{}_z](Si_{12-x}R_x^{+3})O_{30}(OH_2)_4R^{+2}{}_{(x-y+2z)/2} \cdot 8H_2O$

a particle size of up to about 2000 Å with a layer charge of 1.2 e^- per Si_8O_{20} unit that originates from substitution of Li^+ for Mg^{+2} in the octahedral layer while laponite has a particle size of ~200Å with a layer charge of 0.4 e^- per Si_8O_{20} unit as a result of substitution of Li^+ for Mg^{+2} in the octahedral layer. In fluorohectorite all the OH groups are replaced by F. The layer charge that results from substitution in the octahedral layers is distributed over the entire oxygen atom framework. These clays tend to be turbostratic, that is the layers are randomly stacked with respect to the a-b planes of adjoining layers. The negative charge on the layers of the tetrahedrally charged smectites is more localized and these derivatives tend to exhibit greater three dimensional order[14, 18].

The sixth group of 2:1 type silicates is sepiolite-palygorskite (Table II.1). The structures of these minerals can be regarded as containing ribbons of the 2:1 phyllosilicates structure, one ribbon being linked to the next by inversion of SiO_4 tetrahedra along a set of Si-O-Si bonds. Ribbons extend parallel to the x-axis, and they have an average width along the Y axis. The tetrahedral sheet is continuous across ribbons but apices in adjacent ribbons point in different directions, whereas the octahedral sheet is discontinuous. Consequence, of this framework is that rectangular channels run parallel to the x-axis between opposing 2:1 ribbons. As the octahedral sheet is discontinuous at each inversion of the tetrahedra, oxygen atoms of the octahedra at the edge of the ribbon are coordinated to cations of the ribbon side only, and coordination and charge balance are completed along the channel by H^+, H_2O(bound), and a small number of exchangeable. cations. In addition, a variable amount of zeolite water is contained in the channels.(figure II.3) [18].

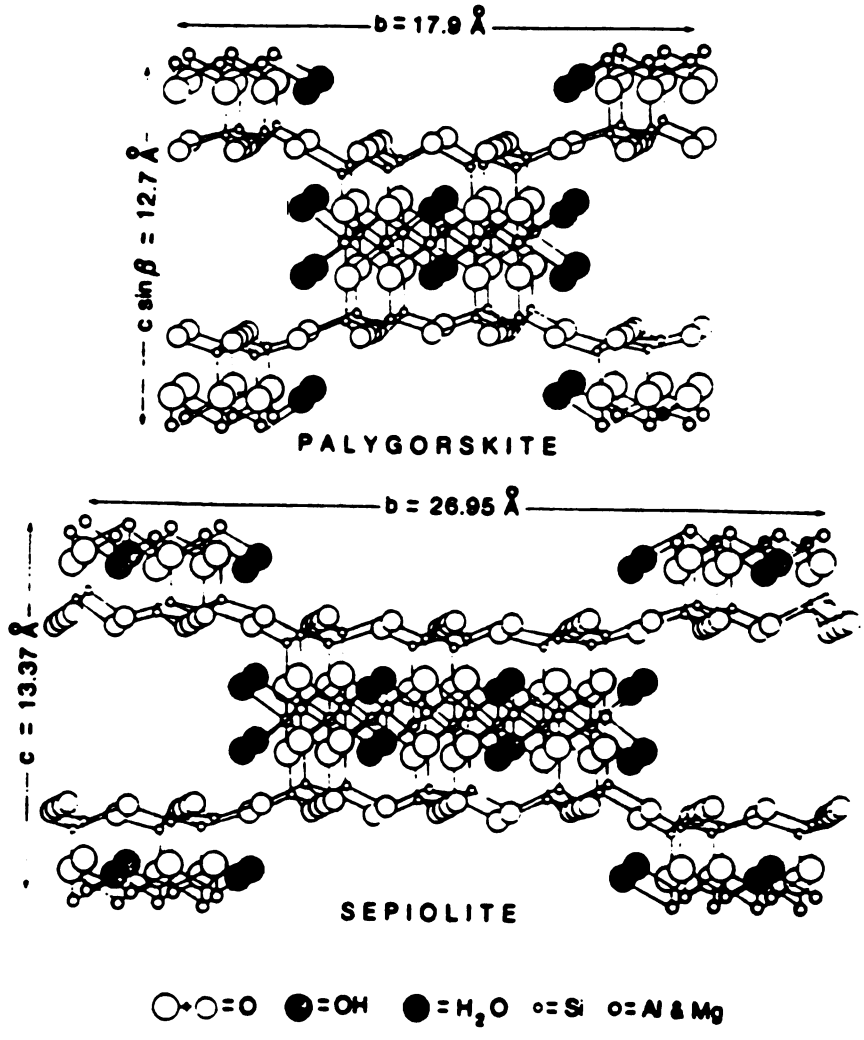

Figure II.3 : Schematic structures of palygorskite and sepiolite[19].

Smectite clays possess a combination of cation exchange, intercalation and swelling properties which make them unique. Their capacity as cation exchangers is fundamental to their intercalation and swelling properties. This distinguishes smectites from the mica and pyrophyllite-talc groups of minerals which have little or no ion exchange capacity[20]. Because of the ability of the minerals to imbibe a variety of cations and neutral molecules, an almost limitless number of intercalates are possible.

The hydrated cations on the interlamellar surfaces of the native minerals can be replaced with almost any desired cation by simple ion exchange methods. Homoionic exchange derivatives are readily achievable with simple hydrated cations, including hydrated transition metal ions. With large, complex exchange cations the extent of ion replacement may be size limited. In hectorite, which typically exhibits a layer charge of 0.67e$^-$ per Si_8O_{20}, the cation exchange capacity on an anhydrous basis is 87 milliequivalents per 100 g, about one-fifth the exchange capacity of sulfonated styrene-divinylbenzene resins. Since the average distance between exchange equivalents in the mineral is 8.3 Å, cations with cross-sectional diameters greater than this value can fully cover the interlamellar surfaces before 100 percent exchange is reached. Thus, although the interlamellar surface is very large (~750 m^2/g), the size of the exchanging ion can be a limiting factor in determining ion loading .

Neutral molecules other than water also can be intercalated between the silicate layers of smectites. Several binding mechanisms may operate in the intercalation process The reaction of the hydrated cation functioning as a Bronsted acid and the intercalant acting as a base is another important intercalation mechanism. Ammonia, for example, binds as the ammonium

ion in Mg^{+2}-montmorillonite.

A variety of experiments have shown that hydrated cations are more acidic in clay interlayers than in homogeneous aqueous solution [21-25]. The enhanced Bronsted acidity under intercalated conditions is due in part to the polarizing influence of the cation on the water molecule in the spatially restricted interlayers. The interlayer acidity is found to increase with increasing charge to radius ratio of the cation and with decreasing water content of the interlayers.

The most important property of smectites from the standpoint of catalyst design is their ability to expand beyond a single molecular layer of intercalant. The extent of interlayer swelling depends on the nature of the swelling agent, the exchange cation, the layer charge, and the location of the layer charge. The Li^+ and Na^+ exchange forms of the minerals are particularly susceptible to swelling by water [26, 27]. As the interlayer water content of Na^+-smectites is increased with increasing partial pressure, a more or less constant interlayer spacing corresponding to monolayer formation is observed. After this, the spacing jumps abruptly to a value corresponding to two intercalated water layers. The stepping of the interlayer spacing is especially well behaved in beidellite and saponite. Further swelling of the interlayers due to osmotic forces is observed when minerals are immersed in liquid water.

Alkylammonium derivatives obtained by cation exchange are distinguished by a great diversity of interlayer structures. Packing density and type of aggregation depend on the density of the negative layer charges, the geometry of the surface, and the degree of exchange.

The alkylammonium ion in 2:1 clay minerals (smectites, vermiculites, micas) lie flat on the silicate surface in mono and bilayers or

form paraffin-type arrangements with the chains radiating away from the surface (fig II.4). In the pseudo trimolecular arrangement, some chain ends are shifted above one another, so that the spacing is determined by the thickness of three alkyl chains. The chains assume the required conformation by kinking. The interlamellar structure depends on the alkyl chain length and the packing density which is determined by the layer charge(see fig II.4). In some cases, the alkyl chains form paraffin-type structures rather than pseudo trimolecular layers. The paraffin-type aggregation allows a better fit of the ammonium groups to the surface oxygen atoms than do the close-packed chains in pseudo trimolecular layers.

Figure II.4 : The surfactant orientation in the interlayers of various layer charge density clay[27].

(a) Monolayer: $[C_{16}H_{33}NMe_3]^+$ Laponite
(Cation exchange capacity, 55meq/100g)

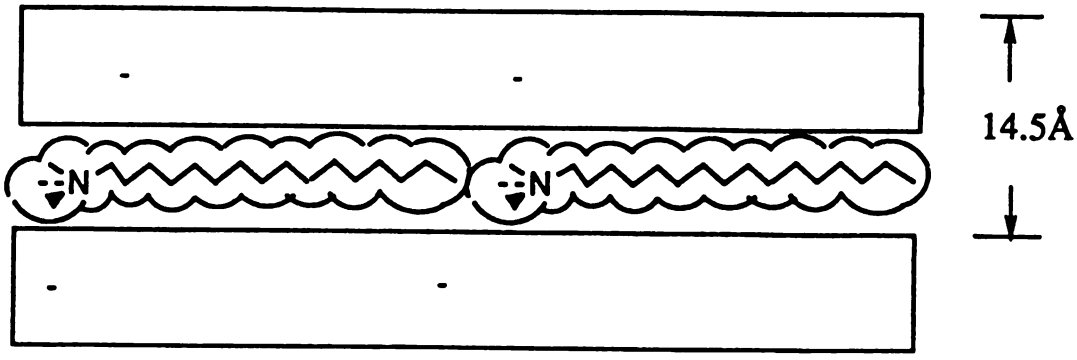

(a) Lateral Bilayer, $[C_{16}H_{33}NMe_3]^+$Hectorite
(Cation exchange capacity, 73meq/100g)

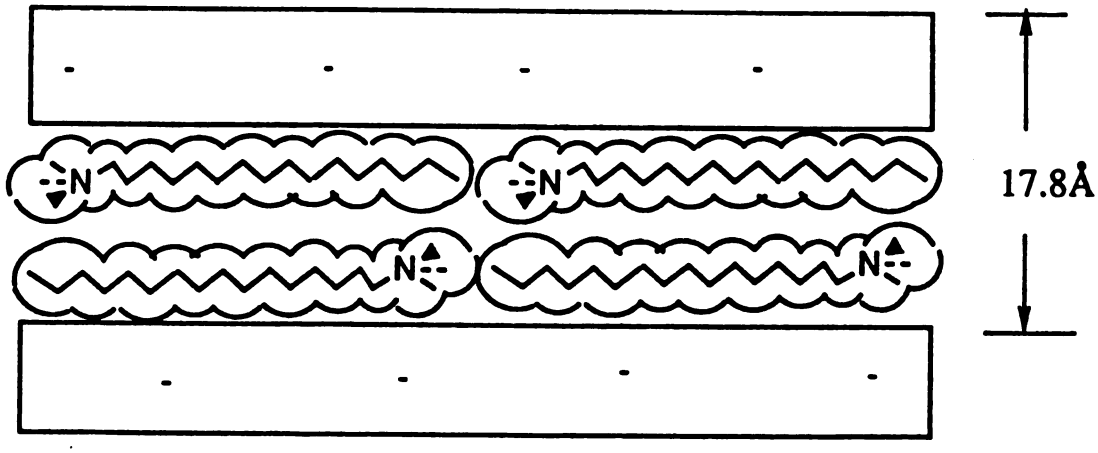

(c) Pseudo Trimolecular Structure:
$[C_{16}H_{33}NMe_3]^+$ Montmorillonite(Arizona)
(Cation exchange capacity, 118meq/100g)

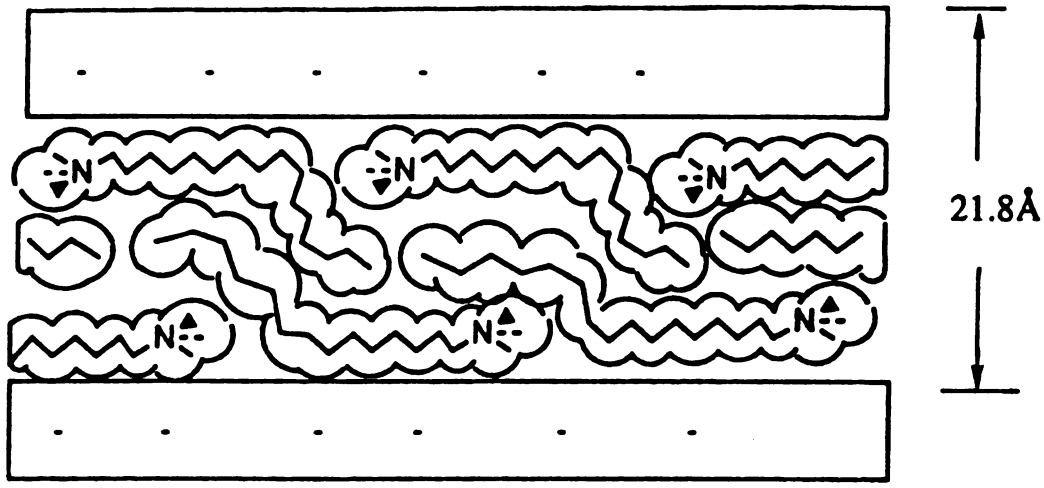

(d) Paraffin Structure, $[C_{16}H_{33}NMe_3]^+$ F-hectorite
(Cation exchange capacity, 140meq/100g)

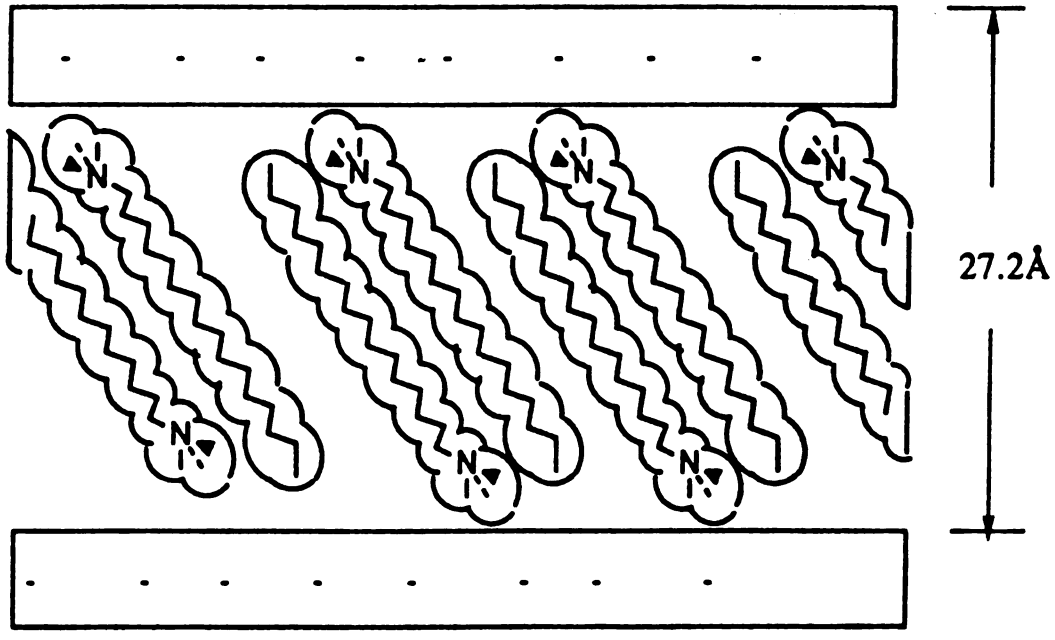

(e) Lipid Structure, $[(C_{12}H_{25})_2NMe_2]^+$ F-hectorite
(Cation exchange capacity, 140meq/100g)

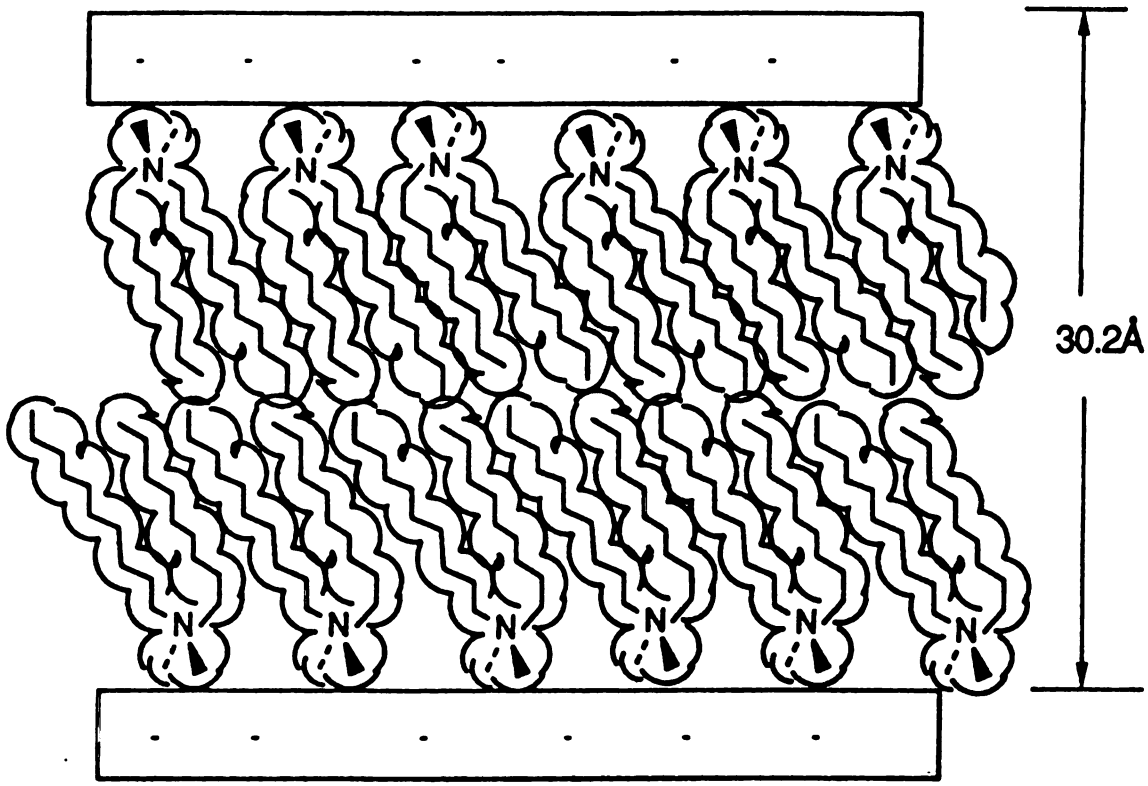

(f) $[(C_{12}H_{25})_2NMe_2^+]$Laponite
(Cation exchange capacity, 55meq/100g)

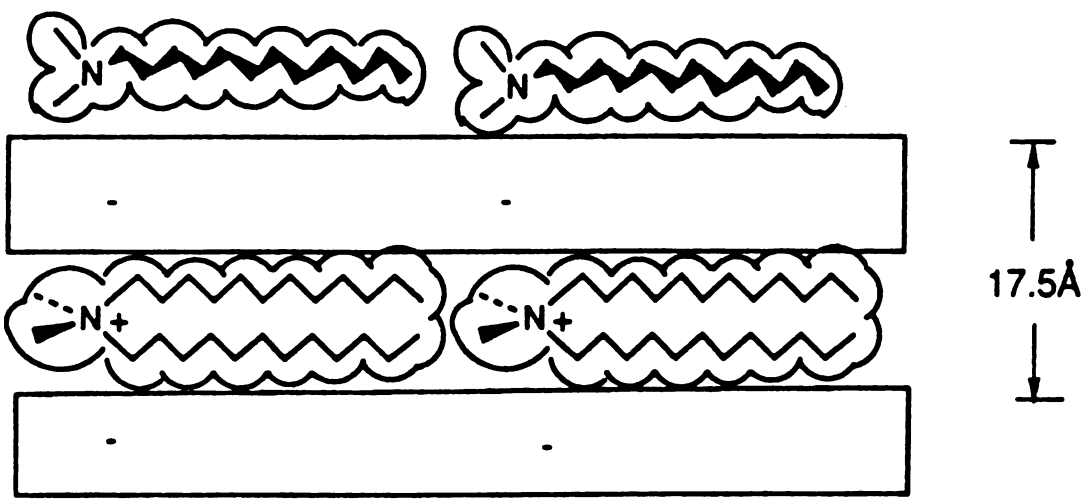

(a) Monolayer: $[C_{16}H_{33}NMe_3]^+$ Laponite
(Cation exchange capacity, 55meq/100g)

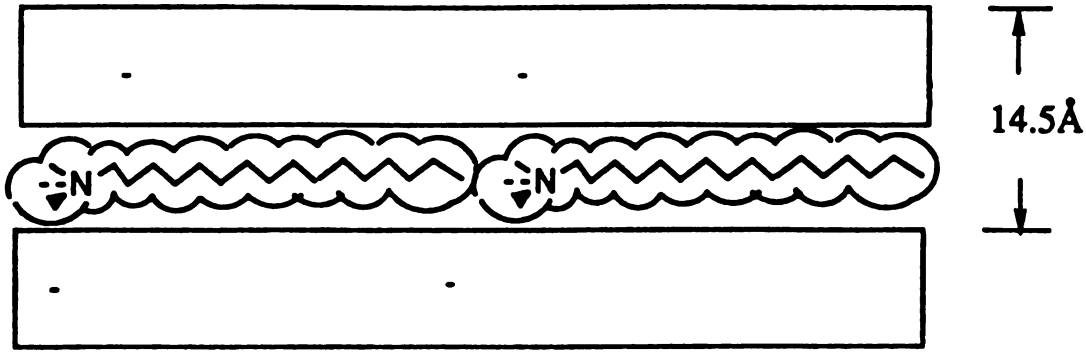

(a) Lateral Bilayer, $[C_{16}H_{33}NMe_3]^+$Hectorite
(Cation exchange capacity, 73meq/100g)

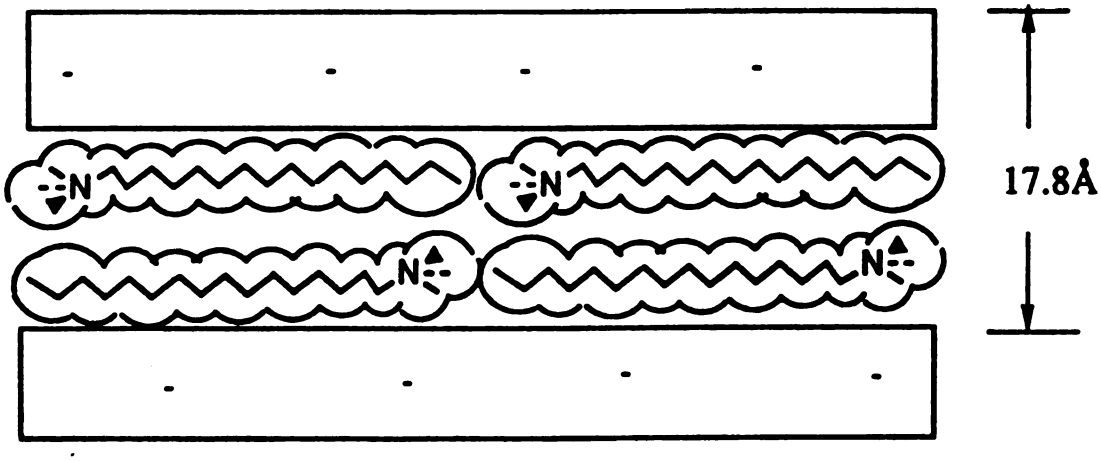

Sol-gel Processing of Silicates [29].

The sol-gel process involves a solution or sol that undergoes a sol-gel transition. At that point, the one-phase solution becomes a two-phase solid solution system due to destabilization, precipitation or supersaturation. The mechanism is not yet understood, but can be divided into five steps: hydrolysis, condensation-polymerization, gelation, drying and densification. The overall chemical reaction can be express in the case of TEOS as:

$$Si(OCH_2CH_3)_4 + 2\,H_2O \text{ -----> } SiO_2 + 4\,CH_3CH_2OH$$

In the hydrolysis reaction of metal alkoxides such as TEOS, water molecules displace alkoxy (e.g. ethoxy) groups to create silanols:

$$\equiv Si(OCH_2CH_3) + H_2O \text{ -----> } \equiv SiOH + CH_3CH_2OH$$

The reaction is an electrophilic substitution in presence of acid, but a nucleophilic substitution in a basic solution. The complete hydrolysis would produce silicic acid $Si(OH)_4$, but some condensation-polymerization occurs simultaneously.

The way in which the species hydrolyze and polymerize determines the propagation of the linking units:

$$\equiv Si(OCH_2CH_3) + \equiv SiOH \text{ -----> } \equiv SiOSi\equiv + CH_3CH_2OH$$

$$\equiv SiOH + \equiv SiOH \text{ -----> } \equiv SiOSi\equiv + H_2O$$

Under acidic condition, the first hydrolysis causes the subsequent hydrolysis of the same unit to be more difficult, so that linear polymer growth will be favored. Furthermore, acid catalyzed reactions in solutions containing a low water concentration produce linear polymers, while solutions containing high water concentration produce cross-linked polymers or branched clusters. Under basic conditions, subsequent

cation exchange capacity is approximately 150 meq./100g of air dried clay.

Natural Brazilian vermiculite which contains iron impurities, was purified by conventional clay purification techniques[30]. From elemental analysis the chemical composition of the material is $Mg_{0.7}$ ($Si_{6.06}$ $Al_{1.94}$) [$Al_{0.48}$ $Mg_{4.05}$ $Fe_{1.5}$] O_{20} $(OH)_4$. The negative charge on the layer arises from the isomorphous substitution of the silicon layer along with some substitution in the octahedral layer. The cation exchange capacity is 180 meq./100g of the air dried clay.

Rectorite mineral was from Ba-Tou, China. Particles larger than 2μm were removed by suspending the mineral in an aqueous solution for 8 hours. Rectorite consists of a regular alternation of mica-like layers and expandable layers having the smectite composition. The chemical composition formula of the material is $\{(Na_{0.72}K_{0.02}Ca_{0.05})(Ca_{0.24}Na_{0.07})\}(Al_{4.00}Mg_{0.02})[Si_{6.58}Al_{1.12}]O_{22}$. The negative charge on the layer arises from the isomorphous substitution on the tetrahedral silica oxygen sheet. The cation exchange capacity is 60 meq./100g of airdried clay.

All reagents were obtained commercially and used without further purification. Hexadecyltrimethylammonium bromide, dodecyltrimethylammonium bromide, and decyltrimethylammonium bromide were obtained from Kodak Chemical Co. Neutral alkylamines with different chain lengths such as hexylamine, decylamine, octylamine, and dodecylamine, were obtained from Aldrich Chemical Co.

Sodium hydroxide, sodium bicarbonate, and sodium acetate were purchased from EM Science company. Hydrochloric acid, and sodium chloride were obtained from Columbus Chemical Industries, Inc. Acetic

acid, sulfuric acid were purchased from Mallinckrodt. Sodium citrate was from J. T. Baker Chemical company. The silica precursor, i.e. tetraethylorthosilicate of 98% purity, was obtained from Aldrich Chemical company.

2. Synthesis.

a. Organoclays-(Q^+-clays)

An aliquot of 1% aqueous suspension of the alkali metal clay was added to an aliquot of aqueous solution of known tetraalkyl ammonium concentration at room temperature. The amount of the onium salts was abou twice that of the clay cation exchange capacity (CEC). For example, for Lithium Fluorohectorite with a CEC of 150 meq./100 g, an aliquot of aqueous solution containing 290 mmole of onium salt was added to the suspension solution with 100 g clay to ensure that all the interlayer alkali ions were replaced by onium ions. After 24 hrs of stirring, the products were purified by repeatedly washing with ethanol to remove excess onium ion and then resuspended in water. This process was repeated until the suspension was free of halide ion as tested by $AgNO_3$. The pure products were collected by centrifugation and air dried at room temperature.

Amine solvated organoclays were prepared by mixing the desired neutral alkylamines to the organoclay (Q^+-clay) with a reaction molar ratio of 20 : 1 between alkylamine : Q^+-clay. The mixture was stirred in a closed beaker for 4 h. The products were analyzed as wet gels or as air dried samples on a glass plate.

b. Templated heterostructures.

A wet amine--solvated organo-clay gel was mixed with tetraethylorthosilicate (TEOS) at different Q^+-clay : Alkylamine : TEOS molar ratios in the range of 1:2:15 to 1:20:200. The suspensions were stirred for 4 h before being separated by centrifugation (10 mins at 6000 rev/min.) The solid gel-like material was then air dried on a glass plate at room temperature. The mass of Q^+-clay used for these preparations ranged from 0.5g (~ 10.0 $*10^{-4}$ mol) to 6.0 g (~60.0 * 10^{-4} mol).

To obtain a porous clay heterostructure, the air dried templated heterostructure was calcined at 650°C in open air for 4 hrs in a programmable furnace with a ramp rate of 2°C/min. The sample was then cooled at a constant cooling rate of 5°C/min to room temperature.

Elemental analysis.

A 50 mg sample was fused with 300 mg (5.5 * 10^{-3} mol) of lithium borate for 10 min at 1000°C in a pre-ignited graphite crucible. The resultant molten glass was transferred to 50 ml of 6% wt nitric acid solution. This solution was stirred until dissolution of the glass was complete and then further diluted to 100 ml with deionized water. The solution was analyzed by inductively coupled plasma atomic emission spectrometry (ICP), at the Inorganic Laboratory of the Michigan State University Toxicology Department, using a Jarnell-Ash atom-comp instrument.

Carbon, hydrogen, and nitrogen analyses were performed at the

University of Illinois Microanalysis Laboratory by oxidation of the elements and chromatographic detection of the gases produced.

b. Physical Measurements.

The basal spacings were determined by X-ray powder diffraction, by using a Rigaku Rotaflex diffractometer equipped with a rotating copper anode and producing K_α radiation of 1.5405 Å. The current and voltage used to operate the anode were 45 mA and 100 kV, respectively. The scan speed was 1°/min, and the sample was scanned over a 2-theta range from 1° to 30°. Peak positions in the angle 2-theta were converted to basal spacing by using a standard chart.

Nitrogen adsorption-desorption experiments were performed on an Omnisorb 360CX sorptometer after outgassing the samples for 12 hours at the specified temperature of 150°C under vacuum. Helium gas was used for volumetric calibration. Surface area values and pore size data were obtained by the BET equation and the t-plot method, respectively.

The Fourier transform infrared spectra were recorded on an IBM IR44 spectrophotometer, by the KBr pressed pellet technique or by preparing pressed pellets of the pure material. Some experiments were conducted, under a flow of helium gas, under reduced pressure, at 150°C. The sample was cooled in situ before recording the spectrum.

Solid state ^{29}Si NMR experiments were performed on a Varian 400 VXR solid state NMR spectrometer operated at 79.5 MHz. A Bruker multinuclear MAS probe equipped with zircon rotors was used for the

measurements. The spectra were obtained by using a 4.6 μs 90° pulse width, a 4 kHz spinning rate, a delay time of 600s and by accumulating 12 scans, unless otherwise specified.

Scanning electron microscopy images were obtained on a JEOL JSM-25 microscope at the Michigan State University Center for Electron Optics.

Transmission electron microscopy images and the electron diffraction patterns were recorded on a JEOL JEM-100CX microscope at the Michigan State University Center for Electron Optics.

Thermogravimetric curves were obtained on a Cahn TG system 121 analyzer. The sample was held at 30°C for 5 min. It was then heated to 700°C at a ramp rate of 5°C/min. The furnace cooling fan was switched off at 400°C.

Results and Discussions.

A. Preparation and structure of organic clay derivatives.

The reaction of an alkali metal ion exchanged smectite in liquid suspension with stoichiometric amounts of onium salts dissolved in water, ethanol or a solution containing 1:1 (v/v) water:ethanol results in products in which the alkali metal ion is displaced by the onium cations. The series of organoclays described in Table II.2 were prepared by this method. If the reaction conditions involved water or ethanol as solvent, displacement of the alkali metal ion by the onium cations was strongly favored. Nearly complete cation exchange was achieved by using stoichiometric amounts of reagents. However, if the ion exchange reaction was carried out in acetone only partial exchange of the organic occured because of the low dielectric constant of acetone limits swelling of the silicate layers. Only those intercalates prepared from exchange reaction in water or ethanol were used for further studies.

The X-ray d-spacing of organoclays depends on the smectite clay layer charge densities and on the structures of the surfactant onium ions. Figure II.5 lists the representative XRD patterns of organoclays : (a) $HDTMA^+$-Fluorohectorite, (b) $HDTMA^+$-Rectorite, (c) $HDTMA^+$-Vermiculite and (d) $DODMA^+$-Fluorohectorite. High d-spacing organoclays are formed for smectites with high layer charge densities. For example, the d-spacing of $HDTMA^+$-Fluorohectorite with a CEC of 150 meq/100 gms is 28 Å. The BET surface areas are dramatically reduced when alkali metal ions are replaced by the surfactant cations in the interlayer. The reduction in surface area is presumed to result from improved

Table II.2 : Surfactant-intercalated Q^+-clays (Organoclays)

Clay	CEC (meq./100g)	Solvent	Surfactant[a]	d_{001} (Å)	Gallery Height (Å)[b]	Onium Orientation	L (Å)
Fluorohectorite	150	Water	$DTMA^+$	22.0	12.4	paraffin	130
Fluorohectorite	150	Water : Ethanol	$DDTMA^+$	24.2	14.6	paraffin	220
Fluorohectorite	150	Ethanol	$HDTMA^+$	28.0	18.4	paraffin	250
Fluorohectorite	150	Ethanol	$DODDMA^+$	40.0	30.4	lipid	325
Vermiculite	180	Water : Ethanol	$DTMA^+$	23.5	13.9	paraffin	145
Vermiculite	180	Water : Ethanol	$DDTMA^+$	26.6	17.0	paraffin	255
Vermiculite	180	Water : Ethanol	$HDTMA^+$	30.0	20.4	paraffin	300
Rectorite	60	Water	$DTMA^+$	26.0	7	pseudoTrilayer	147
Rectorite	60	Water : Ethanol	$DDTMA^+$	28.0	9	pseudoTrilayer	165
Rectorite	60	Ethanol	$HDTMA^+$	31.0	12	pseudoTrilayer	190

[a] $DTMA^+ = C_{10}H_{21}N(CH_3)_3^+$, $DDTMA^+ = C_{12}H_{25}N(CH_3)_3^+$, $HDTMA^+ = C_{16}H_{33}N(CH_3)_3^+$, $DODDMA^+ = (C_{18}H_{37})_2N(CH_3)_2^+$. [b] Gallery height is defined as the observed X-ray basal spacing minus the 9.6Å thickness of the clay layer for smectite and 19.0Å for rectorite.

stacking of the layers the narrow line widths of the XRD patterns support this hypothesis.

In Table II.3 the N_2 BET surface areas for the alkali metal clays and organo clays synthesized from $HDTMA^+$ as the exchange cation.

Table II.3 : The BET surface area of alkali metal clays and organoclays in which the surfactant, [$HDTMA^+$], is intercalated in the clay.

Clay Host	BET Specific Area (m^2/g)	
	Alkali Metal Clay	$HDTMA^+$-Clay#
Fluorohectorite	5.6	3.0
Vermiculite	23.0	4.0

* The clays were outgassed at 100°C for 24 h under vaccum (10^{-6} torr) prior to surface area measurements.
# $HDTMA^+$ $C_{16}H_{33}N(CH_3)_3^+$

Figure II.5 : The X-ray diffraction patterns of various organoclays (Q^+-clays)

(A) Hexadecyltrimethylammonium-Fluorohectorite, air dried.

(B) Hexadecyltrimethylammonium-Rectorite, air dried.

(C) Hexadecyltrimethylammonium-Vermiculite,air dried.

(D)Dioctadecylldimethylammonium-Fluorohectorite,air dried.

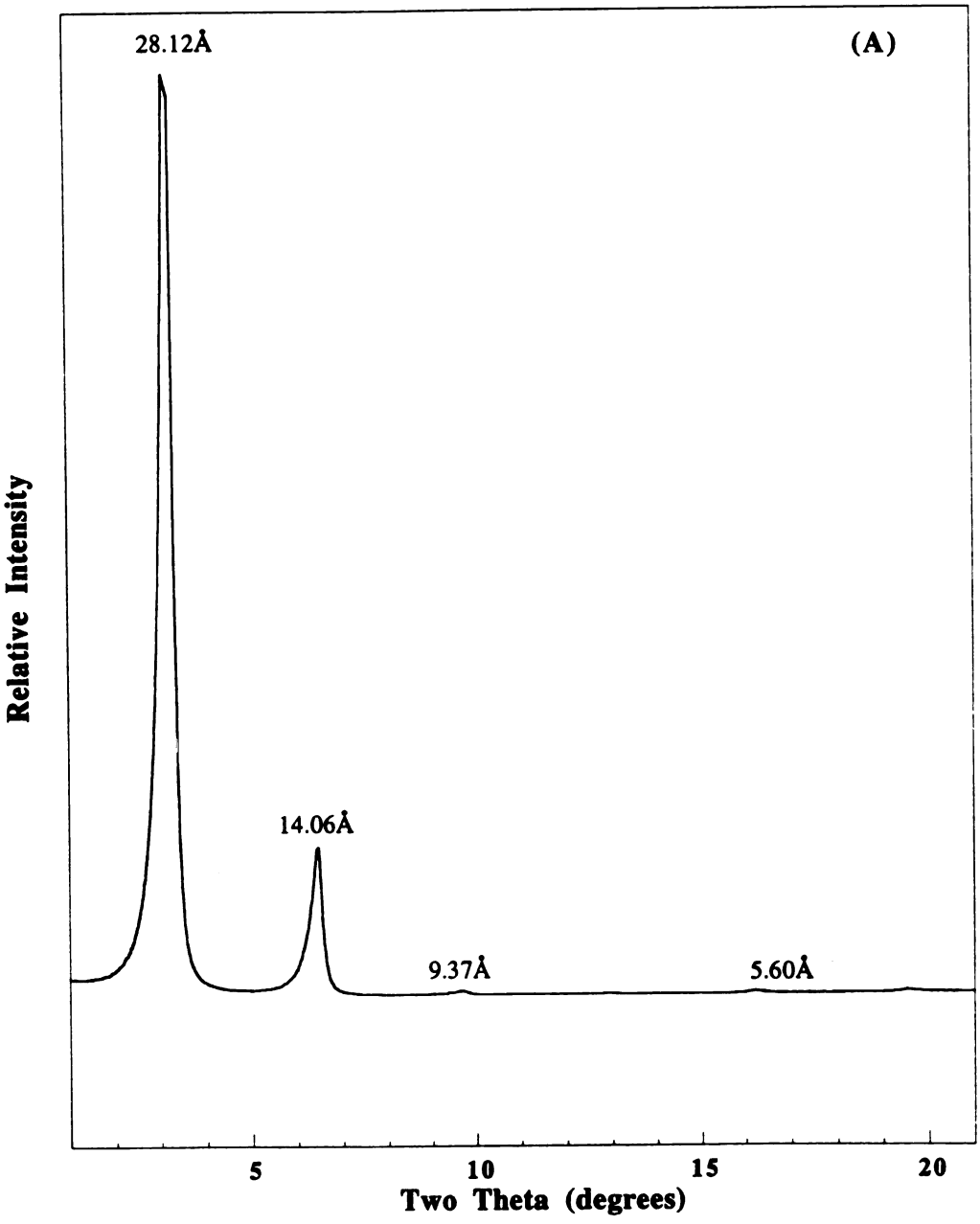
28.12Å
(A)
14.06Å
9.37Å
5.60Å
Relative Intensity
5
10
15
20
Two Theta (degrees)

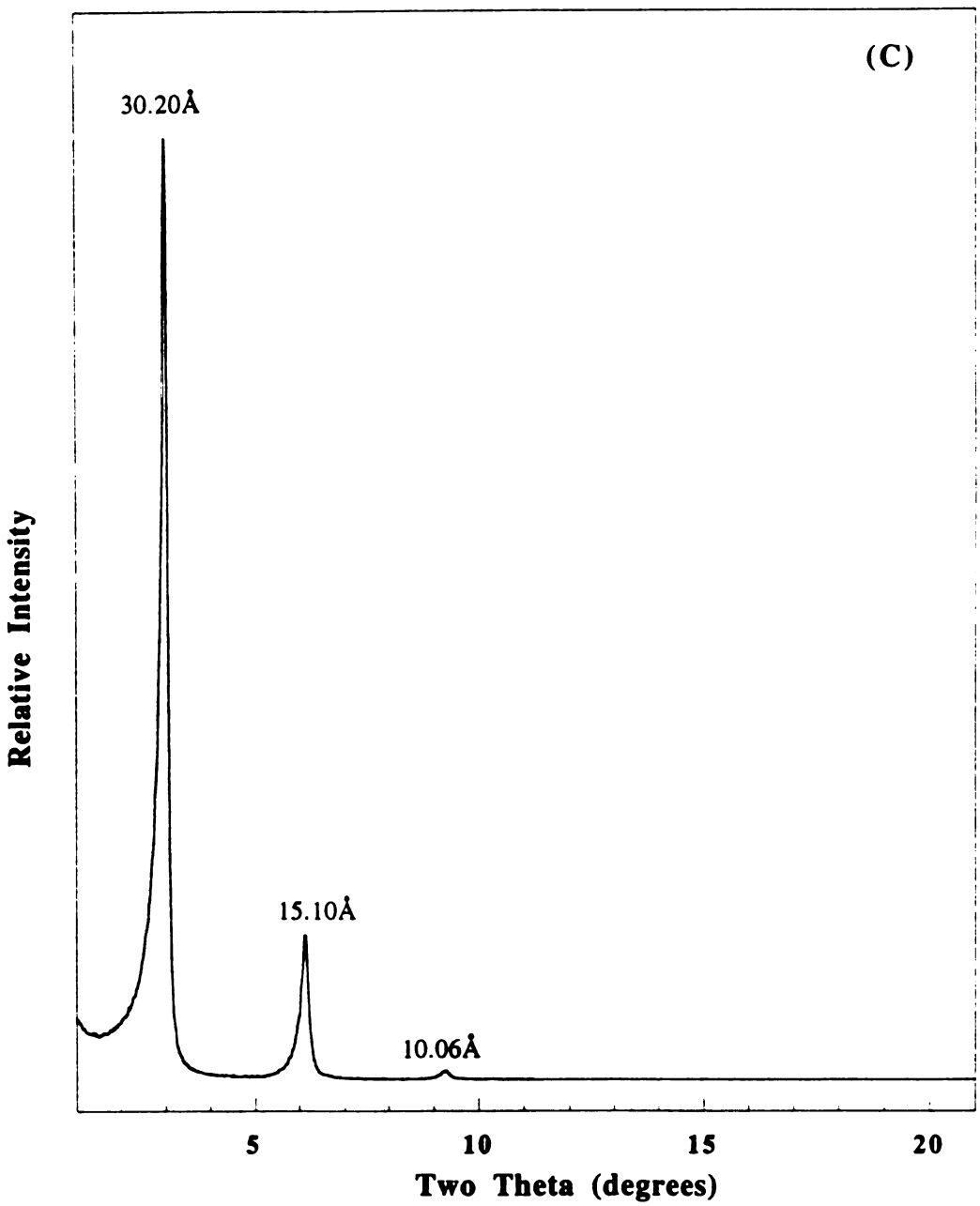
(C)
30.20Å
15.10Å
10.06Å
Relative Intensity
5
10
15
20
Two Theta (degrees)

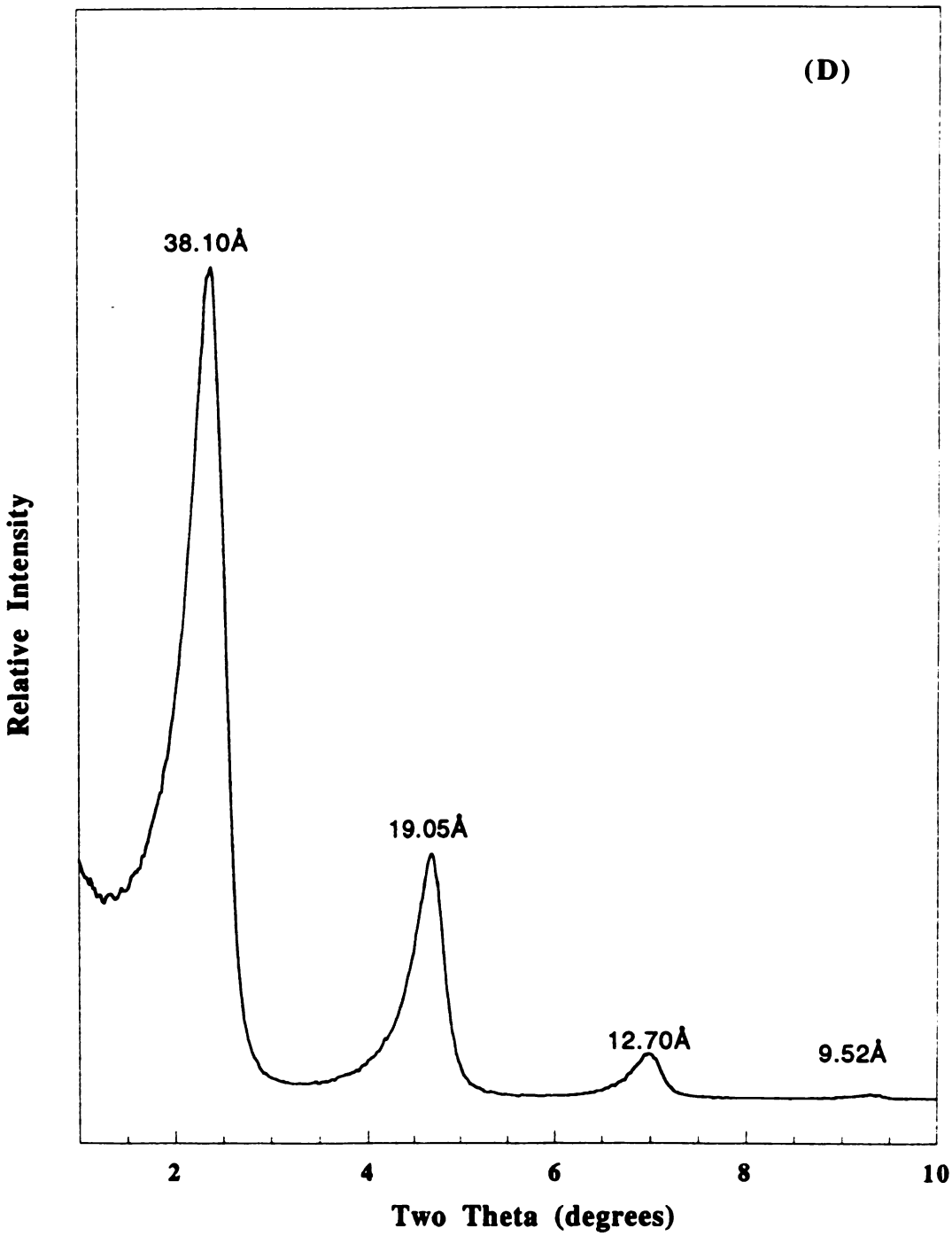
(D)
38.10Å
19.05Å
12.70Å
9.52Å
Relative Intensity
2
4
6
8
10
Two Theta (degrees)

Furthermore the particle size of the silicate layers also helps in improving the layer stacking for the organoclays. From equation 1, the scattering domain L can be calculated :

$$L = \lambda K/\beta\cos\theta \qquad (1)$$

where L is the mean of crystallite dimension in Å along a line normal to the reflection plane, λ is the wavelength of X-ray, K is a constant near unity and β is the width of a reflection at half-height expressed in radians. Values of L are listed in Table II.2. For instance vermiculite derivatives shows better layer stacking compared to synthetic fluorohectorite. Crystallinity is dependent on the particle size of the silicate layers. The surfactant in the clay interlayers does not alter the crystallinity due to the constant particle size of the silicate layers.

The orientation of linear cationic surfactants in the interlayer of clays with various layer charge densities have been studied by Lagaly and Weiss. They observed that the gallery orientation which co-related to basal spacing was depended on the charge density of the smectite clays. For instance, with basal spacings of 14 to 18Å the surfactants laid flat on the silicate surface in mono or lateral bilayer orientations. However, with the increase in basal spacing to ~22Å, the surfactants formed a pseudo trimolecular structure inside the silicate galleries. Further increase in basal spacing made the chains radiate away from the layers to give a paraffin type of orientation inside the galleries. Rectorite derivatives containing $HDTMA^+$ cations are suggested to adopt pseudo trimolecular structures (Figure II.5 b) with a gallery height of ~9-10Å. The surfactants in organo-fluorohectorite and organo-vermiculite interlayers are oriented as in paraffin-like structures (Figure II.5 c and Figure II.5 a, resptively). However, the orientation of the surfactants might differ from the above

structures if the surfactants contain two hydrocarbon chains. For instance, the organo fluorohectorite with dioctadecyldimethylammonium in the interlayer, exhibits a lipid-like orientation and a paraffin-like structure most likely forms on its external surface (figure II.5 d).

As was revealed by the work of Lagaly et.al., amines readily swell organoclays. The swelling is promoted by the solvatation of the onium ions by neutral amine molecules and results in an energy gain from van der Waals interactions, allowing the layers to separate.

The alkylamine/organoclays have been studied under different conditions by using the alkylamines as swelling agents. The alkylamines used were, octylamine, and decylamine. The alkylamine/organoclays were studied in the fully solvated (wetted) state or as air dried compounds. As the amine-solvated products are unstable intermediates, we have only been able to record their X-ray diffraction patterns. However, the air dried compounds formed by evaporation of excess amine at room temperature have been characterized by both X-ray diffraction and ^{29}Si MAS NMR.

X-ray powder diffraction has been our main analytical tool for investigating gallery expansion. The data are gathered in Table II.4

The neutral decylamine/organofluorohectorite pattern in excess amine suspension is displayed in figure II.6. The narrow peak at 30.0Å for the decylamine sample is inconsistent with the presence of a swelled amine/organofluorohectorite. The sharpness of this peak suggests the

Table II.4 : X-ray diffraction data for alkylamine solvated organoclay derivatives.

Clay	Quaternary [a] Exchange Cation	Neutral Amine [d] Co-template	Gallery [d] Height (Å)	Gallery [d] Height [b] (Å)	L (Å)
			Air dried	wet gel [c]	Air dried
Fluorohectorite	$HDTMA^+$	Octylamine	32.4	34.4	300
Fluorohectorite	$HDTMA^+$	Decylamine	34.4	36.5	325
Fluorohectorite	$DTMA^+$	Octylamine	26.3	26.3	145
Fluorohectorite	$DTMA^+$	Decylamine	29.6	31.5	170
Vermiculite	$HDTMA^+$	Octylamine	32.0	34.1	340
Vermiculite	$HDTMA^+$	Decylamine	34.3	36.0	370
Rectorite	$HDTMA^+$	Octylamine	25.0	29.0	210
Rectorite	$HDTMA^+$	Decylamine	27.0	30.1	235

[a] $DTMA^+ = C_{10}H_{21}N(CH_3)_3^+$, $HDTMA^+ = C_{16}H_{33}N(CH_3)_3^+$. [b] Gallery height is defined as the observed X-ray basal spacing minus the 9.6Å thickness of the clay layer for smectite and 19.0Å for rectorite. [c] molar ratio of neutral amine : Q^+-clay is 20 : 1 respectively. [d] Calculated gallery heights for a lipid-like bilayer of neutral amine based on the following estimates of chain lengths (Å) : $C_{16}H_{33}N(CH_3)_3^+$, 21.5; $C_{10}H_{21}N(CH_3)_3^+$, 15.3; $C_6H_{13}NH_2$, 9.0; $C_8H_{17}NH_2$, 11.5; $C_{10}H_{21}NH_2$, 14.0; $C_{12}H_{25}NH_2$, 16.5.

presence of an alkylammonium salt formed by reaction of the amine with atmospheric CO_2 to form an alkylammonium carbonate. To confirm this salt formation hypothesis, we first crystallized the alkylammonium chloride salt by adding concentrated hydrochloric acid to an amine film on a microscope slide. The X-ray diffraction patterns exhibited a narrow peak at 31.0Å for decylammonium chloride. The proximity of this d-spacing to that found on the decylamine/organofluorohectorite pattern suggests a similar packing. On the basis of the amine dimensions (table II.4), the ammonium salt crystallizes in a lipid-like double layers. In organofluorohectorite, no counter-anions are present for alkylamine salt formation. Furthermore, the salt peak intensity is dependent on the aging time of the glass slide: the older the preparation, the less intense the narrow peaks, According to the following equation

$$H_2O_{(g)} + CO_2 \xleftrightarrow{\quad} [H_2CO_3] \xleftrightarrow{RNH_{2(liq)}} [RNH_3^+ , HCO_3^-]_{(solid)}$$

in air <--- drying unstable <--- drying bicarbonate ammo salt

As the excess liquid amine evaporates in air, the equilibrium shifts to the left. So, the bicarbonate ammo salt disappears on aging. These two facts support the hypothesis of a reaction with the atmosphere.

The relatively broad XRD peaks at 46Å for the decylamine solvated organofluorohectorite is assigned to organofluorohectorite swollen by decylamine. This arises due to the intercalation of amine into the organoclay galleries. The gallery height is 36.4Å for decylamine solvated organo fluorohectorite. Furthermore as was stated by Lagaly, alkylamines are arranged in a lipid-like arrangement within the clay galleries.(see figure II.7). By us gallery heights obtained support that hypothesis.

The air dried decylamine/organofluorohectorite exhibits slightly

different basal spacings. The crystallinity decreases upon drying by ~50-100Å in layer ordering along the c axis. (see Table II.4).

Van der Waals interactions between the amine chains play a role in determining the stacking order of the clay layers. The greater the van der Waals interactions, the better the crystallinity. As the number of carbon

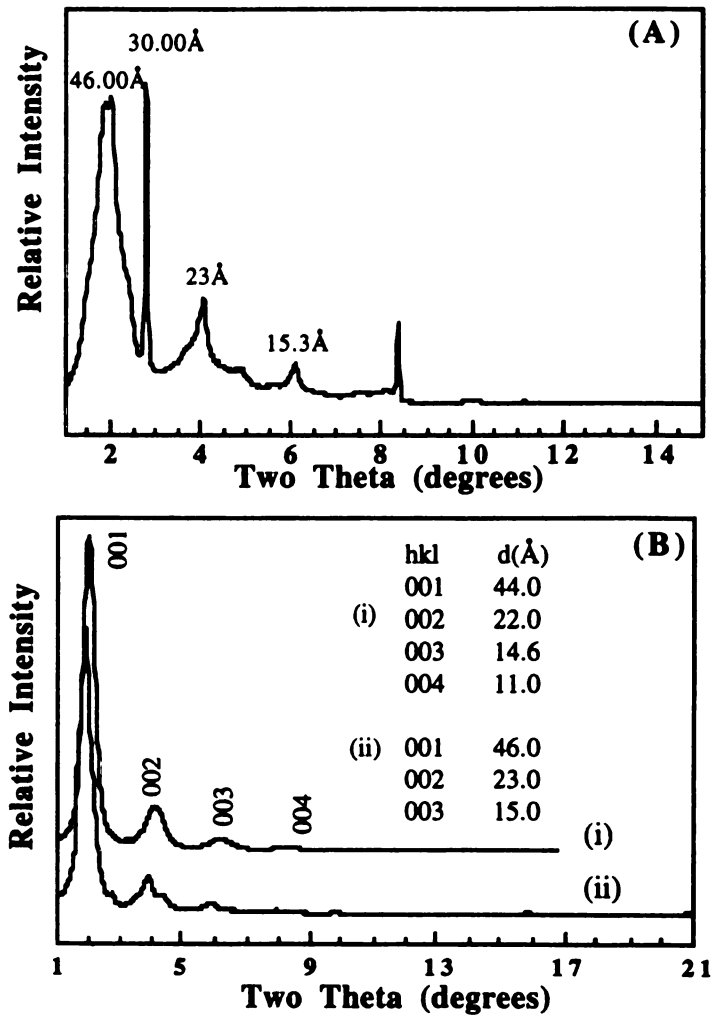

Figure II.6 : (A) X-ray powder diffraction patterns of decylamine solvated HDTMA$^+$-Fluorohectorite gel with a molar ratio of 20 : 1 (B) X-ray powder diffraction patterns of the air dried HDTMA$^+$-Fluorohectorite/amine. (i) octylamine & (ii) decylamine

Figure II.7 : Schematic representation of the exchange reaction of clay with quaternary ammonium cations (filled head groups) to form Q^+-clay with a paraffin structure. Solvation of Q^+-clay with neutral alkylamine (open head groups) affords a lipid like bilayer structure.

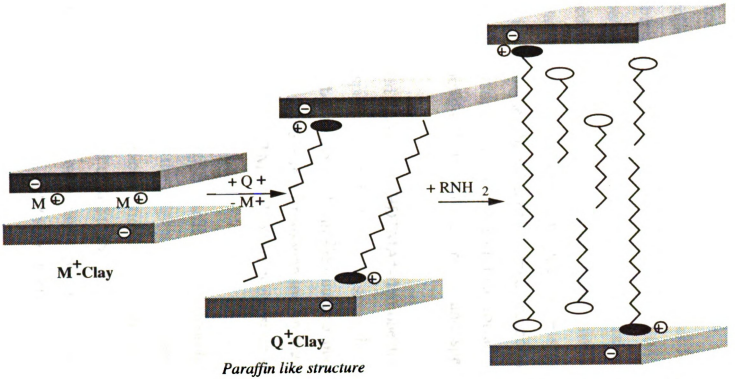
M
M
+ Q +
- M+
M+-Clay
Q+-Clay
Paraffin like structure
+ RNH 2
alkylamine-solvated Q+-Clay
Lipid like bilayer structure

atoms in the alkylamine chain increases from octylamine to decylamine, the size of the scattering domain along the layer stacking direction of the amine/organofluorohectorite increases. For example in $HDTMA^+$-fluorohectorite/octylamine it is 300Å, and for $HDTMA^+$-fluorohectorite/decylamine it is 325Å, however $HDTMA^+$-fluorohectorite exhibits a scattering domain size of 250Å. For the air dried amine/organofluorohectorite, the loss of neutral amine from the galleries caused the lowering of the van der Waals interaction. The crystallinity decreases as compared to that for the amine solvated wet gel. Yet, this value is still higher than that of air dried organofluoorhectorite intercalate. These results support the conclusion that, for amine/organoclays, van der Waals interactions between the chains and specimen crystallinity are related.

Air dried decylamine/$HDTMA^+$-fluorohectorite is stable and exhibits a large basal spacing equal to that of the same clay solvated in liquid amine. We thus have been able to obtain ^{29}Si nuclear magnetic resonance spectra and to determine the effect of alkylamine on the layer structure. The air dried decylamine/$HDTMA^+$-fluorohectorite solid state ^{29}Si NMR spectrum is displayed in Figure II.8.

The air dried decylamine/$HDTMA^+$-fluorohectorite exhibits an NMR spectrum equivalent to the original $HDTMA^+$-fluorohectorite (Figure II.8). The resonance characteristic of the silicon environment for the fluorohectorite layers, i.e., a $Si(OSi)_3(OMg)$ Q^3 at -93.3 ppm, is identical to the value for Li^+-fluorohectorite signifying that the amine co-template only separates the layers and does not affect the layer structure.

B. Porous clay heterostructure formation.

The PCH materials described herein can be synthesized over a broad range of layer charge densities ($3.82 \leq x \leq 1.33$, where "x" is the layer charge per 100Å^2). These materials can be synthesized under ambient conditions where both the type and amount of the exchange cation and neutral amine co-surfactants, along with chain length play an important structure directing influence on the final products. A typical synthesis is Illustrated in Figure II.9. An alkali metal ion exchange clay was converted to a quaternary ammonium exchanged form (Q^+-clay) by ion-exchange with a two fold excess of aqueous $[C_nH_{2n+1}\ N(CH_3)_3]^+\ X^-$, washed free of excess surfactant and air dried. Mixtures of hydrated Q^+-clay (~8.0 H_2O per O_{20} unit cell), neutral amine and TEOS at molar ratios in the range of 1 : 2 : 15 to 1 : 20 : 200 were allowed to react for 4 h at ambient temperature. The resultant intercalates were then centrifuged, dried in the open air to give the as-synthesized *templated heterostructures*. Removal of the template by calcination at 650°C in air for 4 h gave the final as-synthesized *porous clay heterostructure* (PCHs) derivatives. Figure II.10 (a, b, c, d, e, & f), illustrates the X-ray powder diffraction patterns for the air dried *templated heterostructures* and the *porous clay heterostructure* (PCHs), synthesized using rectorite, vermiculite and fluorohectorite as layered hosts. All diffraction patterns exhibited multiple (00l) reflections, indicating the presence of a layered structure. Furthermore, the crystallinity of the air dried *templated heterostructures* was better than that of the calcined PCH's. Depending on the chain length of the exchange cation and neutral amine co-template, the gallery height could be varied from 14.9Å (hexylamine) to 24.0Å (dodecylamine).

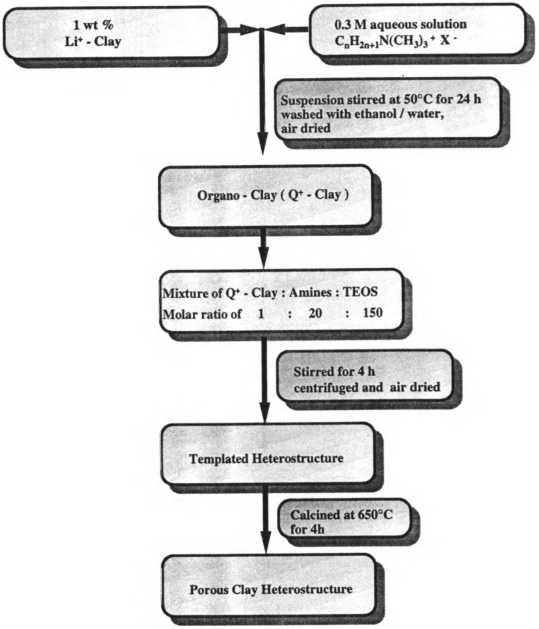

Figure II.9 : Systematic illustrations of the main steps involved in porous clay heterostructure synthesis.

Figure II.10 : The X-ray powder diffraction patterns of air dried *templated heterostructures* and calcined PCH's prepared at a molar ratio of 1 : 20 : 150 for the Q^+-clay : amine : TEOS.
(A) $HDTMA^+$ Fluorohectorite : decylamine : TEOS, air dried.
(B) $HDTMA^+$ Vermiculite : decylamine : TEOS, air dried.
(C) $HDTMA^+$ Rectorite : decylamine : TEOS, air dried.
(D)$HDTMA^+$Fluorohectorite : decylamine : TEOS, calcined at 650°C
(E)$HDTMA^+$ Vermiculite : decylamine : TEOS, calcined at 650°C.
(F)$HDTMA^+$ Rectorite : decylamine : TEOS, calcined at 650°C.

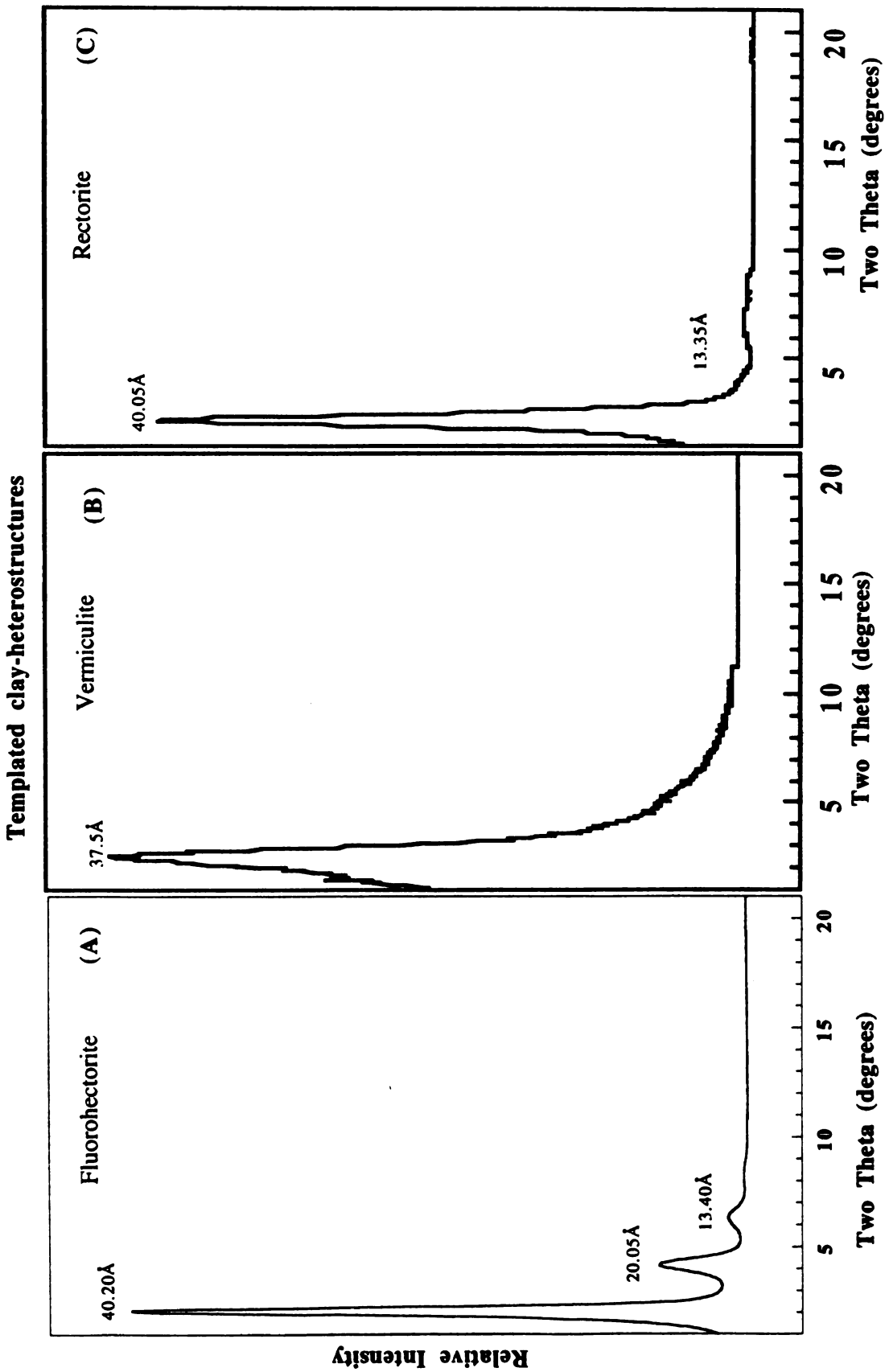
Templated clay-heterostructures
Relative Intensity
Fluorohectorite (A)
40.20Å
20.05Å
13.40Å
Vermiculite (B)
37.5Å
Rectorite (C)
40.05Å
13.35Å
5 10 15 20
Two Theta (degrees)

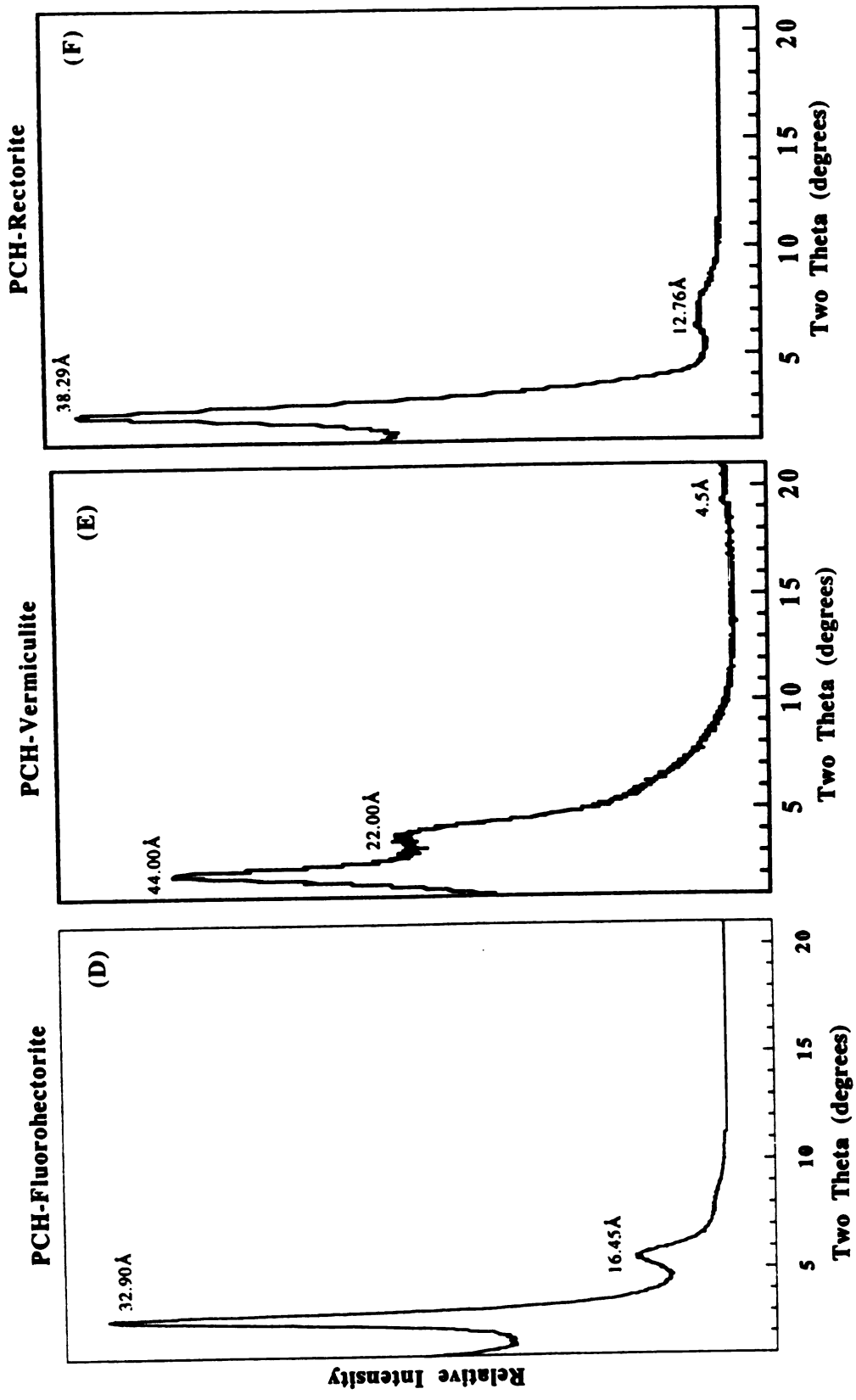
PCH-Fluorohectorite
(D)
32.90Å
16.45Å
PCH-Vermiculite
(E)
44.00Å
22.00Å
4.5Å
PCH-Rectorite
(F)
38.29Å
12.76Å
Relative Intensity
Two Theta (degrees)
5
10
15
20

Thermogravimetric programmed analyses were carried out to study weight losses up to 900°C under flowing N_2. The weight loss curve for PCH prepared from HDTMA$^+$-fluorohectorite/octylamine template is shown in figure II.11. The processes expected with increasing temperature in PCH materials would be :(a) Loss of small amounts of intra-gallery water whose presence is observed in the infra-red spectrum of the as-synthesized material. (b) Loss of the neutral amine by sublimation which occurs at a much lower temperature than the thermal decomposition of the quaternary ammonium surfactants. (c) Finally the loss of water due to silica dehydroxylation. All these features of thermal degradation are observed in PCH materials. The first step of 5% from 25°C to 140°C corresponds to loss of physisorbed water, the weight loss of 16.5% that occurs until 360°C and the weight loss of 14% up to 460°C are due the decomposition of the organic templates. The final weight loss of 1.9% between 460-600°C is related to water losses via condensation of silanol groups to form siloxane bonds. Similar thermogravimetric behavior has been observed in MCM-41.

Nitrogen BET surface areas for PCH materials synthesized using different Q$^+$ and neutral amine co-surfactants ranged from 470-850 m^2/g.

Figure II.12 (A, B & C) illustrates the N_2 adsorption/desorption isotherms for all the PCHs prepared from HDTMA$^+$/decylamine as templates, with rectorite, vermiculite and fluorohectorite as layered hosts. The nearly linear portions of the adsorption curves in the partial pressure region ~0.02-0.25 are indicative of supermicropores (~14-20Å pore diameter) or small mesopores (~20-25Å). As shown in Figure II.12 (inset) a Horvath-Kawazoe analysis of the adsorption data yields average pore sizes of ~21Å. On the basis of the widths at half maximum for the pore

size distribution curves, the pore structures of PCH materials (~7Å peak width) are similar in uniformity to MCM-41 type mesostructures of equivalent pore size (~5Å peak width) formed by surfactant templating.

Table II.5 gives the pore sizes of related PCH prepared using other combination of Q^+ and neutral amine co-template. Increasing the chain length of the amine co-template systematically increases the pore size of the PCH. That the chain length of the Q^+ also is important in the templating

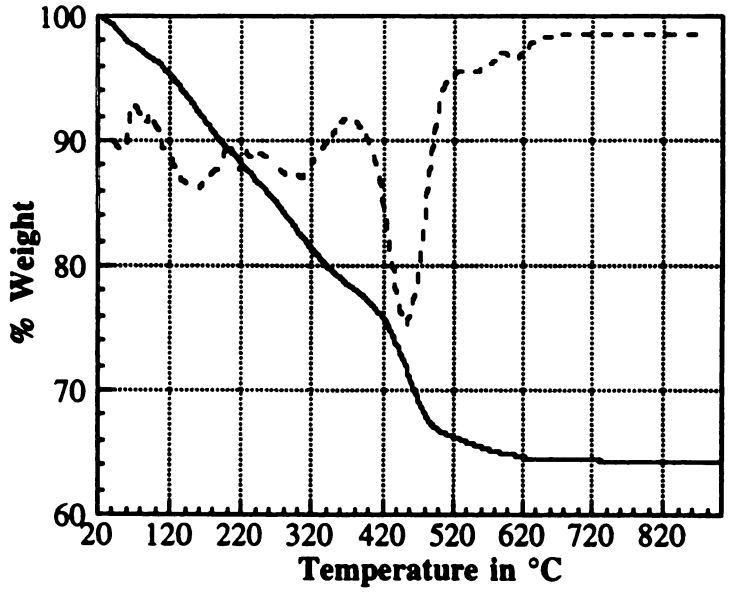

Figure II.11 : Thermal gravimetric analysis of PCH prepared from octylamine-solvated $HDTMA^+$-Fluorohectorite showing five steps of lost weight, the first one attributed to desorption of water (5%), the second and third due to the loss of neutral amine (16.5%), the fourth related to the decomposition of the quaternaryammonium cation (14%) and the fifth related to water losses via condensation of silanol groups to form siloxane bonds (1.9%).

Figure II.12 : Nitrogen adsorption/desorption isotherms for porous silica-clay heterostructures (PCHs) prepared by gallery-templated synthesis using (A)vermiculite, (B) fluorohectorite, & (C) rectorite as layered host. $HDTMA^+$/decylamine were used as templates. The $HDTMA^+$-clay : amine : TEOS reaction stoichiometry was 1 : 20 : 150. Relative pressure is P/P_O, where P is the equilibrium pressure of the adsorbate and P_O is the saturation pressure of the adsorbate at the temperature of the adsorbent; the volume adsorbed is at STP. ***Insert*** **:** The corresponding Horvath-Kawazoe pore size distribution curves. (dW/dR is the derivative of the normalized adsorbate (nitrogen) volume adsorbed with respect to the pore diameter of the adsorbent). Before measurement each sample was heated overnight at 150°C and 10^{-6} torr. The isotherms were measured at -196°C on a Coulter Omnisorp 360CX Sorptometer using standard continuous adsorption procedures.

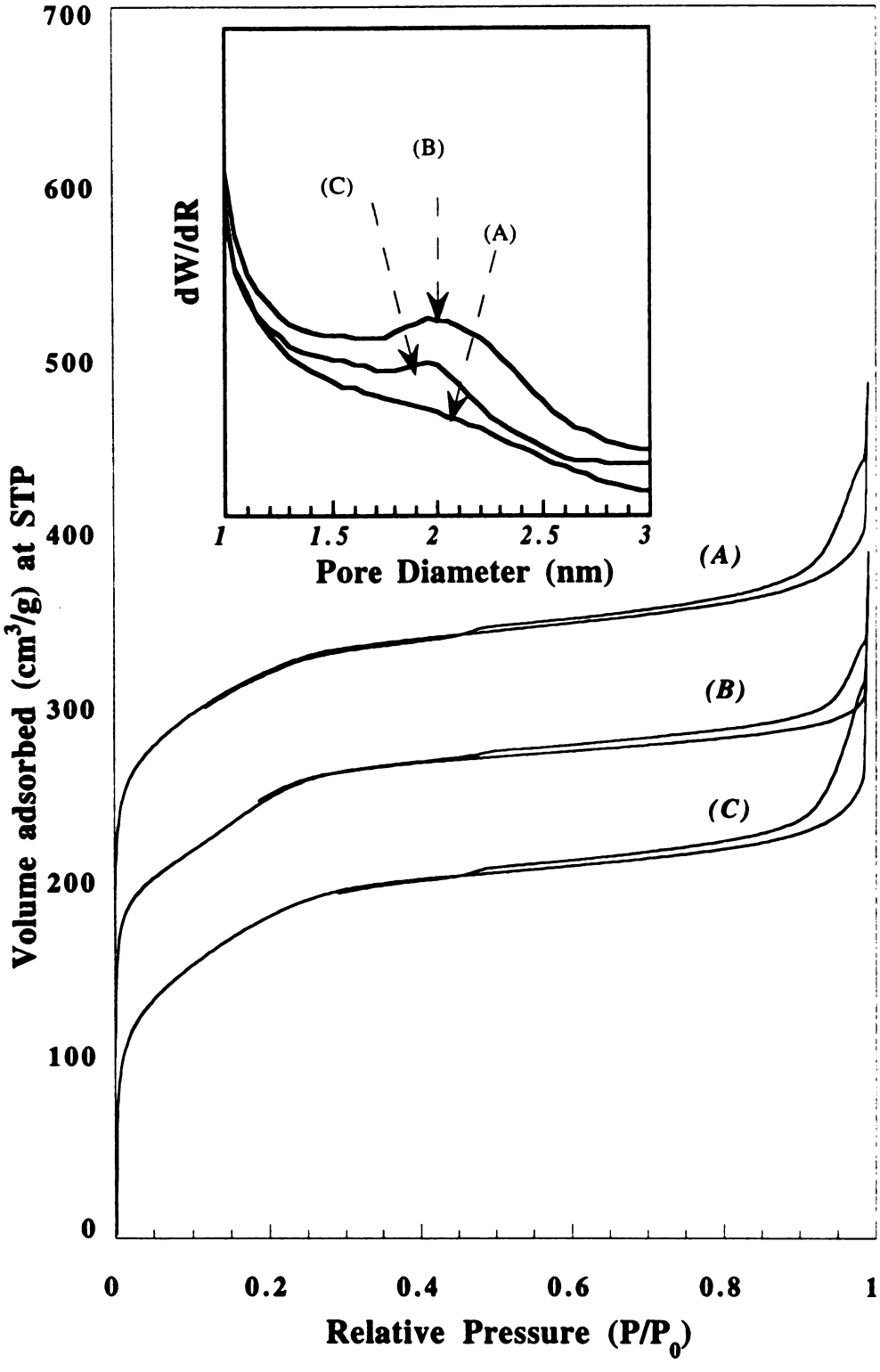
700
600
500
400
300
200
100
0
Volume adsorbed (cm³/g) at STP
0
0.2
0.4
0.6
0.8
1
Relative Pressure (P/P0)
(A)
(B)
(C)
dW/dR
1
1.5
2
2.5
3
Pore Diameter (nm)

Table II.5 : Pore size, gallery heights of air dried and calcined PCHs prepared from fluorohectorites, rectorites and vermiculites as layered hosts.

Clay [d]	Quaternary [a] ammonium exchange cation	Alkylamine co-template	Gallery Heights [c] of air dried products (Å)	Gallery Heights of products calcined at 650°C (Å)	Pore size [b] (Å)
Fluorohectorite	$HDTMA^+$	Hexylamine	22.2	14.9	15.0
		Octylamine	22.4	18.4	18.0
		Decylamine	28.4	22.4	21.0
		Dodecylamine	34.4	23.4	22.0
	$DTMA^+$	Octylamine	17.6	14.0	14.0
		Decylamine	23.9	14.3	14.0
Rectorite	$HDTMA^+$	Octylamine	18.0	19.0	18.0
		Decylamine	21.0	20.0	20.0
Vermiculite	$HDTMA^+$	Octylamine	22.0	23.0	18.0
		Decylamine	25.0	28.0	20.0

[a] $DTMA^+ = C_{10}H_{21}N(CH_3)_3^+$, $HDTMA^+ = C_{16}H_{33}N(CH_3)_3^+$

[b] Pore size obtained by Horvath-Kawazoe analysis of N_2 adsorption data.

[c] Gallery height = basal spacing - layer thickness of clay (9.6 and 19 Å for smectite and rectorite, respectively)

[d] Molar ratio of organoclay : amine : TEOS = 1 : 20 : 150.

process is evidenced by the PCH prepared using $DTMA^+$ and decylamine as gallery co-templates. Consistent with a gallery-templated pathway, this latter surfactant system affords an average pore size of 14Å, substantially smaller than the 21Å pore size provided by $HDTMA^+$ with decylamine as co-template. Included in Table II.5 are the gallery heights for the calcined PCHs, the corresponding air dried PCH precursors and the initial amine solvated Q^+-clay.

As illustrated in Table II.5, the gallery height for the air dried samples increases with chain length of the alkylamine. On calcination of the samples at 650°C there is a slight contraction in the gallery height due to the loss of intragallery water, loss of the template and dehydroxylation of the silica mesostructure. In the case of fluorohectorite and rectorite (see Figure II.13 (a)) the correlation between gallery height and the H-K pore size of the calcined material suggests that the pores of the gallery templated silica are symmetrical and systematically increase with the increase in the length of the carbon chain. However, in the case of vermiculite (see Figure II.13 (b)) the gallery heights observed are much larger than the H-K pore size, suggesting that the walls of the pores are thicker and contribute towards the gallery height of the calcined material. However the effective pore size is very similar to the corresponding fluorohectorite system. Also elemental analyses (given in table II.6) of these samples show the average gallery composition as (~8.0 mol of silica per O_{20} unit cell) for fluorohectorite and for rectorite and for vermiculite as (~11.0 mol of silica per O_{20} unit cell), as the gallery height increases, the amount of amine and silica increases, with the final Si/amine ratio around 3.2 (>3.2 for hexylamine due to its high volatility and < 3.2 for dodecylamine as it is a

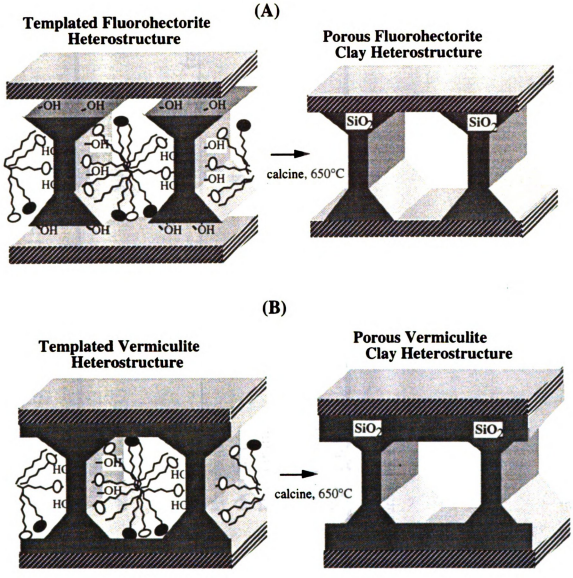

Figure II.13 : Schematic representation of the gallery structures
(A) Symmetrical pore structure formation in fluorohectorite and rectorite
(B) Thicker wall and smaller pore structure of PCH derived from vermiculite.

Table II.6 : Neutral amines and intercalated silica content of porous clay heterostructures synthesized by using fluorohectorites and vermiculites as layered hosts, and $HDTMA^+$ and neutral alkylamines as templates

Clay	Quaternary ammonium exchange cation	Alkylamine co-template	Amount of Alkylamine per O_{20} unit cell	Gallery Silica Composition (mol / O_{20} unit cell)	Si / N (mole ratio)
Fluorohectorite	$HDTMA^+$	Hexylamine	1.2	7.6	6.3
		Octylamine	2.4	8.6	3.6
		Decylamine	3.1	10.4	3.3
		Dodecylamine	4.3	10.4	2.4
Vermiculite	$HDTMA^+$	Octylamine	2.0	11.0	5
		Decylamine	2.9	13.4	4.7

*$HDTMA^+ = C_{16}H_{33}N(CH_3)_3^+$

* Values for alkylamines and Si represent an accuracy of ± 10%

solid at room temperature). A similar Si/N ratio = 3.4 was reported for the bulk templated mesostructure MCM-41 using $HDTMA^+$ as a template.

The relationship between PCH pore size distribution, chain lengths of the templating surfactants and the reaction stoichiometry support a templating mechanism analogous to structure-directed M41S mesostructure syntheses.

Scanning electron micrographs of air dried and calcined *porous clay heterostructures* formed from fluorohectorite using $HDTMA^+$/decylamine as templates are shown in figure ?? B, C respectively. The micrographs reveal the same platty morphology as the initial organofluorohectorite (see Figure A). The similarity between the air dried and calcined PCH product indicates that the templating reaction between the interlayer regions of smectite clays occurs in a topotactic fashion.

Our efforts to image PCH pores by transmission electron microscopy (TEM) have met with limited success owing to the turbostratic nature of the intercalates. For vermiculite as the layered host, the intra-gallery hydrolysis of TEOS in the presence of $HDTMA^+$ and decylamine as co-template affords a calcined PCH with a gallery height of 33.3Å. TEM images of the vermiculite heterostructure as shown in figure ?? reveal clear evidence for a lamellar morphology and uniformly expanded galleries.

Figure II.14-(i): TEM image of a porous silica - vermiculite heterostructure (d_{001} = 37.0Å) showing evidence for regularly ordered lamellar structure. Owing to the turbostratic nature of the intercalate, the galleries pores are not easily oriented for imaging. TEM images do not indicate the presence of significant amounts of extragallery silica. The TEM image was obtained on a JEOL 100CX using an accelerating voltage of 120kV and a 20μm objective lens aperture.

(Note : 2.5 cms = 175Å).

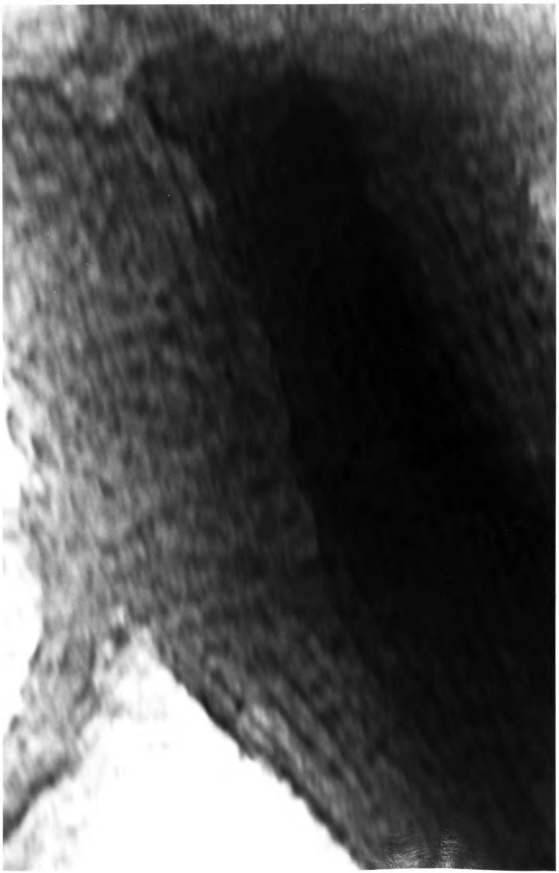

Figure II.14-(ii): TEM image of a porous silica - fluorohectorite heterostructure (d_{001} = 32.0Å) showing evidence for regularly ordered lamellar structure.The TEM image was obtained on a JEOL 100CX using an accelerating voltage of 120kV and a 20μm objective lens aperture.
(Note : 2.5 cms = 400Å)

Figure II.15 : Scanning electron micrographs at X2200 for (A) $HDTMA^+$-fluorohectorite air dried (Top). (B) $HDTMA^+$-Vermiculite air dried (below).

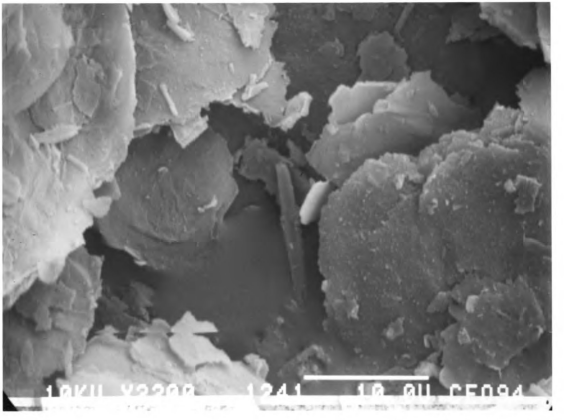

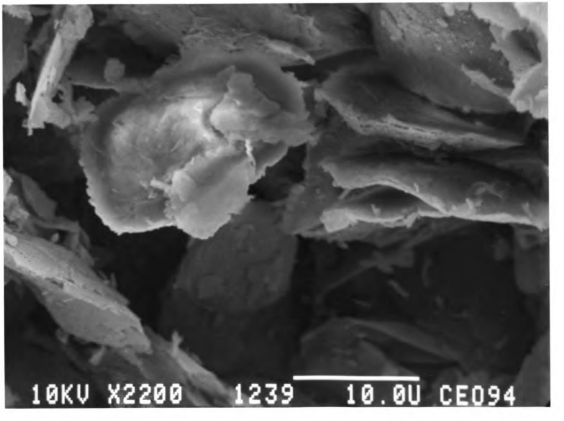
10KV X2200 1239 10.0U CE094

Figure II.15-(ii): Scanning electron micrographs for

(A) $HDTMA^+$-fluorohectorite/decylamine/TEOS mixture with a molar ratio of 1 : 20 : 150 respectively air dried (Top).
(B) $HDTMA^+$-fluorohectorite/decylamine/TEOS mixture with a molar ratio of 1 :20 :150 air dried, calcined at 650°C for 4 h in air (Bottom).

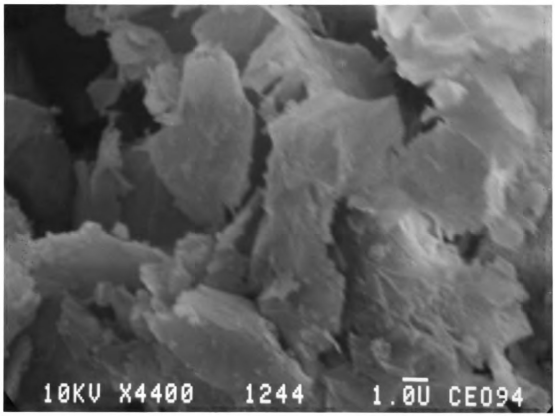
10KV X4400 1244 1.0U CE094

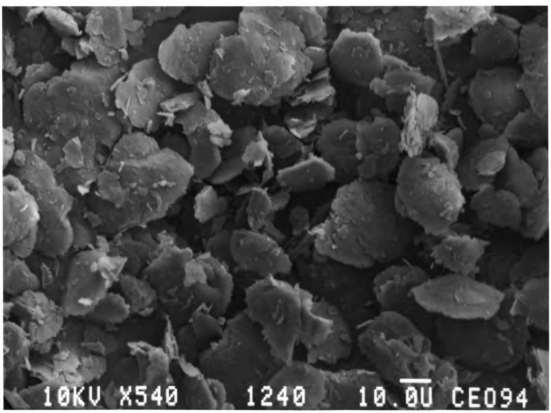
10KV X540 1240 10.0U CE094

Conclusions.

The porous clay heterostructure syntheses set forth here represents a novel strategy for obtaining nanoporous molecular sieves. Because of the complementary chemical functionality of the layered and gallery-templated components, and the stable pore size distributions in the super micropore to small mesopore range (~14-25Å), these porous heterostructures offer new oppurtunities for the rational design of heterogeneous catalyst systems. Also PCHs bridge a potentially important pore size region between microporous zeolites and pillared clays (<10Å) and M41S mesostructures (>20Å). Heavy crude oils, biological molecules (for example metalloprophyrins) and other large macromolecular species can be accommodated in PCH galleries for shape selective processing or catalysis.

References :

1. Kresge, C. T.; Leonowicz, M. E.; Roth, W. J.; Vartulli, J. C.; Beck, J. S., *Nature* **359**, 710-712 **(1992)**.
2 Beck, J.S.; Vartulli, J. C.; Roth, W. J.; Leonowicz, M. E.; Kresge, C. T.; Schmitt, K. D.; Chu, C. T-W.; Olson, D. H.; Sheppard, E. W.; McCullen, S. B.; Higgins, J. B.; Schlenker, J. L., *J. Am. Chem. Soc.*, **114**, 10834-10843 **(1992)**.
3. Tanev, P. T., Chibwe, M., & Pinnavaia, T. J. *Nature,* 368, 321-323 **1994**.
4. Reddy, M. K., Moudrakovski, I. & Sayari, A. *J. CXhem. Soc. Chem. Commun*, 1059-1060, **1994**.
5. Corma, A. , Navarro, M. T.& Pérez Pariente, J. *J. Chem. Soc. Chem. Commun.* 147-148, **1994**.
6. Bein, T. J.& Wu, C.-G. *Science* , 264, 1757-1758, **1994**.
7. Huo, Q. *et al. Nature*, 368, 317-321, **1994**.
8. Huo, Q. *et al. Chem. Mater.* 6, 1176-1191, **1994**.
9. Lagaly, G. *Solid State Ionics* , 22, 43-51, **1986**.
10. Vaia, R. A., Teukolsky, R. K. & Giannelis, E. P. *Chem. Mater.* 6, 1017-1022, **1994**.
11. Galarneau, A.G.; Barodawalla, A.F.; Pinnavaia, T.J.; *Nature*, 374, 529, **1995**.
12. Wells, A.F. *"Structural Inorganic Chemistry"* 4th Ed. **1975** Clarendon Press Oxford.
13. (a) Bailey, S.W. *"Crystal Structure of Clay Minerals and their X-ray Identification"*, Brinley, G.W. and Brown, G. Eds. Mineralogical Society London **1985**. (b) Liebau, F. *"Structural Chemistry of*

Silicates " Springer-Verlag Berlin Heidel Berg **1985**, 93.

14. Farmer, V.C. *"Infra-red Spectra of Minerals"*, Farmer, V.C. Eds. Mineralogical Society London **1974**, 331.
15. Dixon, J.B. *"Minerals in Soil Environments"*, Dinauer, R.C. Eds **1977**, 357.
16. Giese, R.F. Jr. *Clay Miner.* **1975**, 23, 165.
17. Beson, G.; Mitsud, C.T.; Mering, J. *Clays and Clay Miner.* **1974**, 22, 339.
18. Suquet, H.; Calle, de la C.; Pezerat, H. *Clays and Clay Miner.* **1975**,
23, 1.19. Jones, B.F.; Galan, E. *"Reviews in Mineralogy"* , Bailey S.W. Eds. **1988**, 19, 631.
20. Micas can be *"weathered"* to vermiculites, which do exhibit intercalation properties [K. Norrish, *Proc. Int Clay Conf. Madrid* 1, 393 (1968).
21. Raman, K.V. and Mortland, M.M. *ibid.* 16, 393, 1968.
22. Mortland, M.M.; *Phys Chem.* 67, 248, 1963.
23. Russell, J.D. *Trans. Faraday Soc.* 61, 2284, 1965.
24. Fripiat, J.J. *ACS Symp. Ser,* 34, 261, 1976.
25. Conard, J. *ibid.*, p.85.
26. MacEwan, D.M. and Wilson, M.J. in *Crystal Structures of Clay Minerals and Their X-ray Identification*, Brindley, G.W. and Brown, G. Eds. (Mineralogical Society, London, (1980), chap. 3.
27. Glaeser, R. and Mering, C.R. *Acad. Sci. Ser.* D 267, 463 1968.
28. Lee, T. Ph.D. thesis dissertation title "The Catalytic and Mechanistic Properties of Organoclays for Triphase Catalysis". Michigan State University, 1992.
29. Klein, L.C. *Annual Review of Materials Science*, 15, 227, 1987.

30. Pinnavaia et at Michigan State University. 1996.

31. Lagaly, G. *Solid State Ionics*, 22,43-51, 1986.

32. Spartan molecular modelling software, Michigan State University.

33. Brunauer, S.; Emmett, P. & Teller, E. *J. Am. Chem. Soc.*, 1938, 60, 309.

34. Horvath, G. & Kawazoe, K. J. *J. Chem. Eng. Jap.*, 1983, *16*, 470-475.

Chapter III

"Pillaring reaction vs intra-gallery templating processes in a lamellar solid - A comparative study."

Abstract

Our approach to designing porous clay heterostructures (PCHs)[1] is based on the use of intercalated quaternary ammonium cations and neutral amines as co-surfactants, to direct the interlamellar hydrolysis and condensation polymerization of a neutral inorganic precursor such as TEOS within the galleries of smectite clays. Removal of the surfactant by calcination then leaves a mesoporous solid with thermally stable pores in the supermicropore to small mesopore range (~14-25Å) depending on the chain length of surfactants. This concept of gallery templated synthesis gives a new dimension to the old traditional approach of pillaring lamellar solids. Here we describe[2] the fundamental differences that distinguishes an intragallery assembly from a conventional pillaring reaction, namely the effects of the clay layer charge density, surfactant head group size and chain lengths, critical TEOS : amine molar ratio, and the dependence of the pore size on the amount of silica in the reaction. All these factors control PCH formation clearly proving that intragallery templating is involved as opposed to pillaring.

Introduction.

This study investigates the fundamental differences between a pillaring reaction and a new templated synthesis for 2:1 clays which lead to the formation of nanoporous silica structures within the interlayer regions of clays[1]. A great amount of interest has been expressed for all of these large-pore materials with controlled pore size for selective catalysis, molecular sieving, molecular adsorption studies and other materials applications[3-9]. This concept of templating within the constrained gallery regions of a layered solid gives a new dimension to the traditional approach of pillaring layered materials.

Historically, clays (1955) and other layered metal oxides were pillared with polar organic molecules[10]. Also many surfactants such as tetraalkylammonium have been introduced by cation exchange between the layers of smectite clays and hydrous layered silicates such as kanemite; magadiite; kenyaite, etc[11, 12]. The use of these organic intercalated materials has been limited due to their low temperature stability. However thermostable microporous materials have been obtained by pillaring lamellar solids such as clays (1960), silicates, titanates, and phosphates with cationic inorganic precursor such as polyoxocations of aluminum, zirconium with or without the use of a preswelling reagent such as n-alkylamines[13, 14]. The pore size of these pillared materials was determined by the lateral separation of the pillars which in turn was controlled by the charge density of the layers. The pore sizes were typically in the microporous regime (<10Å).

A more recent pillaring procedure[15, 16, 17] (1989) involved the use of a neutral pillaring precursor such as tetraethylorthosilicate (TEOS)

adsorbed into the organophilic gallery regions of n-alkylammonium exchanged silicates (magadiites; kenyaite); titanates ($Na_2Ti_3O_7$); or perovskites ($KCaNb_3O_{10}$). Removal of the organics by calcination leads to stable microporous solids.

Our new approach to the design of porous clay heterostructures (PCHs) is based on the use of intercalated quaternary ammonium cations and neutral amines as co-surfactants to direct the interlamellar hydrolysis and condensation polymerization of a neutral inorganic precursor such as TEOS within the galleries of smectite clays. Removal of the surfactant by calcination then leaves a mesoporous solid with thermally stable pores in the supermicropore to small mesopore range (~14-25Å), depending on the chain length of both surfactants. In some respects, our approach is similar to conventional pillaring reactions of lamellar solids. But in contrast to pillared clays which are formed by the insertion of dense, nanoscale aggregates into the galleries of the layered host, our intra-gallery templating process involves in situ assembly of surfactant inorganic precursor nanostructures, the morphology of which will be determined by the collective energetics of the inorganic and organic species as they assemble together.

Here we report a systematic study of the salient features that differentiate an intra-gallery templating process from a conventional pillaring reaction by using high charge density smectite such as fluorohectorite.

Experimental.

Materials

Synthetic Li^+-fluorohectorite, abbreviated Li^+-Fluorohectorite, with an anhydrous unit cell formula of $Li_{1.12}\{[Li_{1.12}\ Mg_{4.88}](Si_8O_{20})\}F_4$ was obtained as a gift from Dow Corning, Inc.

Quaternary ammonium surfactant compounds ($[(C_nH_{2n+1})(CH_3)_3N]X$, X = Cl or Br) and n = 10 and 16 obtained from Kodak chemicals were used without further purification. Neutral alkylamines with different chain lengths, i.e., $C_6H_{13}NH_2$ to $C_{12}H_{25}NH_2$ were obtained from Aldrich Chem. Co. and used without further purification.

Physical Measurements.

Powder XRD analysis was effected with a Rigaku rotoflex diffractometer by using Cu $K\alpha$ radiation. The gallery height was obtained by subtracting the thickness of the clay unit layer (9.6 Å for a 2:1 smectite and 19.0 Å for a interstratified clay like rectorite).

The chain length of the amines and quaternary ammonium ion were calculated by the Spartan-MSU modelling program [18].

Nitrogen adsorption / desorption isotherms were determined on a Coulter Omnisorb 360 CX sorptometer at liquid N_2 temperatures by using ultra high-purity N_2 and He as adsorbate and carrier gas, respectively. All samples were outgassed at 150°C under vacuum overnight. Surface areas

were determined using the BET[19] equation. The method of Horvath and Kawazoe[20] was used to determine the pore diameters of the product.

TGA curves were obtained on a Cahn-121 type thermal analyser by using nitrogen as a purge gas at a heating rate of 10°C/min.

Elemental analysis was carried out by inductively coupled plasma emission spectroscopy at the University of Illinois Elemental Analysis Laboratory.

Results and Discussions.

Reaction Stoichiometry.

In bulk templated mesostructure synthesis, a critical TEOS/surfactant molar ratio is required for the formation of the final silica templated mesostructure. In PCH synthesis, the amount of cationic surfactant intercalated into the layered silicate host is controlled by the layer charge density. However, the TEOS/amine molar ratio is critical for the successful formation of the final intra-gallery templated silica nanostructure, as illustrated below.

The products obtained by the reaction of the alkylamine/organoclay gel with TEOS at 25°C for 4 h was dependant on the reaction stoichiometry. (see table III.1) Depending on the molar ratio of TEOS to amine, products with different basal spacings were obtained. Figure III.1 (A) illustrates the X-ray diffraction patterns for the uncalcined intercalates isolated from reaction mixtures contain $HDTMA^+$-fluorohectorite and 0.5, 2.5, 5.0, 7.5, and 10.0 moles of TEOS / mole of decylamine. These patterns indicate basal reflections corresponding to spacings of 38.0Å when

Figure III.1 : (a)X-ray powder diffraction patterns for air dried PCH formed by reaction of decylamine solvated $HDTMA^+$-Fluorohectorite with TEOS at $HDTMA^+$-Fluorohectorite : decylamine : TEOS molar ratios of 1 : 20 : X where $10 \leq X \leq 200$.

(b) X-ray powder diffraction patterns of porous clay heterostructures (PCH) obtained by calcination at 650°C for 4 h. Note that at $X \geq 100$, the calcined PCH-fluorohectorite exhibits well ordered c axis spacing of ~32Å.

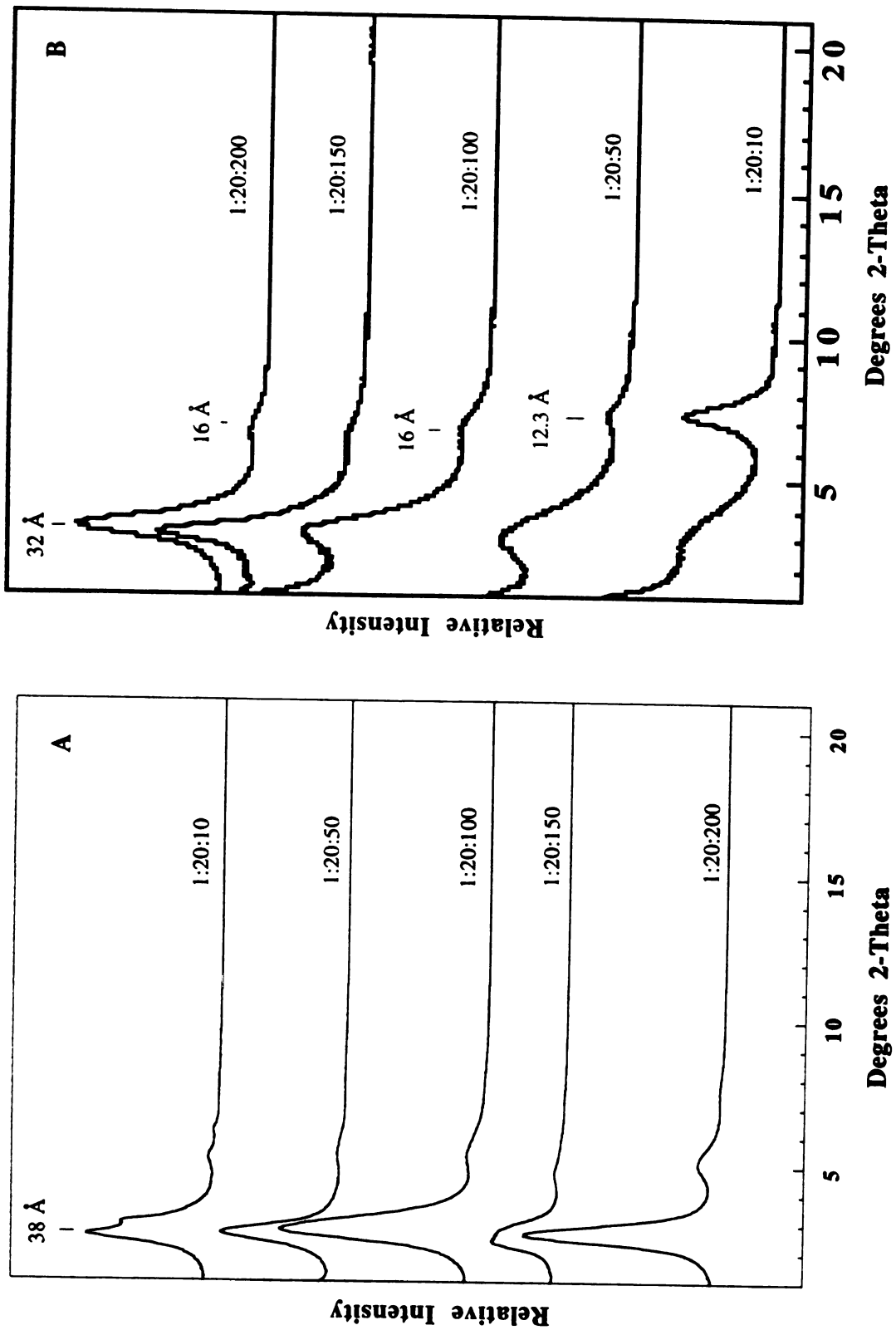
A
38 Å
1:20:10
1:20:50
1:20:100
1:20:150
1:20:200
Relative Intensity
5
10
15
20
Degrees 2-Theta
B
32 Å
16 Å
16 Å
12.3 Å
1:20:200
1:20:150
1:20:100
1:20:50
1:20:10
Relative Intensity
5
10
15
20
Degrees 2-Theta

Table III.1 : Gallery heights of reaction products obtained using quaternary ammonium cation as exchanged-cation and decylamine as co-swelling agent at different TEOS/amine molar ratios.

Clay	TEOS : neutral amine *molar ratio*	Basal Spacings (d_{001}) Å		Gallery Height (Å)	
		air dried	calcined at 650°C	air dried	calcined at 650°C
Fluorohectorite	0.5	38.0	12.2	28.4	2.6
Fluorohectorite	2.5	38.0	12.2	28.4	2.6
Fluorohectorite	5.0	38.0	29.6	28.4	20.0
Fluorohectorite	7.5	38.0	32.0	28.4	22.4
Fluorohectorite	10.0	38.0	32.0	28.4	22.4

*Gallery height is defined as the observed X-ray basal spacing minus the 9.6Å thickness of the fluorohectorite clay layers

HDTMA+/decylamine is used as a template. Since the layer thickness of smectite is ~9.6Å, these basal spacings corresponds to a gallery height of 28.4Å for fluorohectorite. The gallery heights decreases from the initial gallery height of 36.4Å observed for the decylamine solvated HDTMA+/fluorohectorite precursor gel. This means that the gallery shrinks by ~10Å when decylamine is partly replaced by TEOS molecules.

Figure III.1 B illustrates the X-ray diffraction patterns for the products obtained after calcination at 650°C in air for 4 hrs. These patterns indicate a further decrease in gallery heights for all the derivatives. In fact, the diffraction patterns for the products obtained below 5.0 moles of TEOS / mole of amine show the presence of two phases, namely the surfactant templated porous clay heterostructure with a broad basal spacing of ~32.0Å and a second phase of silica intercalated clay derivative with a basal spacing of 12.2Å. The formation of this mixed phase system can be explained by the mixed layering mechanism (see Figure III.2 a, b) which is operative below the critical TEOS / amine molar ratio ~ 7.5.

On increasing the concentration of TEOS in the reaction mixture, the neutral alkylamines in conjunction with the intercalated quaternary ammonium ions impart a structure which is more accessible to TEOS and allows the formation of a reactive intermediate. Some of the neutral amines in the intermediate are displaced from the galleries by TEOS. Subsequent hydrolysis of the gallery TEOS affords a hydrous silica templated around a monolayer of micellar quaternary ammonium and neutral amine assemblies. The final calcination step removes the template and completes the dehydroxylation and cross-linking of the gallery assembled silica structure. Two or more

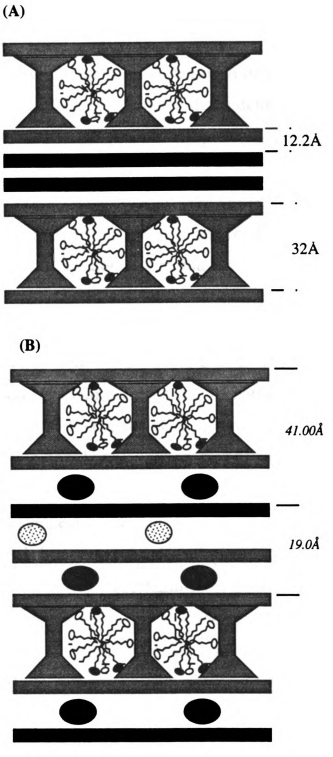

Figure III.2 : A schematic representation for the mixed random layering mechanism.
(A) In smectites with ~9.6Å layer thickness along the c axis.
(B) In interstratified mineral such as rectorite with ~19.0Å layer thickness along c axis.

orders of (001) reflections indicate the presence of a layered structure with good ordering along the c-axis.

This set of experiments also demonstrates that the formation of a porous clay heterostructure is highly dependent on the critical TEOS / amine reaction stoichiometry. The optimum product formation was achieved at a reaction stoichiometry of 1:20:150 of organoclay(Q^+-clay) : amine : TEOS, respectively. This critical TEOS : amine molar ratio is an important feature that differentiates a gallery templated process from a conventional pillaring reaction of lamellar solids.

In a pillaring mechanism formation of dense laterally spaced silica aggregates is dependent on the clay : silica ratio. Such dependence is not observed for the pore size of products obtained in PCH synthesis. The same average pore size and gallery silica composition (~8.0 mol silica per O_{20} F_4 unit cell) are observed for PCH products synthesized at $HDTMA^+$-fluorohectorite : amine : TEOS reaction stoichiometries of 1 : 2 : 15; 1 : 5 : 37.5; and 1 : 20 : 150. However the molar ratio of 1 : 20 : 150 was found to be the most convenient of all.

Figure III.3 illustrates the X-ray powder diffraction patterns of $HDTMA^+$-fluorohectorite : octylamine : TEOS products synthesized at different molar ratios but with a constant TEOS : amine reaction stoichiometry. The air dried intercalates gave similar diffraction patterns with multiple (00l) reflections indicating a highly ordered structure. Calcination at 650°C in air reduced the basal spacing by ~6Å; however, all the samples exhibited similar gallery heights.

Elemental analysis of the samples gave an average gallery silica composition of ~8.0 mol of silica per O_{20} F_4 unit cell. The N_2 adsorption/desorption isotherms were virtually identical and the H&K pore

analysis gave an average pore size of ~18.0Å.

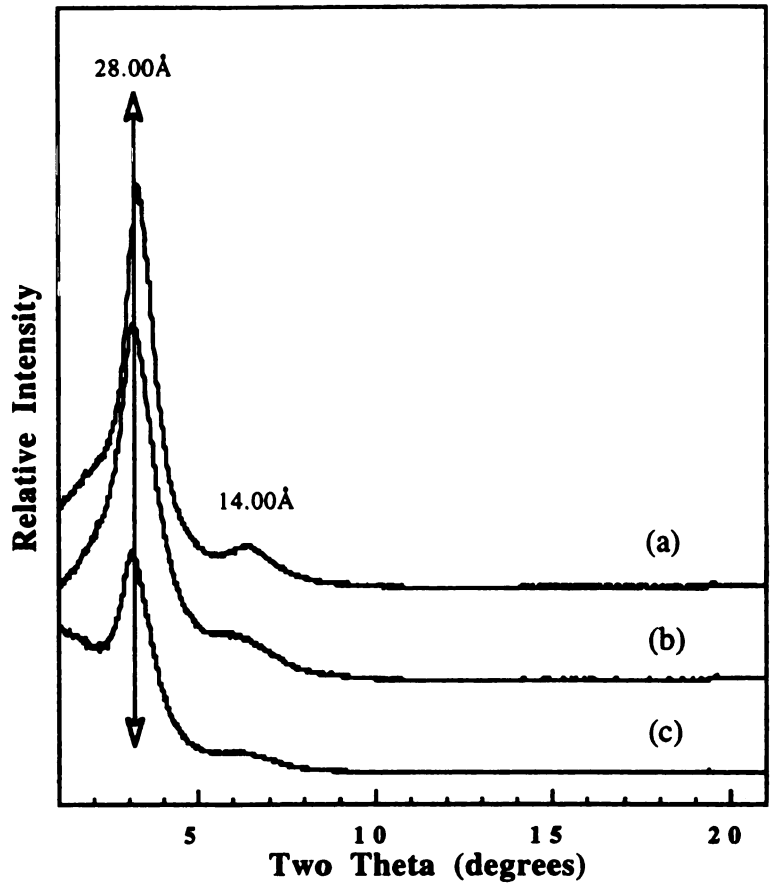

Figure III.3 : X-ray powder diffraction patterns of calcined PCH reaction products formed at a different HDTMA$^+$-fluorohectorite : octylamine : TEOS reaction stoichiometry :
(a) 1 : 20 :150
(b) 1: 5 : 37.5
(c) 1 : 2 : 15.
(Q$^+$-clay : amine : TEOS.)

Pore size dependence on surfactant chain lengths

Both the quaternary ammonium ion and neutral amine co-surfactant as well as surfactant chain length play an important structure directing role in the syntheses of PCH materials. Figure III.4 A and B illustrate the X-ray diffraction patterns from $HDTMA^+$-Fluorohectorite/decylamine/TEOS and $DTMA^+$-Fluorohectorite/decylamine/TEOS systems. Both diffraction patterns exhibit multiple (001) orders of Bragg's reflections indicating a well-ordered structure along the c axis. On calcination of the samples at 650°C there is a slight contraction in the gallery height due to the loss of intragallery water, loss of the template and dehydroxylation of the gallery silica surface. It is important to note that different gallery heights are obtained for different surfactant chain lengths, indicating that the chain lengths of the templates is important in controlling the final gallery heights. This point was further elaborated when surface area measurement were performed on the calcined materials.

Figure III.5 A, B and C illustrate the N_2 adsorption-desorption isotherms for the PCH's prepared from $HDTMA^+$-Fluorohectorite in the presence of hexylamine, decylamine and dodecylamine, respectively as co-templates. The nearly linear portions of the adsorption curves in the partial pressure region ~0.02 - 0.25 are indicative of supermicropores (~14-20Å diameter) or small mesopores (~20-25Å). As shown in Figure III.5(insert), a Horvath Kawazoe analysis of the adsorption data yields average pore sizes of 15Å for hexylamine, 21.0Å for decyalmine, and 23Å for dodecylamine indicating that the neutral amine co-surfactant chain lengths plays an important structure directing role in the synthesis of the gallery intercalated silica.

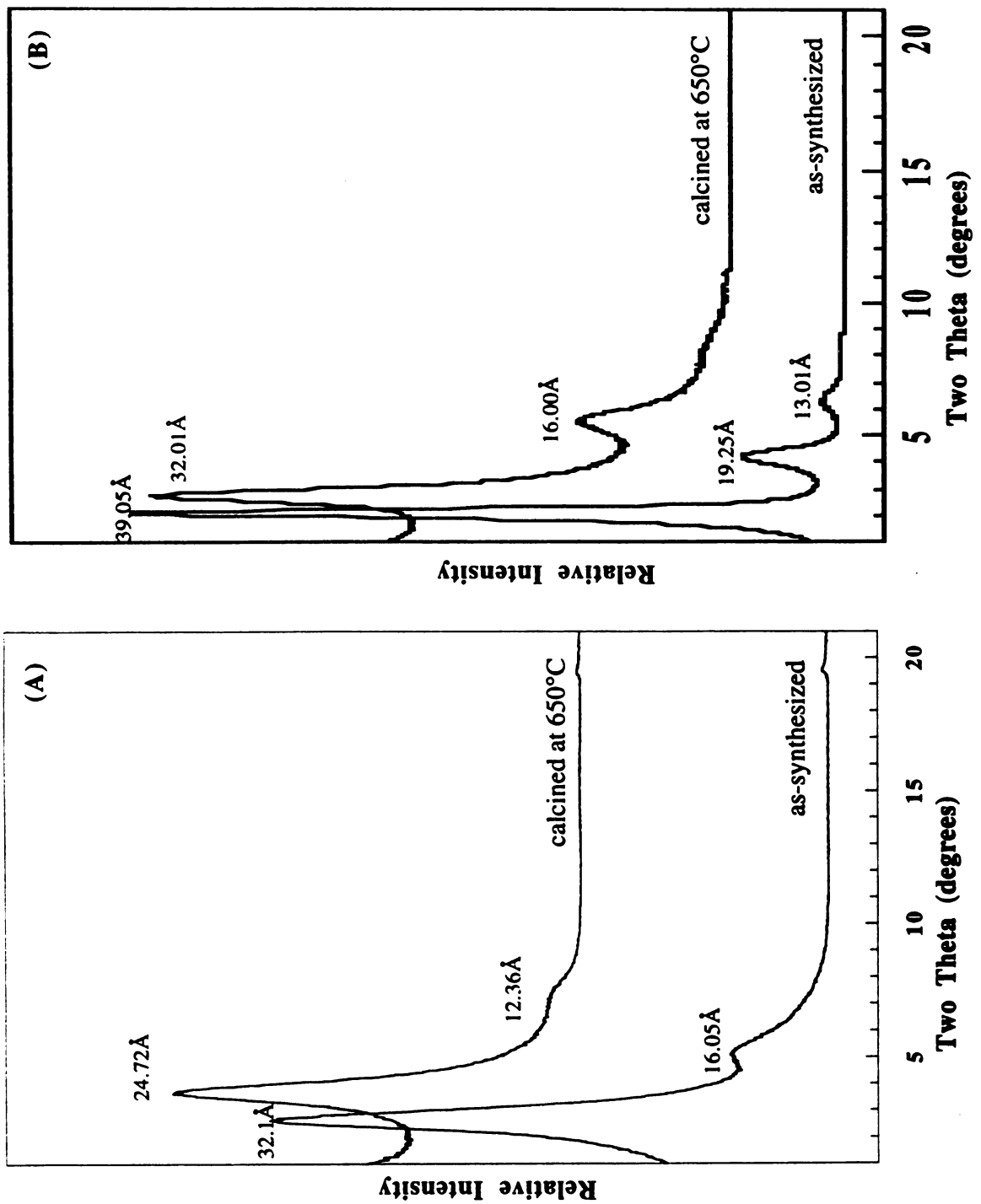

Figure III.4 : X-ray powder diffraction patterns for air dried PCH formed by reaction (A) decylamine solvated $DTMA^+$-Fluorohectorite with TEOS at $DTMA^+$-Fluorohectorite : decylamine : TEOS molar ratios of 1 : 20 : 150. (B) decylamine solvated $HDTMA^+$-Fluorohectorite with TEOS at $HDTMA^+$-Fluorohectorite : decylamine :TEOS molar ratios of 1:20:150.

Figure III.5 : Nitrogen adsorption/desorption isotherms and the corresponding H & K pore size distribution for porous silica-clay heterostructures (PCHs) prepared by gallery-templated synthesis using (a) hexylamine, (b) decylamine, & (c) dodecylamine as co-templates. The $HDTMA^+$-clay : amine : TEOS reaction stoichiometry was 1 : 20 : 150. Relative pressure is P/P_O, where P is the equilibrium pressure of the adsorbate and P_O is the saturation pressure of the adsorbate at the temperature of the adsorbent; the volume adsorbed is at STP. ***Insert*** **:** The corresponding Horvath-Kawazoe pore size distribution curves. (dW/dR is the derivative of t he normalized adsorbate (nitrogen) volume adsorbed with respect to the pore diameter of the adsorbent). Before measurement each sample was heated overnight at 150°C and 10^{-6} torr. The isotherms were measured at -196°C on a Coulter Omnisorp 360CX Sorptometer using standard continuous adsorption procedures.

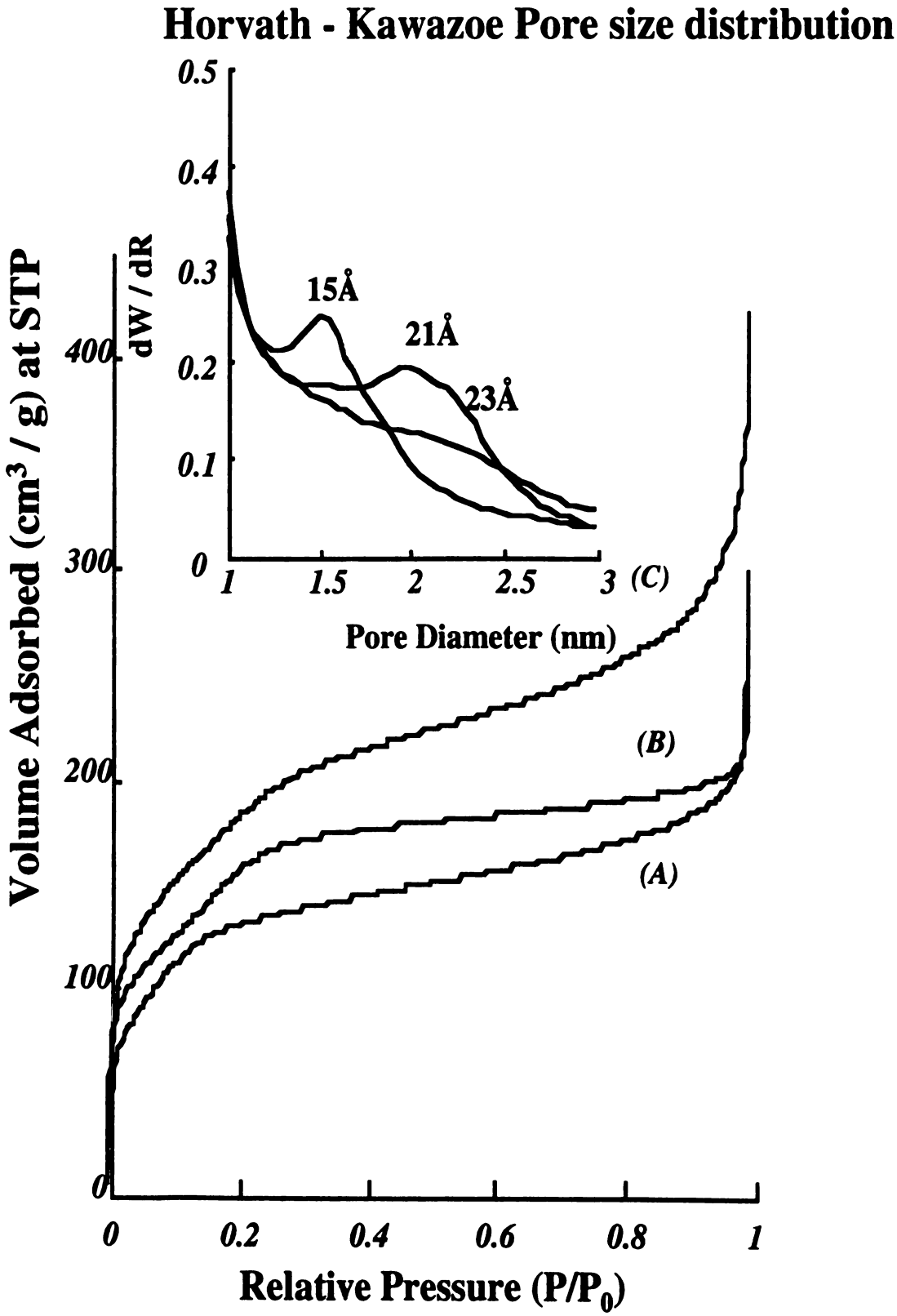
Horvath - Kawazoe Pore size distribution
Volume Adsorbed (cm³ / g) at STP
Relative Pressure (P/P0)
dW / dR
Pore Diameter (nm)
15Å
21Å
23Å
(A)
(B)
(C)
0
100
200
300
400
0.2
0.4
0.6
0.8
1
0.1
0.3
0.5
1.5
2
2.5
3

Table III.2 : Pore Sizes and Gallery Heights (Å) of PCHs Prepared by Gallery - Templated Synthesis.

Alkylammonium Exchange Ion, Q^+	Amine Co-template	PCH b Pore Size	Gallery Heights, Å, a.		
			Calcined PCH	Air-dried heterostructure	Amine-Q^+-FH
$C_{16}H_{33}N(CH_3)_3^+$	$C_6H_{13}NH_2$	15	14.9	22.2	32.2(30.5)c
	$C_8H_{17}NH_2$	17	18.4	22.4	34.4(33.0)
	$C_{10}H_{21}NH_2$	21	22.4	28.4	36.4(35.5)
	$C_{12}H_{25}NH_2$	22	23.4	34.4	38.4(38.0)
$C_{10}H_{21}N(CH_3)_3^+$	$C_{10}H_{21}NH_2$	14	14.3	23.9	29.5(29.3)

a- Gallery height is defined as the observed X-ray basal spacing minus the 9.6 Å thickness of the clay layer. b- Pore size obtained by Horvath-Kawazoe analysis of N_2 adsorption data. c- Values in parenthesis are the calculated gallery heights for a lipid-like bilayer of Q^+ and neutral amine based on the following estimates of chain lengths (Å) : $C_{16}H_{33}N(CH_3)_3^+$, 21.5; $C_{10}H_{21}N(CH_3)_3^+$, 15.3; $C_6H_{13}NH_2$, 9.0; $C_8H_{17}NH_2$, 11.5; $C_{10}H_{21}NH_2$, 14.0; $C_{12}H_{25}NH_2$,16.5.

Table III.2 gives the pore sizes of related PCH's prepared from other combinations of quaternary ammonium and neutral amines co-templates. Increasing the chain length of the amine co-template systematically increases the pore size of the PCH. The fact that the Q^+ chain length is an additional important parameter in the templating process is evidenced by the PCH materials prepared with $DTMA^+$ and decylamine as gallery co-templates. Consistent with the gallery-templated pathway, this latter surfactant system affords an average pore size of 14Å, substantially smaller than the 21Å pore size provided by the $HDTMA^+$ and decylamine templates. Included in Table III.2 are the gallery heights for the calcined PCHs, the corresponding air dried PCH precursors and the initial amine solvated organo fluorohectorite.

Besides serving as co-templates in PCH synthesis, alkylamines improve the intragallery hydrolysis-condensation reaction of TEOS through base catalysis and thereby facilitate the formation of PCH. In addition, the alkylamines enhance the crystallinity of the final product.

Figure III.6 A and B illustrates the X-ray powder diffraction patterns of products formed by reaction of $HDTMA^+$-fluorohectorite and TEOS intercalates in the presence and absence of amines. The air dried samples exhibit multiple (001) orders of Bragg's reflections indicating a well-ordered structure along the c axis. However, on calcination at 650°C in air for 4 h, the sample synthesized in the presence of amines showed multiple (00l) reflections, indicating a layered structure with gallery heigths of ~21Å, but the material synthesized in the absence of amine collapsed to a basal spacing of 12.2Å.

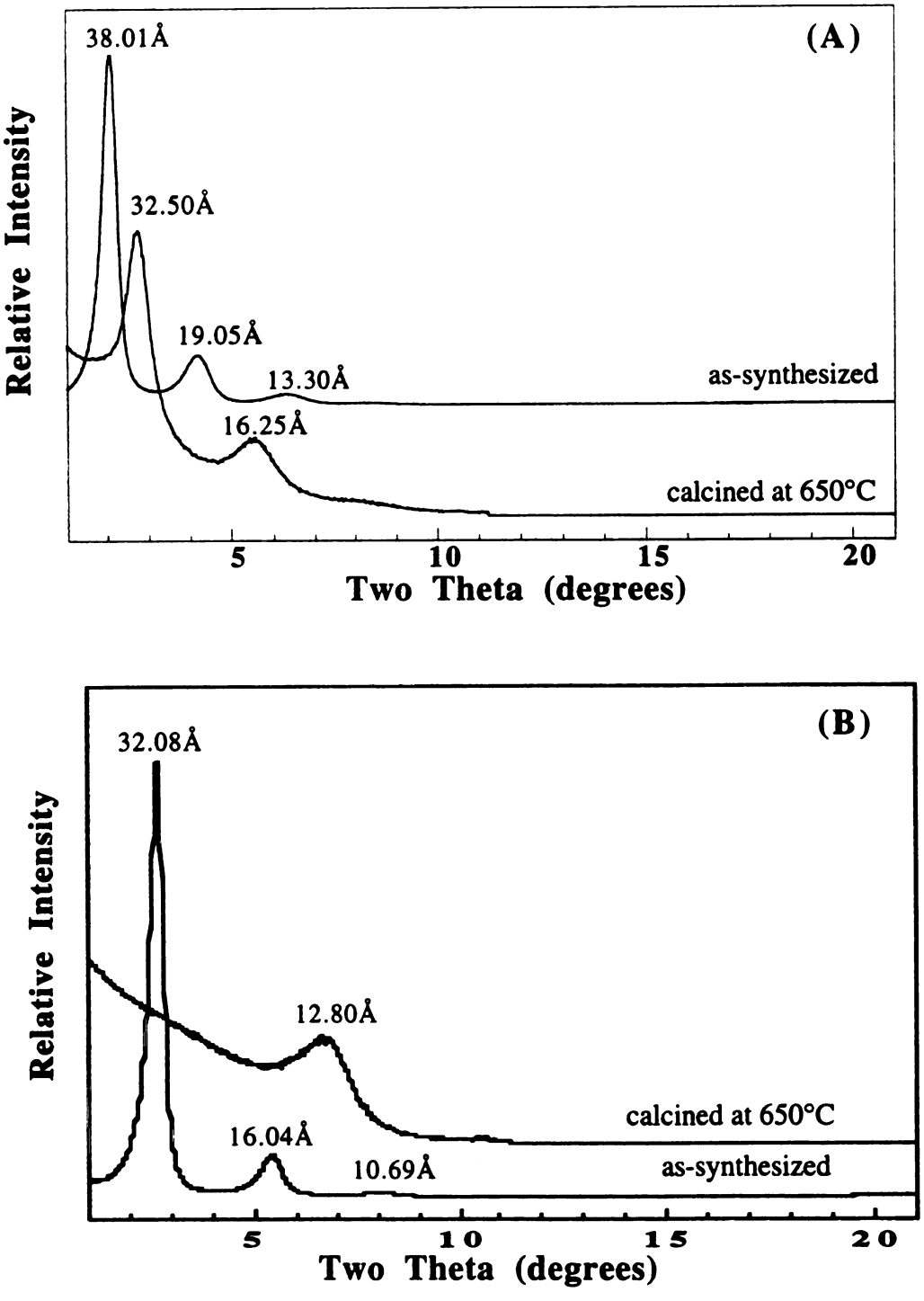

Figure III.6 :(A) XRD pattern of air dried and calcined gallery templated products formed with an amine co-template. (B) XRD pattern of the air dried and calcined silica-pillared products formed in the absence of an amine co-template.

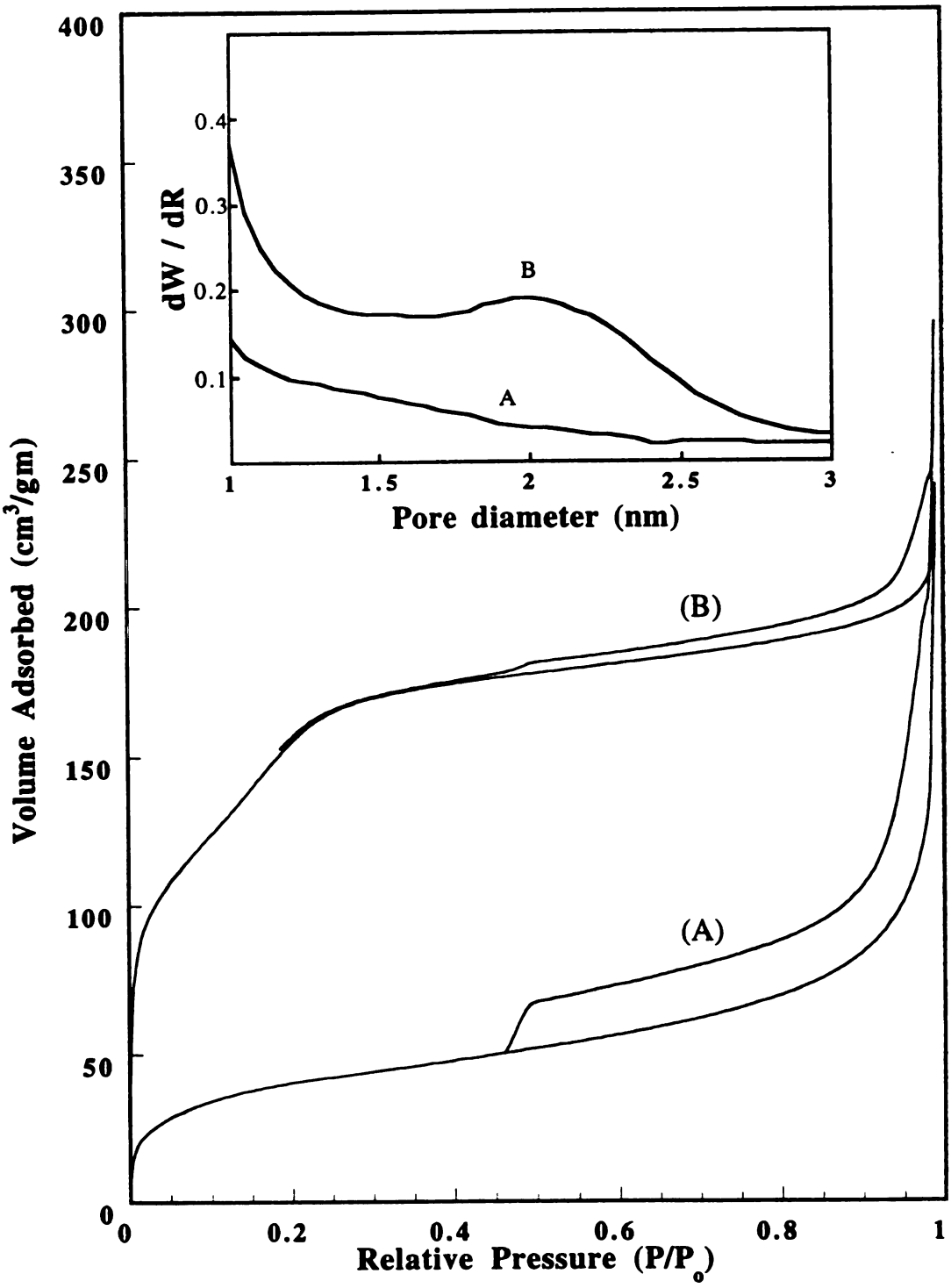

Figure III.7 : (A) Nitrogen adsorption/desorption isotherms and H & K pore size analysis for porous silica-clay heterostructures (PCHs) prepared by gallery-templated synthesis using HDTMA$^+$-Fluorohectorite : decylamine : TEOS with a reaction stoichiometry was 1 : 20 : 150. (B) Nitrogen adsorption/desorption isotherms and H & K pore size analysis for a silica intercalated derivative prepared by using HDTMA$^+$-Fluorohectorite : TEOS with a reaction stoichiometry of 1 : 150.

Figure III.7 A and B illustrate the N_2-adsorption/desorption isotherms for the calcined samples. HDTMA$^+$-Fluorohectorite/TEOS has an isotherm

that lacks the sharp inflection in the low partial pressure region as compared to the one that is synthesized in the presence of amines. As shown in figure III.7 (insert) a Horvath and Kawazoe analysis of the adsorption curves indicates pores around 21Å for the sample synthesized in the presence of amines, while the amine deprived material lacks any useful pore size information.

Effect of surfactant head group size on PCH formation.

Earlier we discussed the effects of templating surfactant chain lengths on the pore sizes of PCHs. We shall now consider the role of the quaternary ammonium surfactant head group size on quantitative PCH formation.

A series of organoclay derivatives containing $C_nH_{2n+1}N(CH_3)_3^+$-Fluorohectorite (denoted as Q_n^+-FH) and $C_nH_{2n+1}NH_3^+$-Fluorohectorite (denoted as P_n^+-FH) were prepared. The difference between the two amphiphiles lies in the effective cross-sectional area of the head groups. The NH_3^+ head group has a cross sectional area of ~10Å^2 and the $N(CH_3)_3^+$ head group has a cross-sectional area of about ~24Å^2.

Mixtures containing Q_n^+-FH : Decylamine : TEOS and P_n^+-FH : Decylamine : TEOS at molar ratio of 1:20:10; 1:20:50; 1:20:100; 1:20:150; and 1:20:200 were stirred for 4 h, centrifuged and air dried. Diffraction patterns for the air dried samples of Q_n^+-FH and P_n^+-FH are similar.

Figure III.1 and III.8 illustrate the X-ray diffraction patterns for Q_n^+-FH and P_n^+-FH surfactant combinations, both as air dried and as calcined products. For the air dried HDTMA$^+$-FH : Decylamine :

Figure III.8 : (a) X-ray diffraction patterns for the air dried products formed by the reaction of decylamine solvated HDA^+-Fluoorhectorite with TEOS at HDA^+-FH : decylamine : TEOS molar ratio of 1 : 20 : X where $10 \leq X \leq 200$.
(b) X-ray diffraction patterns for the calcined material formed by the reaction of decylamine solvated HDA^+-Fluoorhectorite with TEOS at HDA^+-FH : decylamine : TEOS molar ratio of 1 : 20 : X where $10 \leq X \leq 200$.

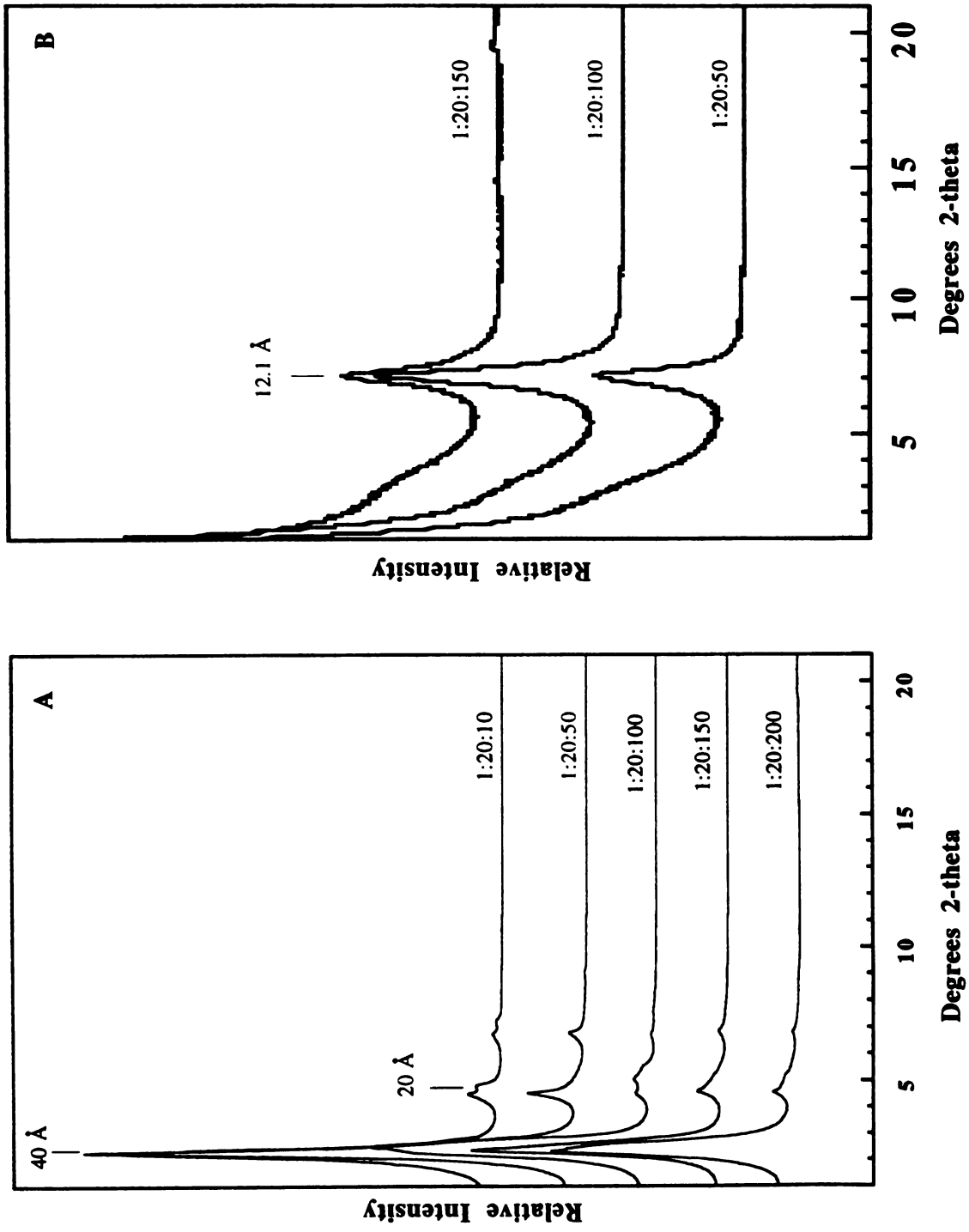
A
40 Å
20 Å
1:20:10
1:20:50
1:20:100
1:20:150
1:20:200
Relative Intensity
5
10
15
20
Degrees 2-theta
B
12.1 Å
1:20:150
1:20:100
1:20:50
Relative Intensity
5
10
15
20
Degrees 2-theta

Table III.3 : Gallery heights of intercalates formed by using a quaternary ammonium cation or a primary ammonium cation as exchanged-cation and decylamine as co-swelling agent at different TEOS/amine molar ratios.

Clay	Exchange cation	Gallery height of air dried sample (Å)	Gallery height of calcined sample (Å)	TEOS : neutral amine *molar ratio*
Fluorohectorite	$DTMA^+$	27.4	2.7	0.5
		24.4	2.7	5.0
		24.4	13.9	7.5
		23.4	14.4	10
	$DDTMA^+$	29.4	2.7	0.5
		26.4	16.4	5.0
		26.4	18	7.5
		26.4	18	10
	$HDTMA^+$	28.4	2.5	0.5
		28.4	20.0	5.0
		28.4	21.0	7.5
		28.4	21.4	10
Fluorohectorite	DA^+	27.4	3	0.5
		24.4	3	5.0
		24.4	3	7.5
		23.4	3.4	10
	DDA^+	29.4	2.8	0.5
		26.4	2.8	5.0
		26.4	2.8	7.5
		26.0	2.9	10
	HDA^+	30.4	2.5	0.5
		27.4	2.5	5.0
		26.4	2.5	7.5
		26.4	2.5	10

*Gallery height = basal spacing - layer thickness of clay (9.6 Å) $DTMA^+ = C_{10}H_{21}N^+(CH_3)_3$, $DDTMA^+ = C_{12}H_{25}N^+(CH_3)_3$, $HDTMA^+ = C_{16}H_{33}N^+(CH_3)_3$, $DA^+ = C_{10}H_{21}NH_3^+$, $DDA^+ = C_{12}H_{25}NH_3^+$, $HDA^+ = C_{16}H_{33}NH_3^+$.

TEOS system, the gallery height remains fixed at 28Å for all reaction stoichiometries. This gallery height is suggestive of a lipid like structure which consists of a single hexadecyltrimethylammonium and neutral decylamine surfactant molecule (see figure II.7). For the air dried HDA^+-FH : Decylamine : TEOS, the XRD data suggests a similar orientation of the hexadecylammonium and decylamine molecules. At the shorter surfactant chain systems a similar correlation in gallery heights between Q_n^+ and P_n^+ is observed.

On calcination of the samples at 650°C for 4h in air, the $HDTMA^+$-FH : decylamine : TEOS system with molar ratios of 1 : 20 : 10 and 1 : 20 : 50 both show diffraction patterns due to the formation of two phases, namely the surfactant templated PCH with a 21Å gallery height and a silica intercalated derivative with a basal spacing of 12.6Å. Increasing the TEOS molar ratio in the synthesis favors the formation of surfactant templated PCH derivative. It can be concluded that PCH formation is not quantitative unless the TEOS : amine ratio is > 7.5

When the P_n^+-FH surfactant is used, the diffraction patterns of all calcined materials consist of a predominantly silica-intercalated derivative with a basal spacing of 12.6Å, which leads to the conclusion that the primary ammonium / neutral amine template combination does not form a gallery nanostructure.

Table III.3 lists the gallery heights of related materials prepared using other combination of Q_n^+ and P_n^+ surfactants.

On performing solvent extraction of the samples by using ethanol as a solvent the role of the quaternary ammonium surfactant head group size on PCH formation becomes crystal clear.

Figure III.9 and III.10 illustrates the X-ray diffraction patterns for

the $DTMA^+$-FH : decylamine : TEOS and DA^+-FH : decylamine : TEOS respectively. It is observed that for the air dried sample prior to any solvent extraction, the diffraction patterns exhibit nearly similar gallery height and multiple (00l) reflections, indicating a layered structure. However upon ethanol extraction of the samples interesting changes are observed. The diffraction pattern for the DA^+-FH : decylamine : TEOS indicates major structural changes, the basal spacing reduces to ~18Å from the initial value of ~33Å and thermogravimetric programmed analysis curve (see figures III.9 &10) showed a single step weight loss between 100°C to 450°C, a weight loss of ~20% was registered due to the thermal decomposition of the organic template. Elemental analysis of the sample showed ~0.8 decylamine per O_{20} F_4 unit cell and ~1.2 mol silica per O_{20} F_4 unit cell. These results along with a sharp decrease in gallery height clearly show the absence of any silica templated nanostructure before calcination. In $DTMA^+$-FH : decylamine : TEOS the gallery height reduces by ~9Å after solvent extraction and thermogravimetric programmed analysis curve (see fig) exhibited a two step weight loss between 100°c to 450°C, the initial step is due to thermal decomposition of the neutral amine co-template, and the second weight loss at a slightly higher temperature is due to the decomposition of the quaternary ammonium surfactants. Elemental analysis of the sample shows ~1.2 decylamine per O_{20} F_4 unit cell and ~7.1 mol of silica per O_{20} F_4 unit cell. These results along with a gallery height of ~15Å after solvent washing clearly indicate the formation of a silica templated nanostructure prior to any thermal treatment and are in agreement with the previous X-ray diffraction data, suggesting a critical structure directing

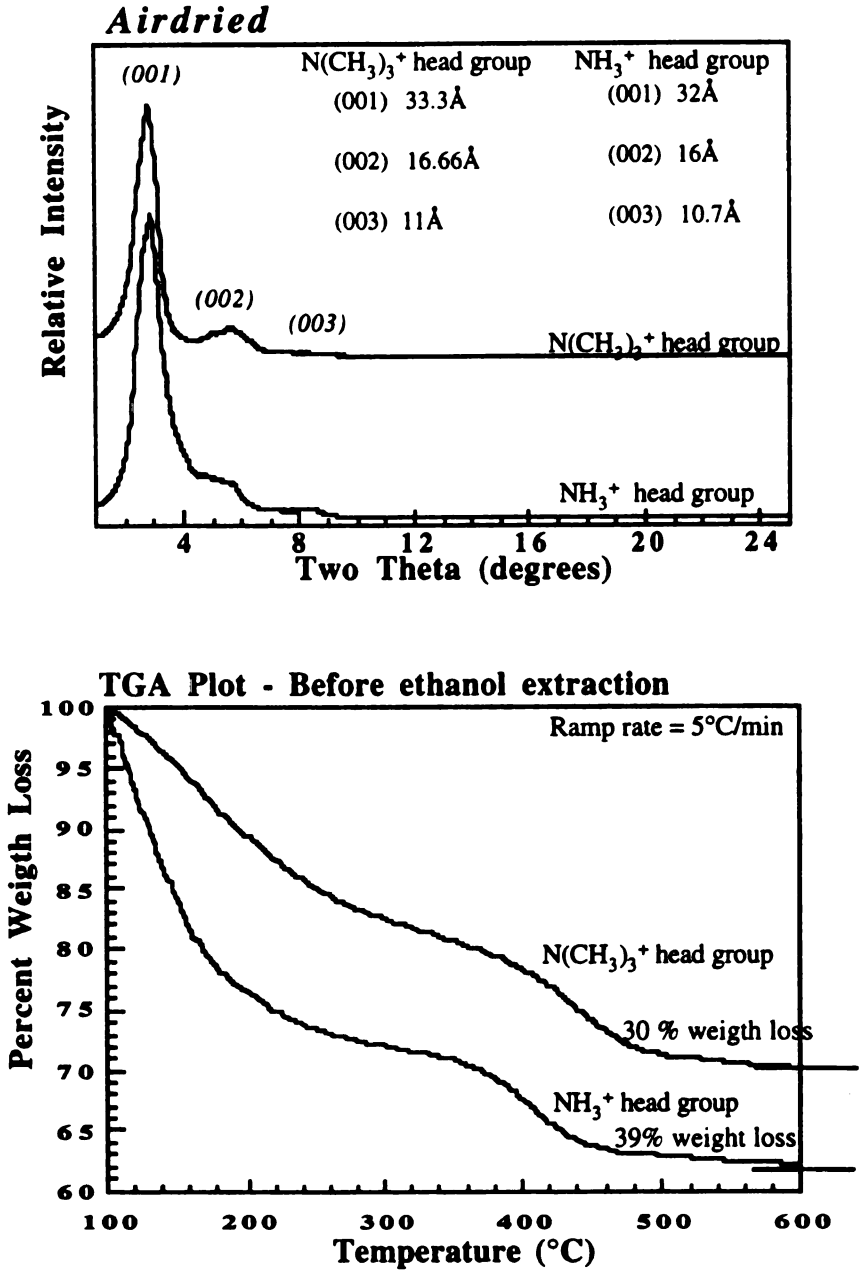

Figure III.9 : (A) X-ray diffraction patterns prior to template extraction Q^+-FH : decylamine : TEOS at a molar ratio of 1: 20 : 150, ($DTMA^+$ as Q^+ ion) and P^+-FH : decylamine : TEOS at a molar ratio of 1: 20 : 150, (DA^+ as P^+ ion). (B) Thermal gravimetric analysis of decylamine solvated n-decylammonium-Fluorohectorite.(P_n^+-FH system) and PCH prepared from decylamine-solvated $DTMA^+$-Fluorohectorite.(Q_n^+-FH system).

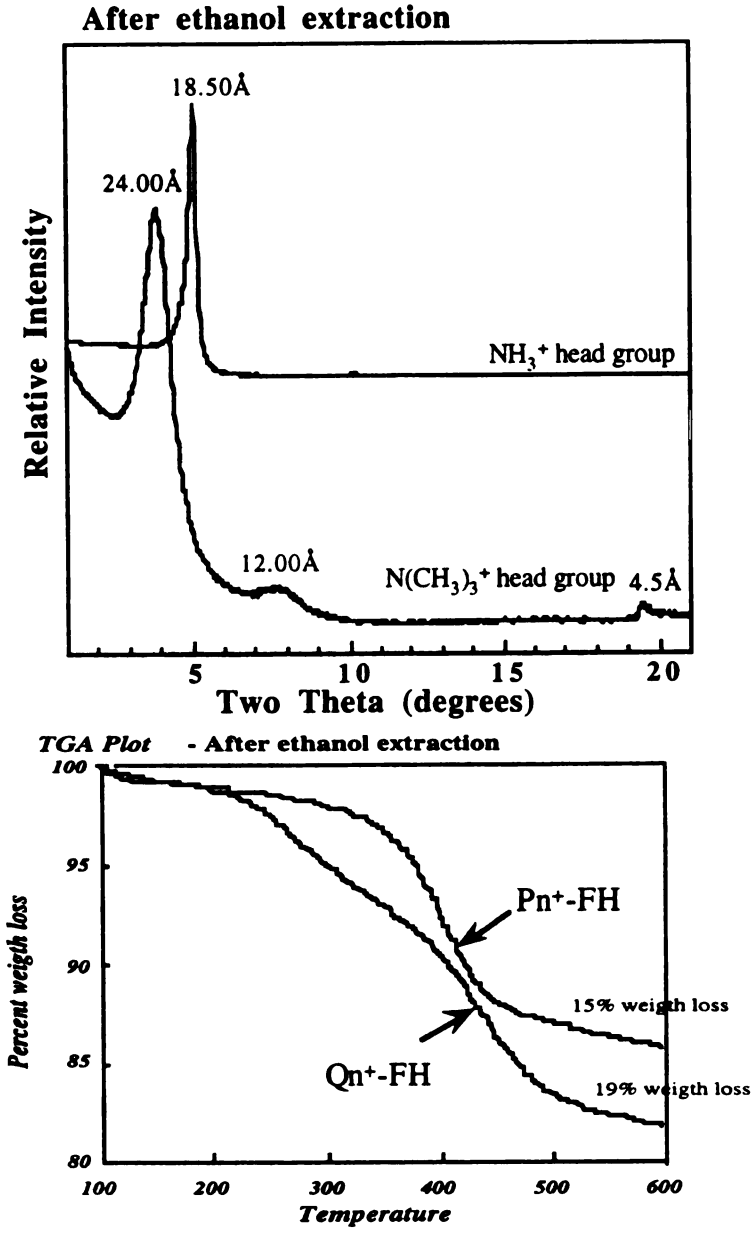

Figure III.10 : (A) X-ray diffraction patterns after template extraction of Q^+-FH : decylamine : TEOS at a molar ratio of 1: 20 : 150, and $DTMA^+$ as Q^+ ion and P^+-FH : decylamine : TEOS at a molar ratio of 1: 20 : 150, and DA^+ as P^+ ion. (B) Thermal gravimetric analysis of decylamine solvated n-decylammonium-Fluorohectorite.(P_n^+-FH system) and PCH prepared from decylamine-solvated $DTMA^+$-Fluorohectorite.

role of the quaternary ammonium surfactant primarily due to the larger head group size.

Surface area measurements and pore structure analysis on calcined samples were performed to further elaborate the differences between the two surfactant system.

Figure III.11 illustrates the N_2 adsorption/desorption isotherms for the Q_n^+-FH : decylamine : TEOS surfactant system. The presence of the linear portion in the low P/P_0 region is suggestive of the presence of pores between (~14-25Å); which is a characteristic feature for all PCH materials. Figure III.11 A & B (insert) shows the H and K analysis of the adsorption data which gives average pore size ~15Å and 21Å for the $DTMA^+$/decylamine and $HDTMA^+$/decylamine templates respectively. Nitrogen BET surface areas were in the range of 470-750m^2/g for two different surfactant chain lengths.

Figure III.12 A and B illustrate the N_2 adsorption isotherms for P_n^+-FH : decylamine : TEOS system. The adsorption curves illustrates virtually non-porosity in the low partial pressure region and hence lack the charateristic feature of a nanoporous adsorbent. Figure III.12 (insert) shows the H-K pore analysis of the adsorption curve. The differential of the N_2 adsorbed with respect to the pore diameter of the adsorbent clearly lacks any useful pore size evaluation.

Table III.4 illustrates the BET surface area, H-K pore size and t-plot analyses of related samples prepared by using other combinations of Q_n^+ and P_n^+ surfactants.

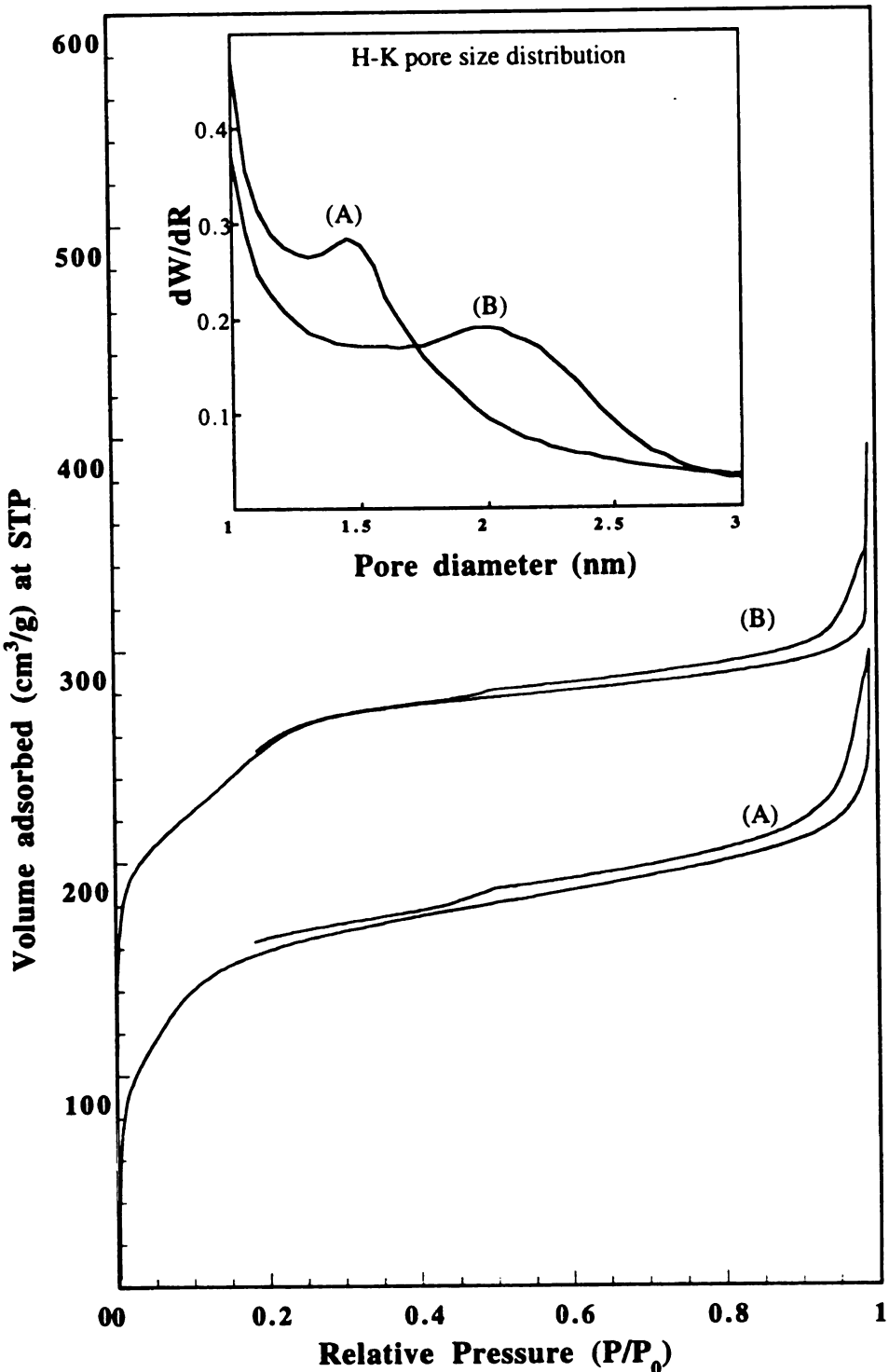

Figure III.11 : Nitrogen adsorption/desorption isotherms and H-K pore size analysis for porous silica-clay heterostructures (PCHs) preparedby gallery-templated synthesis using (A) $HDTMA^+$-fluorohectorite : decylamine : TEOS with a reaction stoichiometry was 1 : 20 : 150, respectively. (B) $DTMA^+$-fluorohectorite : decylamine : TEOS with a reaction stoichiometry of 1 : 20 : 150, respectively.

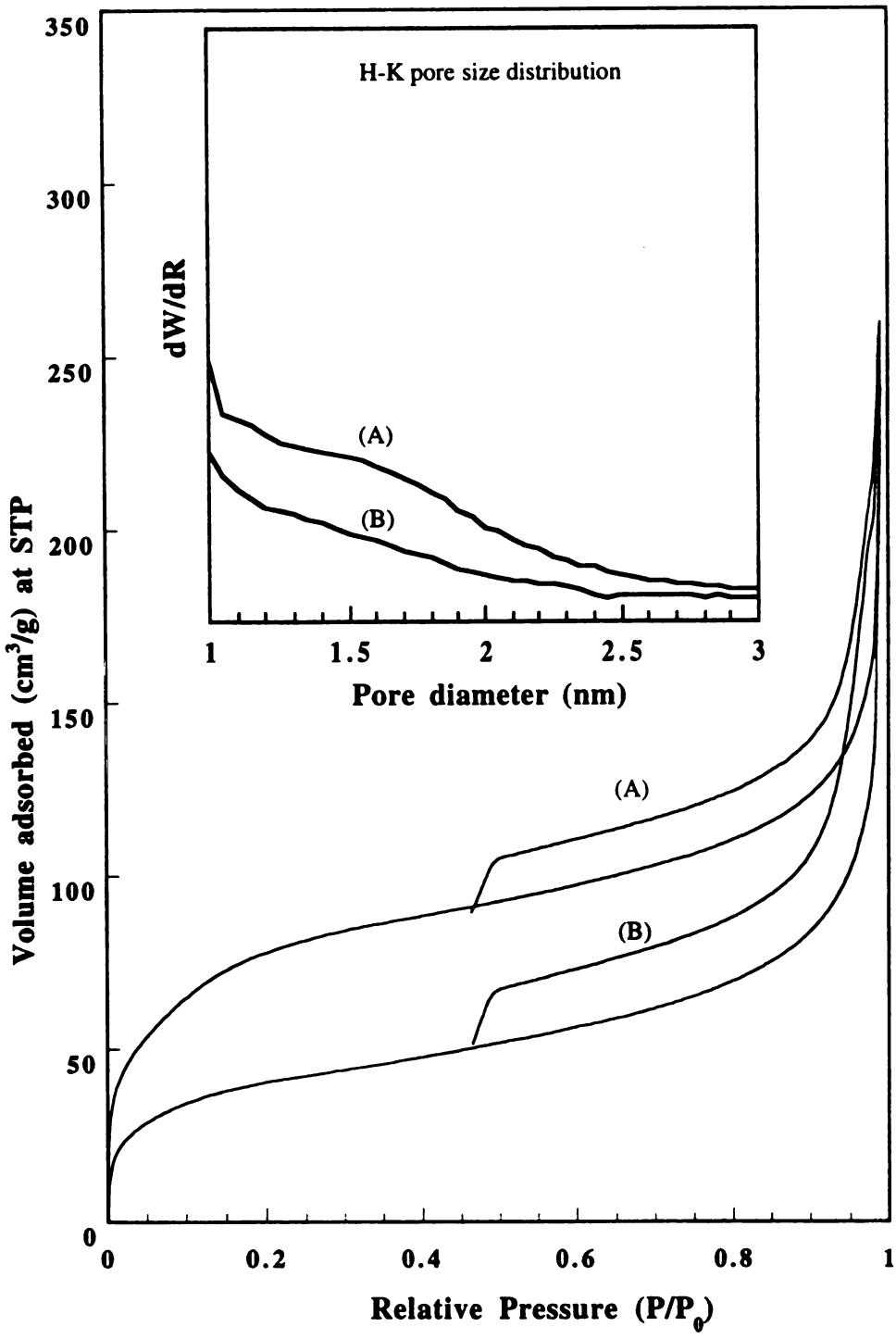

Figure III.12 : Nitrogen adsorption/desorption isotherms and H-K pore size analysis for

(A) HDA^+-fluorohectorite : decylamine : TEOS with a reaction stoichiometry was 1 : 20 : 150 respectively.

(B) DA^+-fluorohectorite : decylamine : TEOS with a reaction stoichiometry of 1 : 20 : 150 respectively.

Table III.4 : Horvath and Kawazoe (H-K) pore size, BET surface area, and t-plot analysis of materials prepared using quaternary Q_n^+ and primary P_n^+ ammonium as exchanged-cation in fluorohectorite with decylamine as co-solvent. Molar ratio of Q_n^+ or P_n^+-FH : decylamine : TEOS of 1 : 20 : 150; and materials were calcined at 650°C.

Ammonium	H&K pore size (Å)	BET surface area (m^2/g)	t-plot analyses S_T	S_μ (m^2/g)	$S_{non\text{-}\mu}$
$DTMA^+$	14	560	620	520	100
DA^+	<9	280	280	170	90
$DDTMA^+$	17	660			
DDA^+	<9	330	350	220	130
$HDTMA^+$	21	800	760	690	70
HDA^+	<9	150	150	80	70

$DTMA^+ = C_{10}H_{21}N^+(CH_3)_3$, $DDTMA^+ = C_{12}H_{25}N^+(CH_3)_3$, $HDTMA^+ = C_{16}H_{33}N^+(CH_3)_3$, $DA^+ = C_{10}H_{21}NH_3^+$, $DDA^+ = C_{12}H_{25}NH_3^+$, $HDA^+ = C_{16}H_{33}NH_3^+$.

To further emphasize the effect of the quaternary ammonium surfactants head group size on PCH formation, we carried out reactions with intercalated cations of larger head group cross-sectional areas. With $P(C_4H_9)_3^+$ replacing the $N(CH_3)_3^+$, the difference in the effective cross-sectional area is ~80Å^2. When we used the larger head groups such as the $HDTBP^+$ ion (Hexadecyltributylphosphonium), no intra-gallery assembly process occurs, as a result of which there is no gallery nanostructure

formation. Both X-ray diffraction data and surface area measurements confirm this observation. Furthermore if long chain dialkyl quaternary ammonium intercalated ions are used, no PCH formation is observed

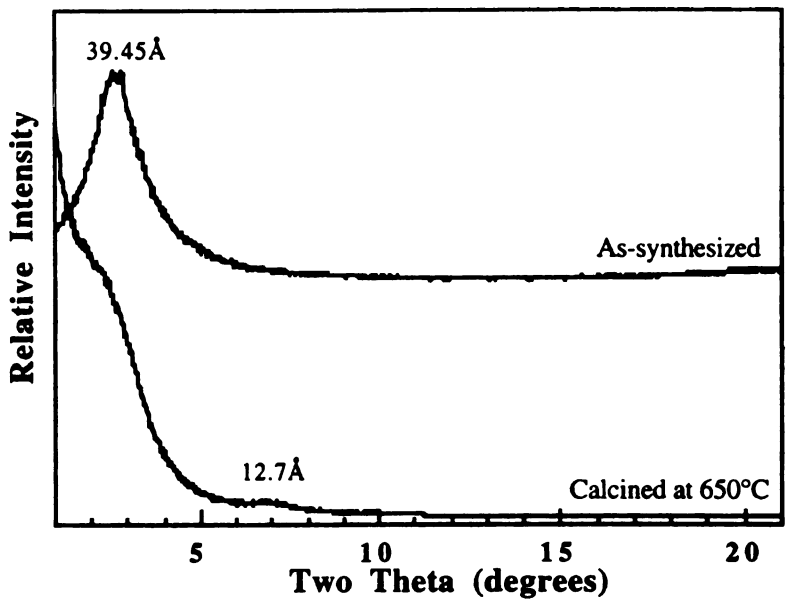

Figure III.13 : (A)X-ray powder diffraction patterns for air dried PCH formed by reaction of decylamine solvated DODDMA$^+$-Fluorohectorite with TEOS at DODDMA$^+$-Fluorohectorite : decylamine : TEOS molar ratios of 1 : 20 : 150. (B) X-ray powder diffraction patterns of air dried (PCH) obtained by calcination at 650°C for 4 h.

Figure III.13 illustrates the X-ray powder diffraction patterns for

the as-synthesized and calcined DODDMA$^+$-fluorohectorite : decylamine : TEOS , with 1 : 20 : 150 molar ratios, respectively (DODDMA$^+$→ Dioctadecyldimethylammonium). The air dried sample shows a substantial amount of gallery height indicating lipid-like structure formation of the surfactants within the galleries. However, on calcination of the as-synthesized sample at 650°C for 4 h, a collapsed silica-intercalated derivative with a basal spacing of ~12.7Å results. This observation clearly show that the packing density of the organic templates is crucial for the successful formation of porous clay heterostructures. It just works out that the monoalkyl long chain quaternary ammonium ion along with the neutral amine, co-surfactants in conjunction with the neutral silicate species allows for the formation of intra-gallery micellar units. N_2-Adsorption-desorption measurements of the calcined sample confirm the presence of a collapsed structure, with a BET surface area of ~150 m^2/gm.

Unfortunately attempts at PCH formation in magadiite by using long chain quaternary ammonium surfactants and neutral amines as co-surfactants failed; no intra-gallery templated products formed. However when the monoalkyl quaternary ammonium exchanged were replaced by dialkyl long chain quaternary ammonium exchanged ions and neutral amines were used as co-templates, gallery structure was observed after calcination.

Figure III.14 illustrates the X-ray diffraction powder patterns for as-synthesized, ethanol extracted, ion-exchanged and air dried, calcined DDDMA$^+$-magadiite : decylamine : TEOS, with a reaction molar ratio of 1 : 20 : 150, respectively (DDDMA$^+$→ Didecyldimethylammonium ion) The as-synthesized sample shows a gallery height of ~21Å. Calcination of the sample to 500°C in air for 4 h, yielded no reduction in gallery height.

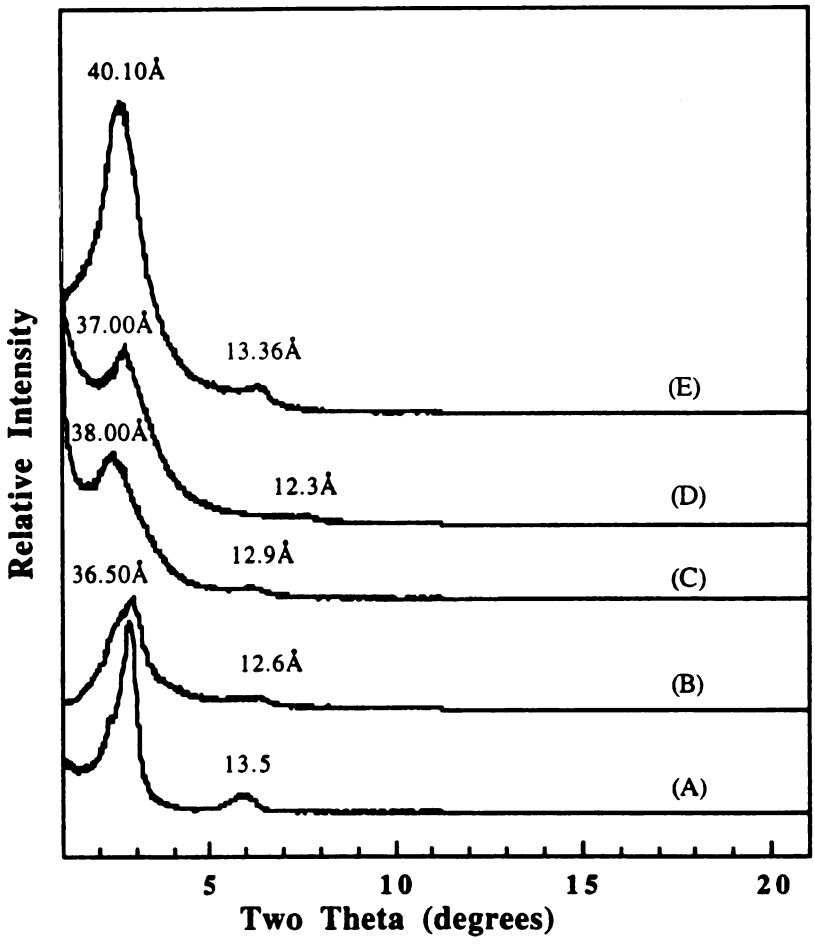

Figure III.14 : X-ray diffraction powder patterns for DDDMa+-magadiite : decylamine : TEOS, with a molar ratio of 1 : 20 : 150, respectively. (A) $DDDMA^+$-magadiite, (B) As-synthesized, (C) Ethanol-extracted, (D) As-synthesized, calcined at 650°C, (E) Ethanol-extracted, ion-exchanged.

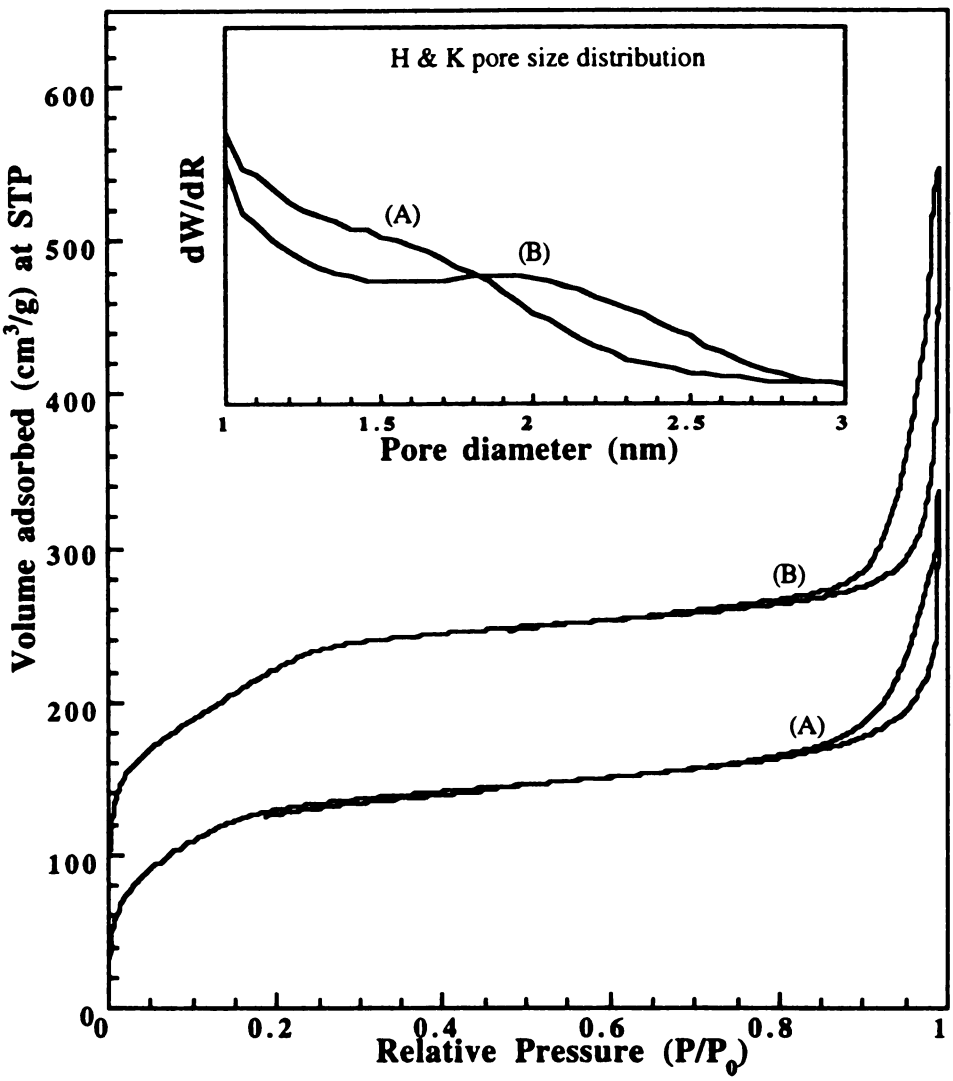

Figure III.15 : N_2 adsorption/desorption isotherms and the corresponding H-K pore size distributionfor (a) As-synthesized, calcined, (b) Ethanol-extracted, ion-exchanged material.

Ethanol extraction of the as-synthesized sample shows an increase in gallery height from ~21Å to 26Å. Ion exchange with 0.12N HCl solution for 24 h results in the complete removal of the template and shows a gallery height of ~22Å. That the template was removed completely was checked by thermogravimetric analysis of the ion-exchanged sample.

Figure III.15 illustrates the N_2 adsorption-desorption isotherms and the corresponding H-K pore size distributions for the as-synthesized, calcined and the template extracted, ion-exchanged samples. The adsorption isotherms for both samples show a small step in the low partial pressure region between 0.02 to 0.25 P/P_0, indicating the presence of gallery nanopores; however the H-K pore size distribution curve show maxima at different pore diameters. For the as-synthesized, calcined material the average pore size was ~17Å, whereas for the ethanol extracted and ion exchanged material the average pore size was ~21Å. These results are in agreement with the X-ray diffraction data. The BET surface areas for both materials were ~450 m^2/gm.

Use of larger head group intercalated ions such as $P(C_4H_9)_3^+$ instead of $N(CH_3)_3^+$ in magadiite did not negatively affect gallery nanostructure formation. Figure III.16 shows X-ray diffraction patterns for the as-synthesized, ethanol extracted, ion-exchanged, and air dried,calcined $HDTBP^+$-magadiite : decylamine : TEOS mixtures with 1 : 20 : 150 molar ratio, respectively ($HDTBP^+ \rightarrow$ Hexadecyltributylphosphonium ion). The as-synthesized sample shows a gallery height of ~25Å. On calcination of the sample to 500°C in air for 4 h, a gallery height of ~26Å was obtained. Ethanol extraction of the as-synthesized material yields a gallery height of ~27Å. Ion-exchange with 0.12N HCl solution results in complete removal of the template and a gallery height of ~29Å is obtained.

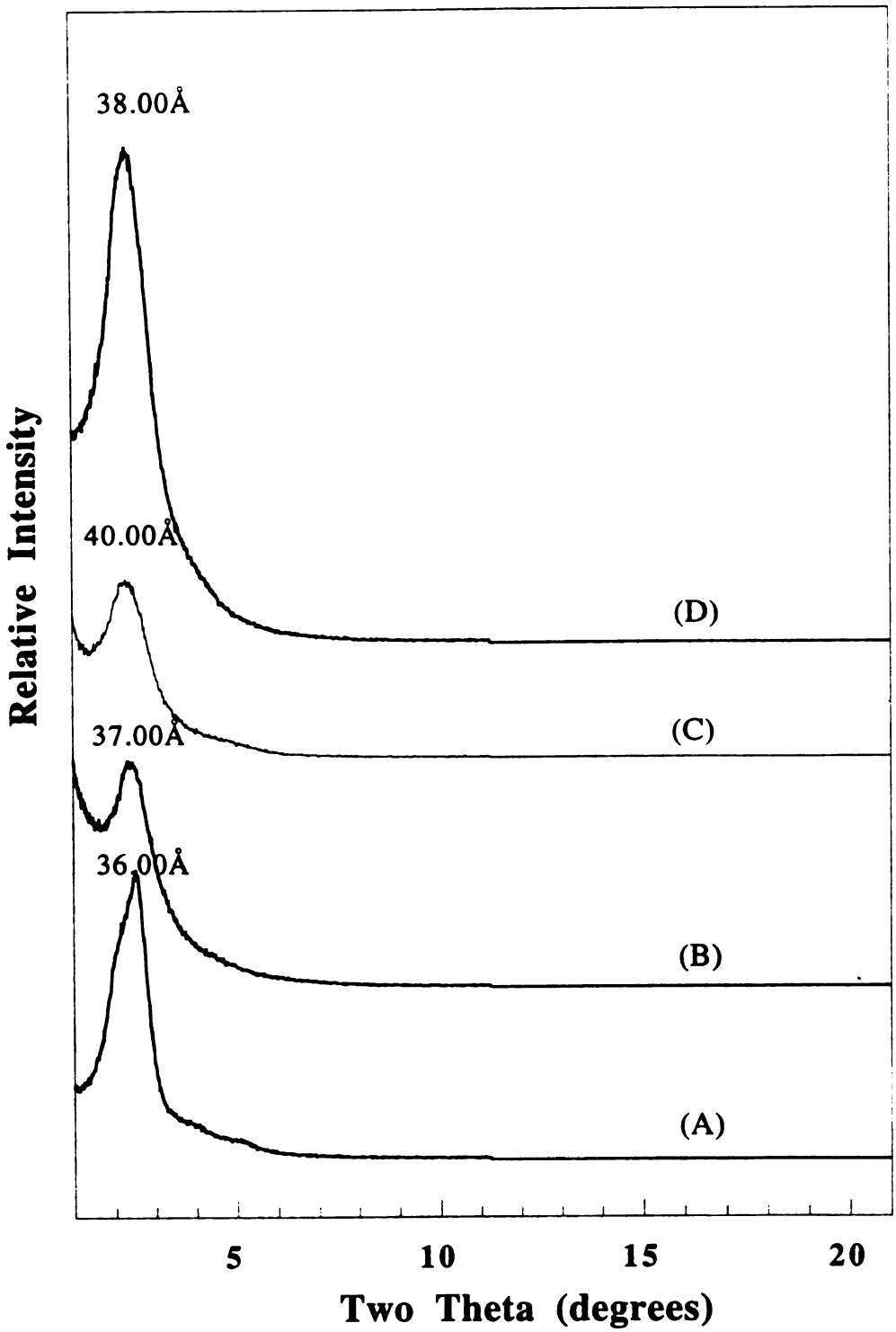

Figure III.16 : X-ray diffraction powder patterns for $HDTBP^+$-magadiite : decylamine : TEOS mixture with 1 : 20 : 150 molar ratio, respectively. (A) As-synthesized, (B) As-synthesized, calcined at 650°C, (C) Ethanol-extracted, ion-exchanged, (D) Ethanol-extracted.

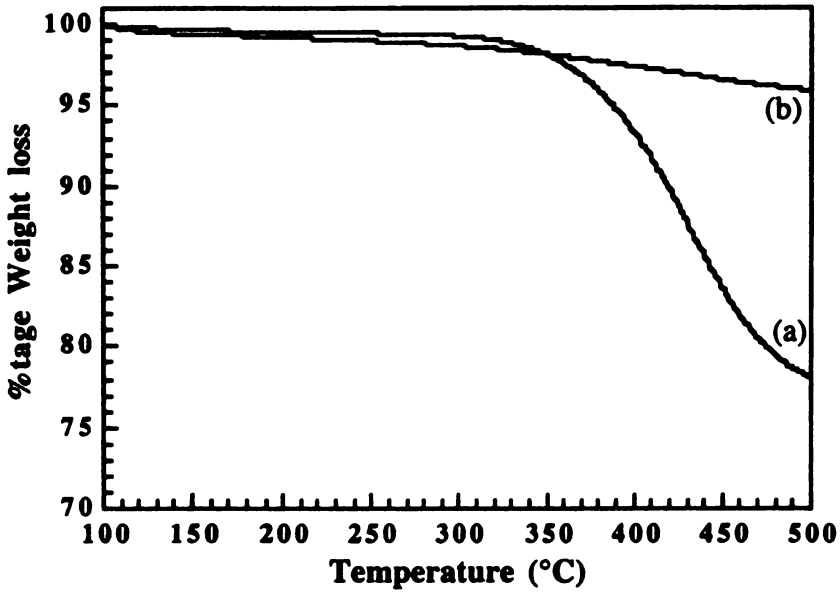

Figure III.17 : Thermogravimetric plot of (a) HDTBP+-magadiite (b) Ethanol-extracted, ion-exchanged HDTBP+-magadiite : decylamine : TEOS mixture.

Thermogravimetric analysis of the HDTBP+-magadiite and the HDTBP+-magadiite/decylamine/TEOS ethanol-extracted, ion-exchanged material is shown in Figure III.17. It is observed that the weight loss curve for the HDTBP+-magadiite shows beyond 100°C, a single step at around 380°C, which is due to the decomposition of the HDTBP+ ions. In the ethanol extracted and ion-exchanged material a total weight loss of < 3% beyond 100°C is observed which clearly indicates the complete removal of the organic templates from the structure. N_2 adsorption-desorption measurements were performed on the as-synthesized, calcined and

completely template-removed but not calcinated materials.

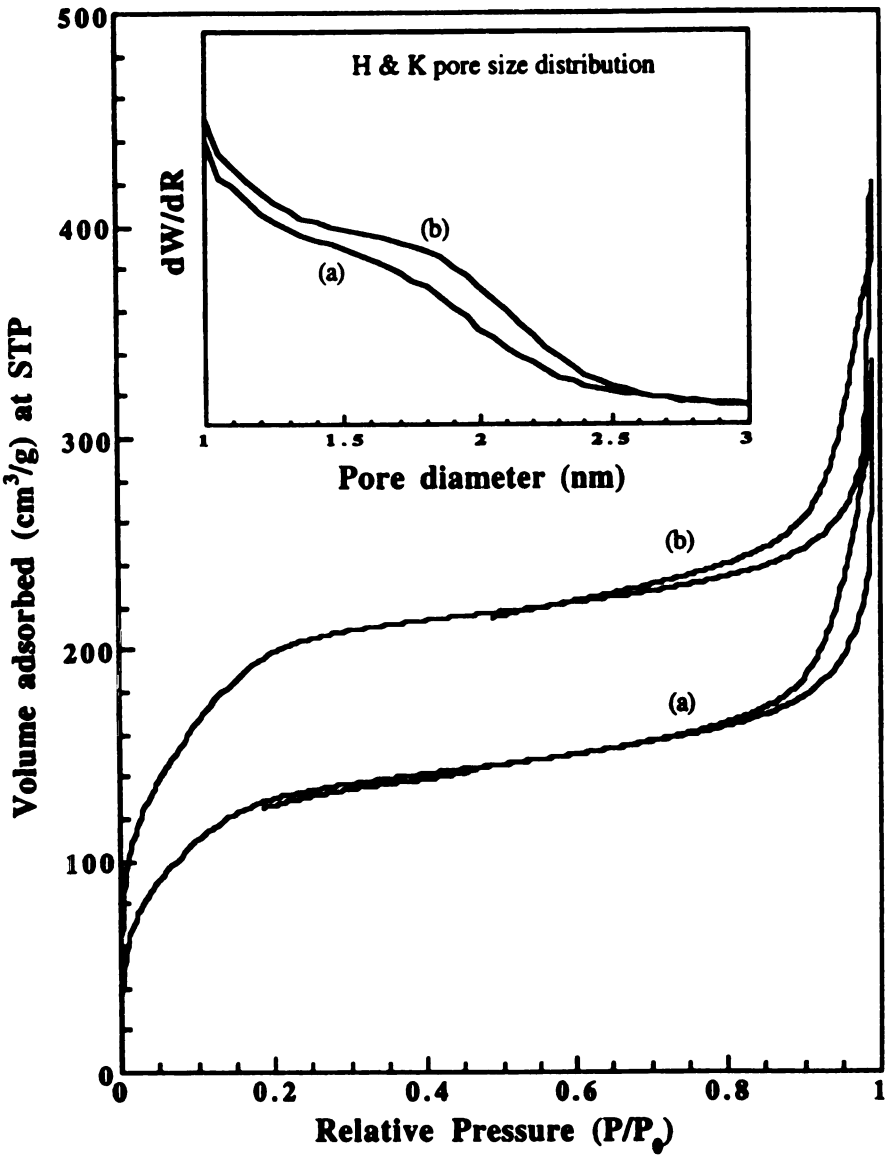

Figure III.18 : N_2 adsorption/desorption isotherms and the corresponding H-K pore size distribution for $HDTBP^+$-magadiite : decylamine : TEOS mixture at 1 : 20 :150 molar ratio. (A) as-synthesized, calcined (B) Ethanol-extracted, ion-exchanged.

Figure III.18 illustrates the N_2 adsorption-desorption isotherms and the corresponding H-K pore size distribution for the as-synthesized, calcined and completely template removed materials. The adsorption isotherm for both materials shows the presence of a small step in the low P/P_0 region, indicating the presence of nanopores; however a BET surface area of ~600 m^2/g was obtained for the templated extracted materials and the as-synthesized, calcined sample gave a BET surface area of ~530 m^2/g. H-K pore analysis shows a similar pore size is present in both samples.

Thus, these few preliminary intra-gallery reactions in magadiite suggest that the surface OH groups have an effect on the rate of hydrolysis and condensation of the silicate species, and also suggest that the optimum surfactant packing requirements are different from those of the corresponding smectite clay PCH formations.

Furthermore, earlier studies have reported the intragallery hydrolysis of TEOS for primary alkylammonium exchanged forms of magadiites in both the presence and absence of primary amines. However, these silica intercalated magadiites have been described as pillared structures. For instance, octylamine solvated octylammonium magadiite as a reaction precursor affords silica intercalates with 9-15Å gallery heights depending on the magadiite : TEOS ratio. The average pore size of these derivatives (~6Å) is substantially smaller than the gallery heights, a feature characteristic of metal oxide pillared clays. Also, the observed pore size is smaller than expected (~12Å) for a micelle-templated nanostructure. The amine solvated galleries of primary ammonium-ion exchanged forms of magadiite are thus accessible to TEOS for microporous pillaring, but not for nanoporous templating.

Gallery templated synthesis of PCH materials is not limited to

fluorohectorite. We have also prepared PCH derivatives of vermiculite and rectorite by gallery templated TEOS hydrolysis in the presence of quaternary ammonium surfactants with neutral amines as co-surfactants. Each of these PCH derivatives had an average pore size equal (within experimental uncertainity) to the pore size observed for the corresponding fluorohectorite system. These results further support intragallery templating and unequivocally rule out pillaring. If the intra-gallery hydrolysis of TEOS simply involved the formation of dense silica pillars between the quaternary ions; the pore size should decrease with increasing charge density on the host layers. For the layered hosts investigated in the present work, the layer charge per 100Å^2 increases in the order rectorite (1.33) < fluorohectorite(2.5) < vermiculite(3.82). Yet the observed pore sizes are invariant over the entire layer-charge range. This result precludes pillaring, but supports templating by micellar units comprised of neutral amines and quaternary ammonium ions in the appropriate layer charge-compensating ratio.

Mechanistic considerations.

As outlined in figure III.19, we propose that PCH pore structures are determined solely by intrinsic structure-directing interactions between the intra-gallery sufactants and the inorganic precursor. The initial amine-solvated organoclay (Q^+-clay) is assigned a lipid-like structure (fig III.19 A). This structure is substantiated by gallery heights that are close to the values expected based on the chain lengths of quaternary ammonium surfactants and the neutral amine (see table III.2). Upon introduction of TEOS, some of the neutral amine is displaced from the galleries and a reactive intermediate is formed (figure 19B). Also the extra-gallery water

concentration is low, as judged by the water content of the amine (~0.4 wt%). Thus, the base-catalysed hydrolysis of TEOS is much faster in the clay galleries than in solution, and this minimizes the formation of extra-gallery silica. Subsequent hydrolysis of the gallery TEOS affords a hydrous silica templated around a monolayer of micellar Q^+ and neutral amine assemblies. Surfactant assemblies formed exclusively from Q^+ or neutral amines are precluded by the fact that both templating components are needed for the formation of a gallery nanostructure. Spherical micelles in van der Waals contact or, more likely (by analogy to the templating of hexagonal mesostructures,such as, MCM-41), rod-like micelles are formed, as shown in cross-section in Figure III.19C. These latter assemblies are structurally analogous to the layered silica-surfactant intercalates that have been postulated to form as intermediates in the synthesis of MCM-41, with the important exception that the layers in the case of PCHs consist of preformed anionic 2:1 layered silicate. The final calcination step (Fig III.19D) removes the template and completes the dehydroxylation and cross-linking of the gallery-assembled silica structure.

Figure III.19 : Proposed mechanism for the formation of a PCH by gallery - templated synthesis: (A) Amine - solvated bilayer structure with a thickness equivalent to the length of the quaternary cation (filled head groups) and the neutral amine (open head groups) surfactants; (B) Intercalation of TEOS by partial displacement of neutral amine ; (C) Templated heterostructure in which a 2D hydrated silica is organized around micellar assemblies of Q^+ and neutral amine; (D) Calcined porous clay heterostructure with a 2D framework of porous silica intercalated between the clay layers.

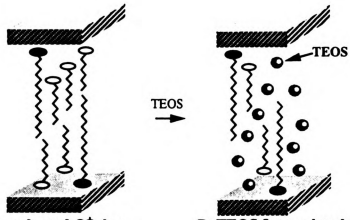

A. Amine-solvated Q^+-clay B. TEOS-Intercalated intermediate

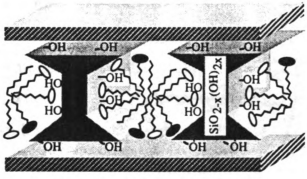

C. Templated Heterostructure

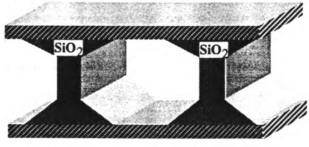

D. Porous Clay Heterostructure

Conclusions.

Porous clay heterostructures are synthesized by using intercalated quaternary ammonium surfactants and neutral amines as co-surfactants to direct the inter-lamellar hydrolysis of a neutral silicate precursor such as TEOS within the galleries of an ionic lamellar solid. The nature and amount of the exchange cation and neutral amine co-template, along with its chain length, are critical to the formation of PCH materials. In fact the relationship between PCH pore size distribution, surfactant chain length and reaction stoichiometry supports a templating mechanism analogous to that of the structure-directed M41S mesostructure synthesis. The fundamental differences between pillaring a layered solid and the gallery templation process are listed below.

(1) A critical value of the molar ratio of amine : TEOS is essential for the formation of a gallery nanostructure in porous clay heterostructure synthesis, whereas in a conventional pillaring process such a dependence on reaction stoichiometry is not critical for the quantitative formation of dense metal oxide aggregates inside the galleries of an ionic lamellar solid.

(2) A conventional pillaring process is characterized by the dependence of the pore size on the total cation exchange capacity of the layered host with an increase in charge density decreasing the pore size of the final pillared solid. However, while in the PCH synthesis the layer charge per 100Å^2 for the host layers investigated increased from 1.33 for rectorite to 3.82 in vermiculite, the observed pore size remained invariant.

(3) The pore size of the calcined PCH does not change when changing the clay : TEOS ratio is changed, suggestive of an intra-gallery templating process, whereas in a pillaring reaction the pore size decreases with an increase in the amount of TEOS in the reaction mixture.

(4) A systematic increase in PCH pore size with an increase in the chain length of the templating surfactants precludes pillaring, but supports templating by micellar units comprised of neutral amines and quaternary ammonium ions in the appropriate layer charge-compensating ratio.

(5) Finally, the head group size of the exchange cation on quantitative PCH formation strongly implies important intra-gallery assembly interactions between the exchange cation, the neutral amine co-template and the inorganic silicate precursor, suggesting a gallery templating reaction.

References :

1. Galarneau, A.; Barodawalla, A.; Pinnavaia, T. J., *Nature*, 374, 529-531, **1995**.
2. Barodawalla, A.; Galarneau, A.; Pinnavaia, T.J.; manuscript in preparation, **1996**.
3. Kresge, C. T.; Leonowicz, M. E.; Roth, W. J.; Vartulli, J. C.; Beck, J. S., *Nature* 359, 710-712 **1992**.
4 Beck, J.S.; Vartulli, J. C.; Roth, W. J.; Leonowicz, M. E.; Kresge, C. T.; Schmitt, K. D.; Chu, C. T-W.; Olson, D. H.; Sheppard, E. W.; McCullen, S. B.; Higgins, J. B.; Schlenker, J. L., *J. Am. chem. Soc.*, 114, 10834-10843 **1992**.
5. Tanev, P. T.; Chibwe, M.; Pinnavaia, T. J., *Nature*, 368, 32221-323, **1994**.
6 Tanev, P. T. and Pinnavaia, T. J., *Science*, 267, 865-867, **1995**.
7. Reddy, M. K., Moudrakovski, I.; Sayari, A. *J. Chem. Soc. Chem. Commun*. 1059-1060, **1994**.
8. Corma, A. , Navarro, M. T.; Pérez Pariente, J. *J. Chem. Soc. Chem. Commun*. 147-148 **1994**.
9. Bein, T. J.; Wu, C.-G. *Science* , 264, 1757-1758 **1994**.
10. Barrer, R. M.; MacLeod, D. M., *Trans. Faraday Soc.*, 51, 1290, **1955**.
11. Lagaly, G. *Solid State Ionics*, 22,43-51, **1986**.
12. Vaia, R. A.; Teukolsky, R. K.; Giannelis, E. P., *Chem. Mater.*, 6, 1017-1022, **1994**.
13. Pinnavaia, T. J., *Science*, 220, 365, **1980**.
14. Clearfield, A.; in M. L. Occeli and H. E. Robinsoon (Eds.),

Expanded Clays and other Microporous Solid. Van Nostrand Reinhold, New York, **1992**, p. 245.

15. U. S. Pat. Nos 4,859,648, *1989.*, 4,728,439, **1988.**, 4,929,587, **1990.**; Can. Pat. No. 1,252,432, **1989**.
16. Landis, M. E.; Aufdembrink, B. A.; Chu, P.; Johnson, I. D.; Kirker, G. W. & Rubin, M. K. *J. Am. Chem. Soc.* , **1991**, *113*, 3189.
17. Dailey, J. S.; Pinnavaia, T. J. *Chem. Mater.*, 4, 855-863, **1992.**
18. Spartan program modelization, Michigan State University, Department of Chemistry.
19. Brunauer, S.; Emmett, P.; Teller, E. *J. Am. Chem. Soc.*, **1938**, 60, 309.
20. Horvath, G.; Kawazoe, K. J. *J. Chem. Eng. Jap.*, **1983**, 16, 470-475.

Chapter IV

Physico-chemical properties of PCH materials.

Abstract

Thermochemical studies were carried out on porous clay heterostructure (PCH) materials that were prepared by using hexadecyltrimethylammonium / decylamine as templates , TEOS as the silica precursor, and fluorohectorite as the layered host. The gallery heights, surface areas, pore structures, and the degree of crosslinking of the gallery silica mesostructures were studied by using X-ray powder diffraction, N_2 adsorption-desorption, ^{29}Si MAS NMR, ^{19}F MAS NMR, TGA, & elemental analysis.

PCH-fluorohectorite prepared by gallery templating gave surface area in the range of 555 - 790 m^2/g and stable pore sizes between 19 to 23Å at temperatures ranging from 200 to 550°C. ^{19}F NMR shows the depletion of the structural fluorine at calcination temperature of around 350°C and ^{29}Si MAS NMR shows evidence for the crosslinking of the gallery silica nanostructure to the clay layers. Partial removal of the template prior to calcination results in decomposition of the gallery nanostructure. PCH-rectorite exhibits hydrothermal stabilities up to 700°C for 2 to 3 hrs, and pyridine chemisorption studies on PCHs shows that silica-interlayered PCHs are intrinsically acidic, whereas pure silica mesostructure possess little or no acidity. In addition metal ion substitution in the gallery framework structure was also attempted and PCH formation using low charge density smectites was attempted.

Introduction.

Because of growing environmental concerns, there is interest in replacing tradition catalysts, such as aluminium trichloride, sulfuric acid and hydrofluoric acid, with recyclable solid catalysts. Pillared interlayered clays (PILC) have been extensively studied and are very attractive as solid acid catalysts[1,2]. These solids exhibit a tunable acidity, regular microporosity and relatively high thermal stability. Montmorillonite, hectorite, beidellite and saponite pillared by Al_{13} hydroxy cations have been the most studied. These materials revealed a substantial activity for petroleum cracking and for fine chemical synthesis via alkylation and isomerization. Recently Butruille *et al.* reported an improvement in the acid catalytic properties of alumina-pillared fluorohectorite[3,4]. The presence of fluorine in the layer structure enhanced the Brönsted acidity of the pillared clay at outgassing temperatures below 350°C. This catalyst exhibited significant Brönsted acidity, which is unusual for smectite clays.

We recently reported a new templating route which allows us to expand the use of lamellar compounds for the design of nanoporous materials. By appropriate choice of a reaction medium and combinations of neutral and ionic co-surfactants, new intercalated structures containing large channels similar to those formed in mesoporous molecular sieves (MCM-41) can be synthesized[5]. We call these materials porous clay heterostructures (PCHs). PCHs provide unique oppurtunities to improve the chemical and physical properties of surface active lamellar structures by enhancing diffusion. Here we report some important thermochemical alterations that occur in PCH-Fluorohectorite, formed with $HDTMA^+$/decylamine as the templating surfactants. Because the pore

structure is confined in a two-dimensional lattice, these new porous clay heterostructures are more stable than large pore molecular sieves such as MCM-41. Hydrothermal studies on PCH-rectorite showed steam stability of the gallery nanostructure for 2 to 3 h, at tempeartures up to 650°C. In addition, pyridine chemisorption properties of PCHs showed that due to the presence of protons which are necessary to balance the clay layer charge. Silica-intercalated PCHs are capable of transferring protons to organic substrates adsorbed in the gallery nanopores thereby making them intrinsically acidic, whereas pure silica mesostructures possess little or no acidity.

Experimental

Materials

Synthetic lithium fluorohectorite (Li-FH) with the chemical composition $Li_{1.12}\{[Li_{1.12}\ Mg_{4.88}](Si_8O_{20})\}F_4.xH_2O$ was obtained as a gift from Dow Corning, Inc.. Li-Fluorohectorite has a 2:1 layered structure consisting of two layers of silica tetrahedra sandwiching a central layer of magnesium octahedra. Lithium ions replace some of the magnesium ions in the octahedral sheet, generating a net negative charge. This charge is then balanced by the Li^+ ions inside the gallery. These latter Li^+ ions are solvated by water and are ion exchangeable, the cation exchange capacity (CEC) is 150 meq/100g.

The quaternary ammonium surfactant $[(C_{16}H_{33})(CH_3)_3N]^+Br$ was obtained from Kodak chemicals. Decylamine and TEOS were purchased from Aldrich Chemical Co.

Porous clay fluorohectorite heterostructure synthesis.

To a 1 wt % suspension of Li^+-FH was added a 0.3 M aqueous solution of $[(C_{16}H_{33})(CH_3)_3N]Br$ in two-fold excess of the CEC value of the clay. The suspension was stirred for 24 h at 50°C to ensure complete ion exchange. Next, the resulting solid was centrifuged, washed repeatedly with ethanol to remove the excess surfactant and then resuspended and washed with water until free of halide ions. The pure product was collected by centrifugation and air-dried at room temperature. The resulting $[(C_{16}H_{33})(CH_3)_3N]^+$-fluorohectorite henceforth is noted $HDTMA^+$-Fluorohectorite.

Decylamine was added to $HDTMA^+$-fluorohectorite in the molar proportion $HDTMA^+$-Fluorohectorite : decylamine = 1 : 20, and the resulting suspension was stirred for 30 minutes. Tetraethylorthosilicate was then added to achieve a final molar ratio of $HDTMA^+$-FH : decylamine : TEOS = 1 : 20 : 150. The mixture was vigorously stirred for 4 hours at room temperature in a closed container. The reaction products were recovered by centrifugation and air-dried in the open atmosphere.

As-synthesized PCH-fluorohectorite was then calcined at the desired temperature in the range 200°C to 650°C for 4 h. i.e, ramped at the corresponding temperature, then held at that temperature for 4 h.

Porous clay rectorite heterostructure synthesis.

To a 1 wt % suspension of alkali-metal-Rectorite was added a 0.3 M aqueous solution of $[(C_{16}H_{33})(CH_3)_3N]Br$ in two-fold excess of the CEC value of the clay. The suspension was stirred for 24 h at 50°C to ensure

complete ion exchange. Next, the resulting solid was centrifuged, washed repeatedly with ethanol to remove the excess surfactant and then resuspended and washed with water until free of halide ions. The pure product was collected by centrifugation and air-dried at room temperature. The resulting $[(C_{16}H_{33})(CH_3)_3N]^+$-rectorite henceforth is noted $HDTMA^+$-Rectorite.

Decylamine was added to $HDTMA^+$-Rectorite in the molar proportion $HDTMA^+$-rectorite : decylamine = 1 : 20, and the resulting suspension was stirred for 30 minutes. Tetraethylorthosilicate was then added to achieve a final molar ratio of $HDTMA^+$-Rectorite : decylamine : TEOS = 1 : 20 : 150. The mixture was vigorously stirred for 4 hours at room temperature in a closed container. The reaction products were recovered by centrifugation and air-dried in the open atmosphere.

As-synthesized PCH-rectorite was calcined at 700°C and then exposed to steam at different temperatures in the range of 400°C to 700°C for 2 to 3 hrs.

Steaming Procedure and apparatus

Steam treatment was performed by using a iron steaming tube. Samples placed in a tubular iron crucible were inserted in the steaming vessel. It was then heated to the required temperature by using a programmed heating coil. Water was boiled in a 1000 ml two neck round bottom flask to produce steam which was introduced through one end of the tube and collected at the other end in an ice trap.

Porous clay vermiculite-(aldrich) heterostructure synthesis

An inexpensive source of vermiculite, from Aldrich Chemical packaging material, was used for pyridine chemisorption studies. The flaky packaging material was first ground into a fine powder in a electric grinder and then sieved through a 300 mesh mechanical sieve. The fine powder obtained after sieving was saturated with Mg^{+2} ions by refluxing it in a 2 M $MgCl_2$ solution for 48 hrs. The hot solution was cooled and repeatedly washed with distilled water till free of excess Cl^- ions. The Mg^{+2}-vermiculite was next ion-exchanged for $HDTMA^+$ ions by using a 0.1N $HDTMA^+Br^-$ solution with a final 1 wt% clay suspension. The $HDTMA^+$-vermiculite was washed with water and then with ethanol to remove excess ion pairs from the clay structure. The pure product was collected by centrifugation and air-dried at room temperature.

Decylamine was added to $HDTMA^+$-vermiculite in the molar proportion $HDTMA^+$-vermiculite : decylamine = 1 : 20, and the resulting suspension was stirred for 30 minutes. Tetraethylorthosilicate was then added to achieve a final molar ratio of $HDTMA^+$-vermiculite : decylamine : TEOS = 1 : 20 : 150. The mixture was vigorously stirred for 4 hours at room temperature in a closed container. The reaction products were recovered by centrifugation and air-dried.

MCM-41 synthesis

MCM-41 was prepared following the synthetic procedures of Beck et al. A 46.7 mmole specimen of a 29 wt% hexadecyltrimethylammonium chloride solution was combined with 10 wt% TMA-silicate solution (41.5

mmoles) and 96.8 mmoles of HiSil 233 amorphous silica under stirring. The reaction mixture was loaded in an autoclave and heated under moderate stirring at 100°C for 36 hrs. The resulting solid was recovered by filteration, washed with deionized water and dried in air at room temperature. To remove the organic species occluded in the pores of the as-synthesized MCM-41 samples were calcined in air at 660°C for 4 hrs at the rate of 2°C/min.

Template removal.

Partial template removal was achieved by solvent extraction. The solvent extraction was performed by using a soxhlet extractor with ethanol as the extracting agent. Typically ~1g of the as-synthesized PCH-fluorohectorite was extracted for ~24 h and the wet product was then placed in the oven at 70°C for ~1 h and dried in open air.

Physical Measurements.

Powder XRD analysis was carried out with a Rigaku rotoflex diffractometer using Cu-K_α radiation. The products were prepared as powdered samples for X-ray analysis. The gallery height was obtained by subtracting 9.6 Å, the thickness of the clay unit layer, from the XRD (001) basal spacing of the intercalated clays.

Nitrogen adsorption / desorption isotherms were determined on a Omnisorb 360 CX (Coulter) sorptometer at liquid N_2 temperatures by using ultrahigh-purity N_2 and He as adsorbate and carrier gas, respectively. All samples were outgassed at 150°C under vacuum overnight. Surface

areas were determined with the BET[6] equation. The method of Horvath and Kawazoe[7] was used to determine the pore diameters of the product.

FTIR spectra of PCH samples in the range 400-4000 cm^{-1} were recorded by using a Nicolet IR/42 spectrometer. The samples, were prepared as KBr wafers. FTIR spectra in the range 4000-2500 cm^{-1} and FTIR spectra for the adsorption of pyridine were obtained on an IBM IR44 spectrometer. Self supported pellets of sample (15 mg) were used. The heating rate was 5°C/min and the compounds were calcined for 2 hours at the choosen temperature under vacuum. The pyridine adsorption at 150°C was performed by outgassing the pellets for 2 h at this temperature prior to admitting pyridine. The pyridine was then removed by evacuation and by heating the sample at 150°C for 2 H. All spectra were recorded at 150°C.

^{29}Si MAS (magic angle spinning) NMR spectra were performed on a Varian VXR 400 spectrometer. A Bruker probe was used to spin the samples at 4 kHz. For the ^{29}Si spectrum, a pulse duration of 9 μs and a delay time of 870 s allowed full relaxation of the Si nucleus. An external reference of talc (δ = -98.1 ppm relative to tetramethylsilane) was used to determined chemical shift values.

^{19}F MAS-NMR spectra were obtained using a Doty probe with 35 s delay time and a spinning rate of 7 kHz. The ^{19}F chemical shifts are relative to hexafluorobenzene ($\delta(CFCl_3)$ = 164.9 ppm relative to hexafluorobenzene).

Elemental analysis were carried out by inductively coupled plasma emission spectroscopy at the University of Illinois Elemental Analysis Laboratory.

Results and Discussions.

A. Thermochemical Alterations in PCH-fluorohectorite.

Figure IV.1 illustrates the X-ray powder diffraction patterns of PCH-fluorohectorite formed by calcination at different temperatures for 4 hrs in air. All patterns exhibit three or more orders of (00l) reflection along with the presence of the clay (021) in-plane reflection at 19.6° 2-theta (d_{021} = 4.5Å). The dependence of d-spacing values on the calcination temperature is summarized in the insert in figure IV.1.

It is observed that on calcining the material up to 200°C, the basal spacing decreases from the initial value of 41.2Å to 38.5Å. This decrease in d-spacing results from the loss organic template molecules from the structure

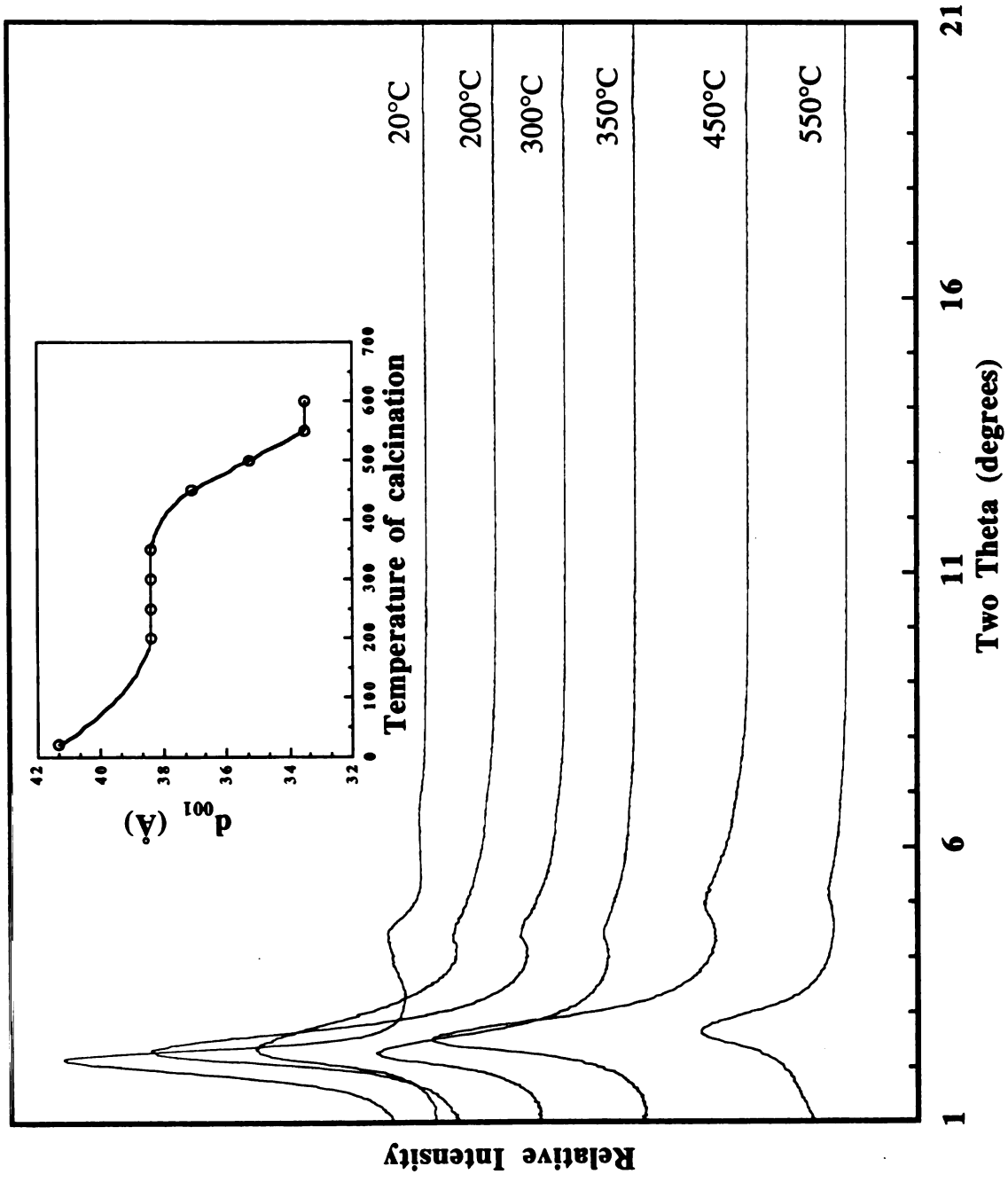

Figure IV.1 : X-ray diffraction pattern of PCH-Fluorohectorite calcined at different temperatures for 4 hours in air. **Insert** : The corresponding evolution of the d-spacing.

and from gallery silica dehydroxylation. On further heating the sample between 200°C and 350°C, no additional change in d-spacing is observed. However, on calcinating it above 350°C to 650°C the basal spacing is reduced further by 4Å up to 650°C calcination temperature. This reduction in gallery height is further explained by IR spectroscopy, ^{29}Si MAS NMR and ^{19}F MAS NMR data.

The oxide framework of the clay layers gives rise to several characteristic vibrations in the mid-infrared region. For fluorohectorite, bands at 990 and 1111 cm^{-1} are characteristic of symmetric and asymmetric Si-O stretching modes, respectively, and a band at 470 cm^{-1} is indicative of an O-Si-O bending mode. The vibrations at 990 and 1111 cm^{-1} relating to the stretching of the Si-O-Mg linkage are structure sensitive. The shoulder at 530 cm^{-1} corresponds to the Mg-O stretching mode. The metal-fluorine stretching vibration occurs at around 718 cm^{-1}.

As shown in Figure IV.2, all of these characteristic fluorohectorite vibrations are observed for as-synthesized PCH-fluorohectorite. Additional broad vibrational bands due to the Si-O stretching modes of the gallery silica mesostructure are observed at ca. 1067 cm^{-1} (which is overlapping with the clay layer Si-O stretching modes), a shoulder at 1200 cm^{-1}, and two weak vibrations at 957 and 800 cm^{-1}. These vibrations are similar to those observed in mesoporous MCM-41[9] as well as hydrated silica or fumed silica Cab-O-Sil which have linked SiO_4 tetrahedra.[10] The vibrations due to the structure-directing amine and alkylammonium cation surfactants are revealed by the bands at 2855 and 2924 cm^{-1} for the symmetric and asymmetric stretching CH_2 modes and at 1468 cm^{-1} for CH_2 scissoring mode. These surfactant vibrations disappear completely at a calcination temperature of 300°C.

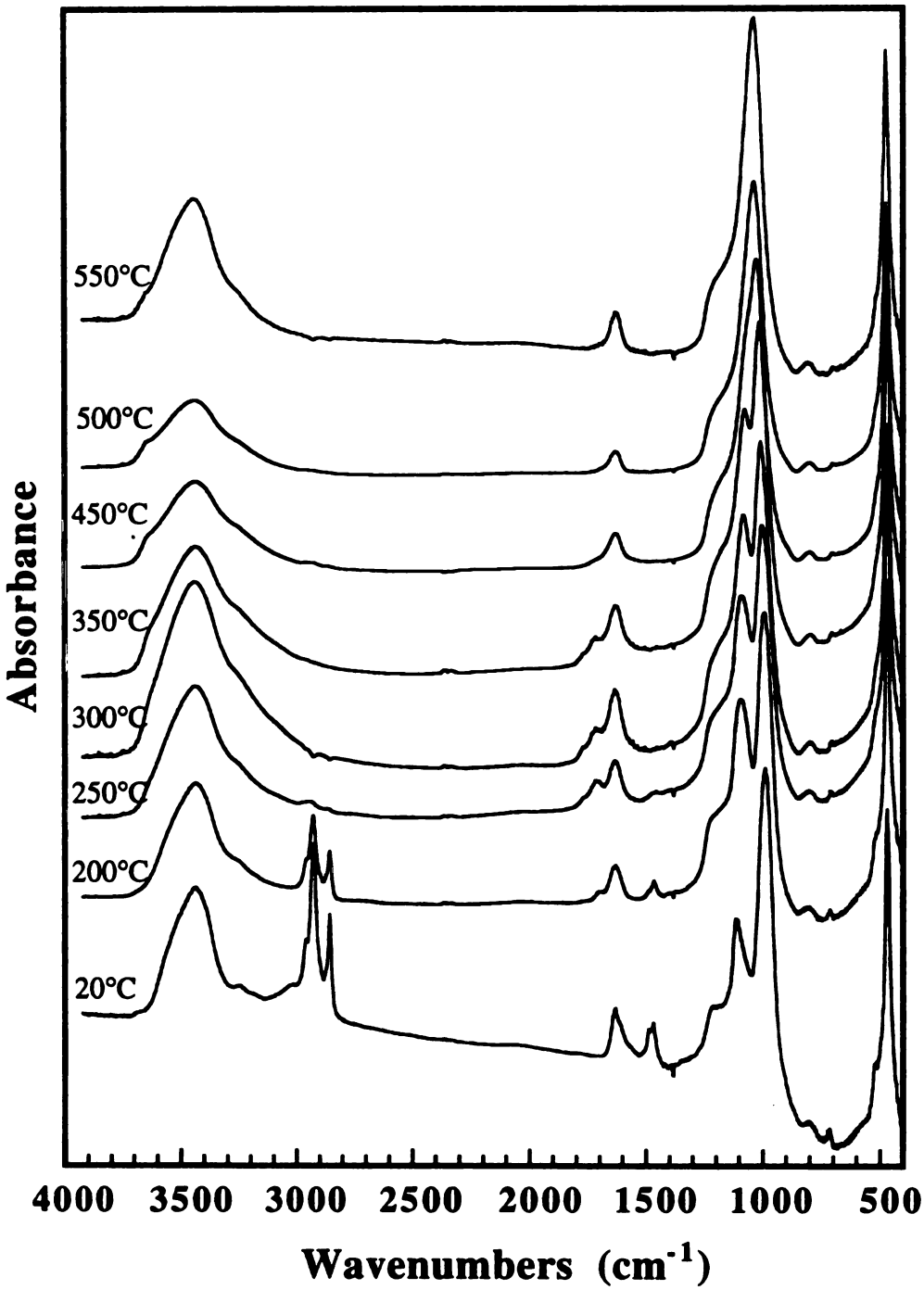

Figure IV.2 : Infrared spectras of PCH-Fluorohectorite calcined at different temperatures for 4 h. The samples were prepared as KBr wafer. No effort was made to remove physisorbed water.

Upon calcination (350°C) of the structure we observe a shift in the symmetric and asymmetric Si-O stretching modes. The vibration at 990 cm^{-1} shifts to 1017 cm^{-1} and the one at 1111 cm^{-1} shifts to 1076 cm^{-1}. The metal-fluorine stretching vibration gradually decreases in intensity and shifts from 718 cm^{-1} to 703 cm^{-1}. These shifts parallel the structural changes in the clay layer structure that we observed in the NMR study, i.e. hydrolysis of the layer by loss of fluorine and its replacement by hydroxyl groups. At 450°C the asymmetric and symmetric Si-O stretching modes of the clay layer merge into one broad stretching vibration at 1040 cm^{-1}, also indicative of some important changes in the structure at this temperature.

The OH stretching mode region in as-synthesized FH-PCH is masked by the adsorption of molecular water at 3430 cm^{-1} and hydrogen bonds so created. This region is observable for the as-synthesized and calcined samples after dehydrating overnight under vacuum at room temperature (Figure IV.3 a). A vibration at 3696 cm^{-1}, corresponding to the O-H stretching of the Si-OH groups of the gallery silica mesostructure, is retained until 150°C. The high energy shift upon removal of surfactant shows that the silanol groups are hydrogen-bonded to the primary amine. Calcining PCH-fluorohectorite at 250°C removes most of the remaining organics and causes the Si-OH vibration to shift to higher frequency, leaving a strong sharp band at 3740 cm^{-1} due to isolated Si-OH groups. This Si-OH band at ~3740 cm^{-1} has been previously assigned to a weakly acidic hydroxyl[11], capable of just hydrogen-bonding to basic adsorbates.[12]

It is noteworthy that a similar weak acidic hydroxyl (band at 3740 cm^{-1}) also is observed at 250°C in mesoporous MCM-41 (Figure IV.3 b). Yet, for PCH-fluorohectorite calcined at 250°C and 350°C two new O-H stretching modes also appear in the region between 3450 and 3700 cm^{-1},

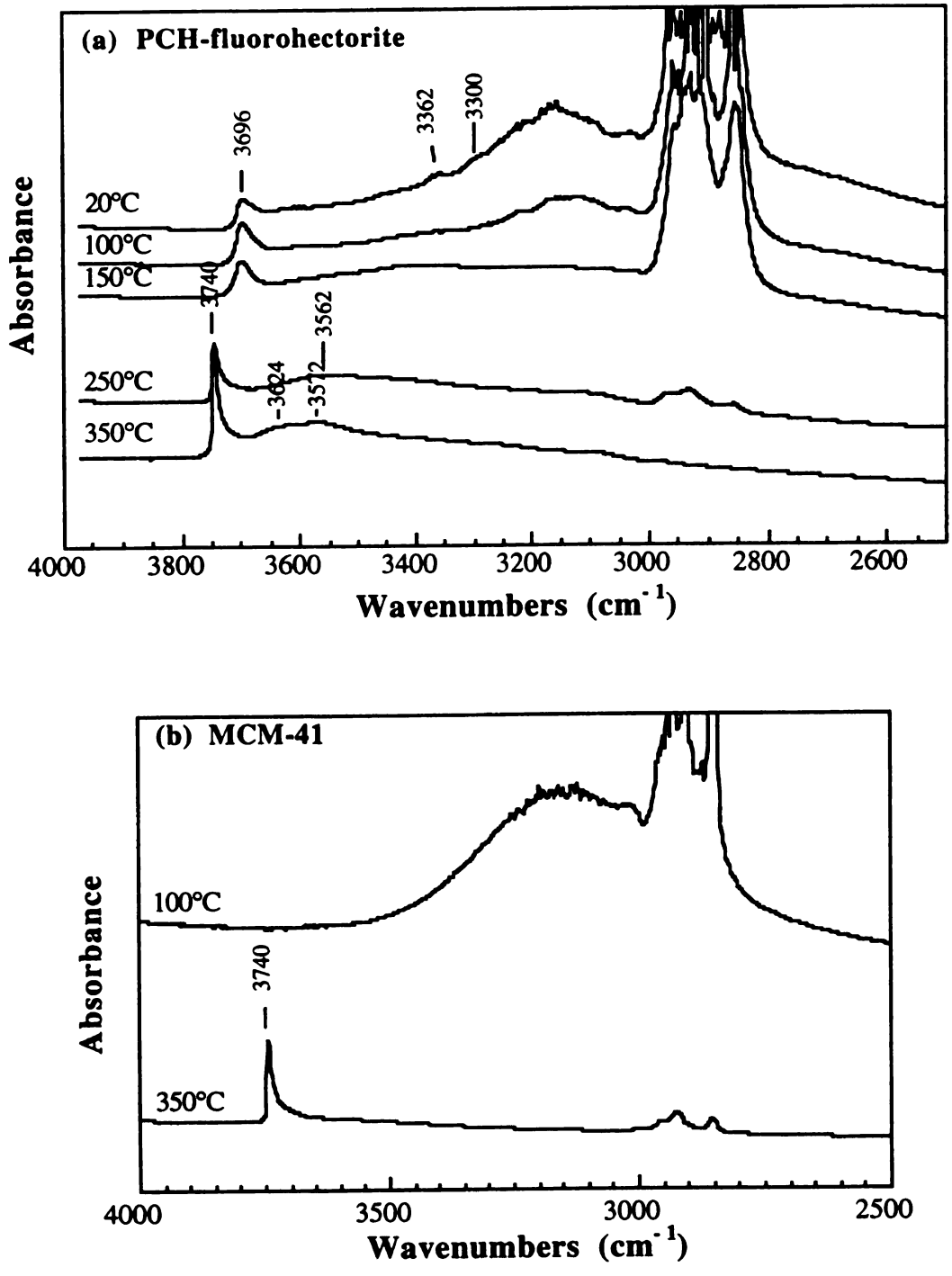

Figure IV.3 : (a) Infrared spectra of PCH-Fluorohectorite calcined at 20, 100, 150, 250 and 350°C for 4 h. (b) Pure silica MCM-41 mesostructure calcined at 20, 100, 150, 250 and 350°C temperatures. Spectra were recorded after removing the adsorbed water under vacuum. Self supported pellets were used.

frequencies which are not observed in mesoporous MCM-41. Such low frequency O-H stretching modes in aluminosilicates are usually attributed to medium to strong Brönsted acid sites. For siliceous Y-zeolites two vibrations were reported[13] with a low frequency (LF) band at ca. 3560 cm^{-1} due to the OH groups pointed in the β-cages and a high frequency (HF) band at ca. 3630 cm^{-1} corresponding to hydroxyls vibrating in the supercages. In PCH-fluorohectorite there is no aluminium in the structure, so we might explain these vibrations as originating from Mg-OH-Li groups (due to the hydrolysis of the layer) in very strong interactions with Si-OH groups of the gallery silica mesostructure. These bands might also be due to Mg-OH-Si groups formed by protonated Mg-O-Si groups of the layer by protons formed in the decomposition of the quaternary alkylammonium cations. Thus, three types of acidic hydroxyls are detected by infrared in PCH-fluorohectorite at 350°C calcination temperature. At 650°C the intensity of these vibrations decreases dramatically due to the condensation of silanol groups giving Si-O-Si bonds and dehydration of the clay layer.

^{29}Si MAS NMR Spectroscopy

The thermochemical alterations occurring for the calcined PCH-fluorohectorite derivatives were studied by ^{29}Si MAS-NMR spectroscopy (see Figure IV.4). As-synthesized air-dried PCH-fluorohectorite shows three silica resonances, the first being characteristic of the silicon environment of the fluorohectorite layers, i.e., a $Si(OSi)_3(OMg)$ Q^3 site at -93.3 ppm. The higher field peaks are due to the gallery-templated silica framework. The gallery silica mesostructure consists of $(SiO)_3SiOH$ groups (Q^3 at -103 ppm) and of completely crosslinked $Si(OSi)_4$ units (Q^4 at -110 ppm).

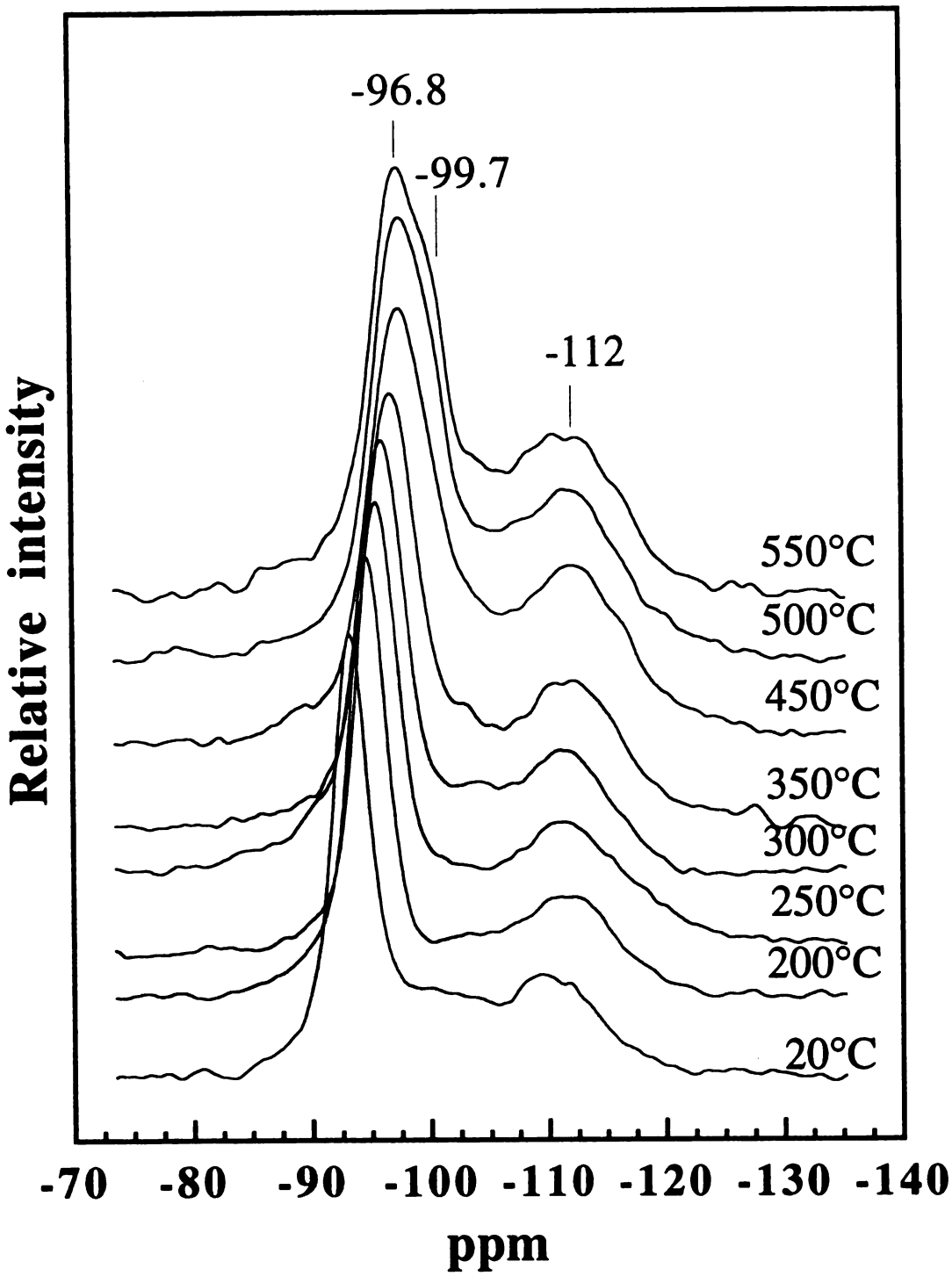

Figure IV.4 : ^{29}Si MAS-NMR spectra of PCH-Fluorohectorite calcined at different temperatures for 4 h. Chemical shifts are relative to TMS.

The Q^3 resonance of the fluorohectorite layers shifts progressively from -93.3 ppm to -96.6 ppm upon calcination at temperature to 350°C, which suggests a widening of the Si-O-Si bond angle.[14] The line width of the resonance remains unchanged from 20°C to 250°C, but it starts increasing upon further calcination. This increase in the line width may indicate a dispersion of isotropic chemical shifts due to structural disorder or to unaveraged dipolar interactions of ^{29}Si nuclei with other NMR active nuclei, particularly ^{1}H. The resonances due to the gallery silica mesostructure are not greatly affected in this range of temperature calcination.

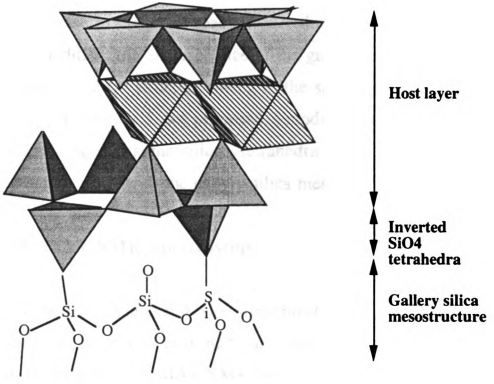

Figure IV.5 : Schematic of crosslinking between the gallery silica mesostructure and the layers showing inversion of some silica tetrahedra of the layer.

Further interesting changes in the ^{29}Si MAS NMR spectrum take place for PCH-fluorohectorite calcined at 450°C to 550°C. The line width of the Q^3 peak due to the clay layer gradually increases and finally gives rise to a second resonance at higher field (-99 ppm) with almost equivalent intensity. A new Q^4-like environment is created for almost half of the silica of the clay layer. This can be explained by two mechanisms, either by the dehydroxylation of the clay layers or by a formation of Si-O-Si linkages between the silicate sheet and the silica tetrahedra of the intragallery nanostructure during condensation, which is the favored explanation in our case. In fact Plee[15] et al. and Pinnavaia[16] et al. suggest the formation of Si-O-Al linkages between the pillars and the layers in alumina-pillared clays. This hypothesis is also supported in our system by the 4 Å decrease in the basal-spacing over the temperature range of 450-550°C. In addition, the Q^3 resonance of the gallery silica mesostructure is transformed into a Q^4 structure owing to the silanol groups condensation. As shown in Figure IV.5, we proposed a model for layer cross-linking in PCH, suggesting that some silicon tetrahedra in the clay layers are first inverted before linking to the gallery silica mesostructure.

^{19}F MAS NMR Spectroscopy

To better understand the structural changes occuring upon calcination, an effort was also made to examine the structural fluorine of the clay layers using ^{19}F MAS NMR spectroscopy. The ^{19}F MAS NMR spectrum of a natural fluorine-containing hectorite has been reported by Huve[17] et al. to exhibit two resonances, and this has been confirmed and explained by Butruille[4] et al. for alumina-pillared fluorohectorite. Two

non-equivalent environments at -10 and -16 ppm have been observed with relative intensities that are determined by the composition of the clay layers. In fluorohectorite all tetrahedral sites are occupied by silicon and the octahedral sites are occupied by Mg^{2+} and Li^{+}. The fluorine atoms bridge three octahedral metal positions, which they referred to as "octahedral triads". Each octahedral triad consists of one M1-type octahedron in which the fluorine atoms are arranged at *trans* positions and two M2-type octahedra

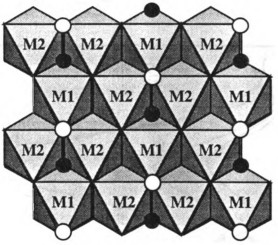

Figure IV.6 : Representation of the octahedral sheet in fluorohectorite (see text). Fluorine atoms are represented by white or black circles, depending whether they are above or below the layer plane.

with the fluorines at *cis* positions (see Figure IV.6). The upfield line at -16 ppm is assigned to the fluorine atoms in electrically charged triads with

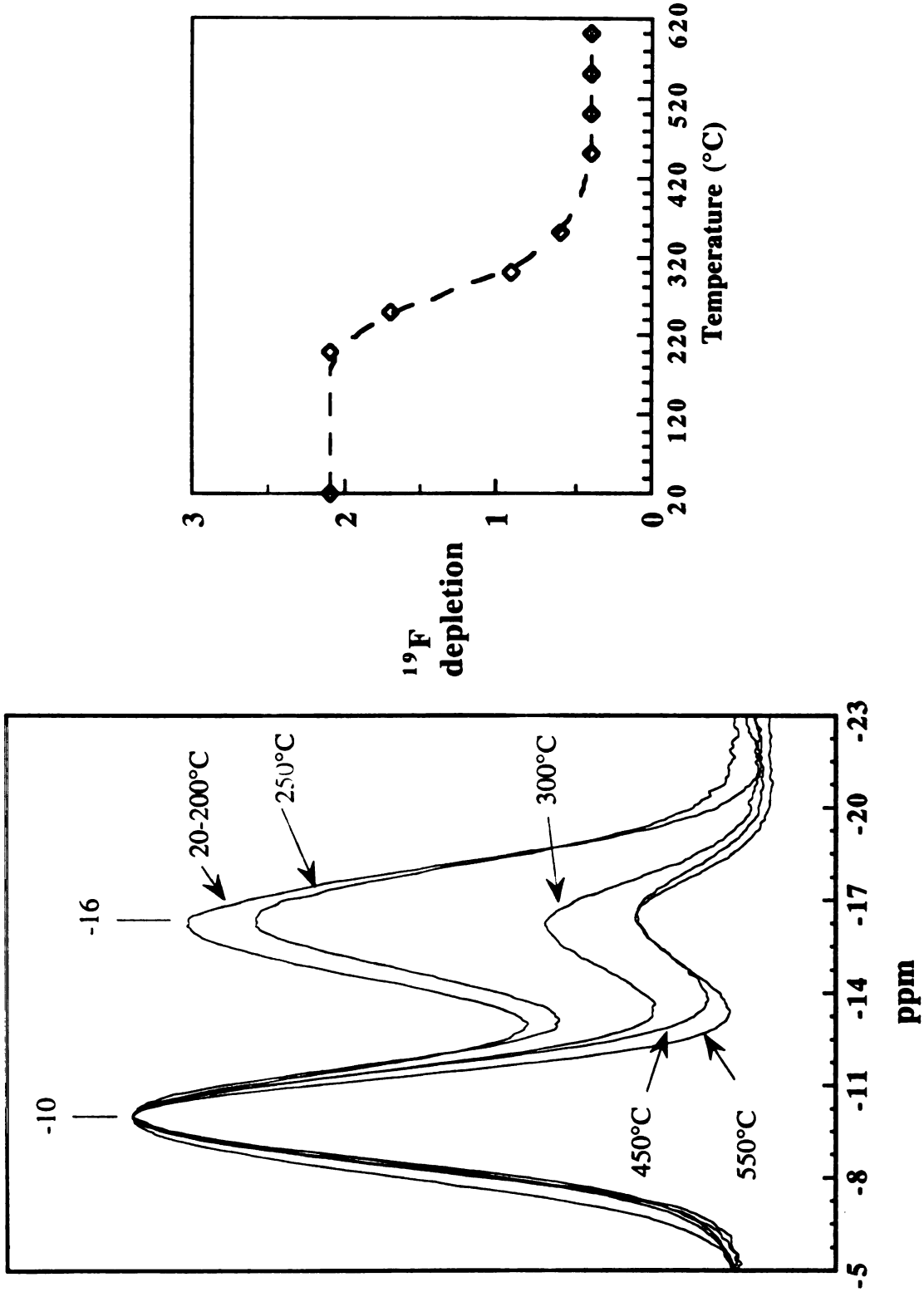

Figure IV.7 : ^{19}F MAS-NMR spectra of FH-PCH calcined at different temperatures.

Li^+ in a M1 site and two Mg^{2+} ions in M2 sites. The downfield line at -10 ppm is attributed to the fluorines of neutral triads with M1 and M2 sites filled by Mg^{2+}. The relative intensities of ^{19}F resonances depend on layer charge density. In fluorohectorite, the low-field/high-field peak intensity ratio was 0.90, as expected for a $O_{20}F_4$ unit cell with a net negative charge of 1.12.

The air-dried PCH-fluorohectorite exhibits the same two ^{19}F resonances as described above (see Figure IV.7). Upon increasing the calcination temperature from 250°C to 450°C, the intensity of the high-field resonance of FH-PCH decreases to ~25% of its initial value. Similar results were obtained by Butruille[4] *et al.* for the alumina-pillared fluorohectorite. This loss of structural fluorine was attributed to hydrolysis of lattice fluorine. A plausible pathway for the hydrolysis of the fluorine in electrically charged triads is the interlayer transport of water to the basal hexagonal cavities of the tetrahedral sheet, below which the fluorine atoms are located, the hydrolysis being catalyzed by protons, coming from the degradation of the quaternary ammonium cations for PCH-fluorohectorite. We also note that a similar hydrolysis occurs for the hexadecyltrimethyl ammonium exchanged form of fluorohectorite ($HDTMA^+$-Fluorohectorite), while no hydrolysis is observed for the Li^+-exchanged form of fluorohectorite (Li^+-Fluorohectorite).

BET surface area measurements and pore size distribution.

Nitrogen adsorption-desorption experiments were performed on FH-PCH calcined at different temperatures (see Figure IV.8 a & b). The surface areas were calculated by using the BET equation for multilayer

surface coverage by the adsorbate molecule. The method of Horvath and Kawazoe was adapted to determine the pore size distribution of the products after calcination at 300, 350, 450, 500 and 550°C. The surface area and pore size distribution for the samples are summarized in Table IV.1. The BET surface area for the FH-PCH progressively increases with the calcination temperature up to 550°C. For FH-PCH-300 the BET surface area is 570 m^2/g while PCH-fluorohectorite calcined at 500°C exhibits a BET surface area of 750 m^2/g. The pore size for the calcined product also

Table IV.1 : Gallery heights, BET surface area, Horvath and Kawazoe pore sizes, carbon and nitrogen content determined by chemical analysis of PCH-fluorohectorite derivatives calcined at different temperatures.

Calcination Temperature (°C)	Gallery Heights (Å)	S_{BET} (m^2/g)	Pore diameter (Å)	Carbon per (O_{20} unit cell)	Nitrogen per (O_{20} unit cell)
300	28.5	575	18.9	11.6	1.15
350	29.1	555	19.6	8.4	0.8
450	27.5	630	22.3	6.0	0.8
550	23.9	790	21.7	0.9	<0.1

*Gallery height is defined as the observed X-ray basal spacing minus the 9.6Å thickness of the fluorohectorite clay layers

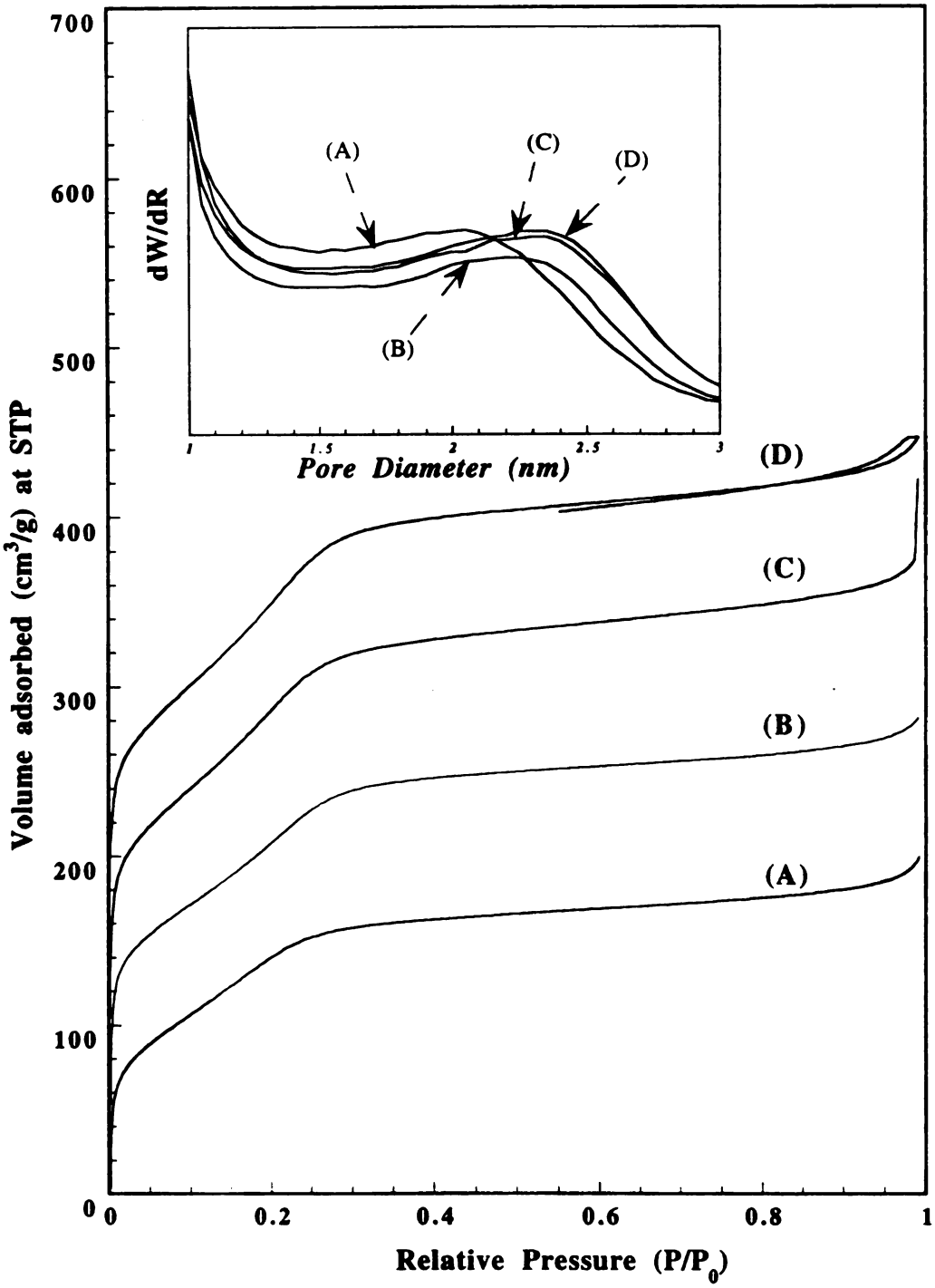

Figure IV.8 : Nitrogen adsorption/desorption isotherm for PCH-Fluorohectorite calcined at different temperatures ranging from 300 to 550°C. **Insert** : The correspoding Horvath-Kawazoe pore size distribution curves of PCH-Fluorohectorite calcined between 300°C to 550°C.

increases with the calcination temperature, from 19 to 23 Å for FH-PCH-300 and FH-PCH-550, respectively. This increase in pore size and surface area is explained by the more efficient removal of carbon residues from the pore structure with calcination temperature (see Table IV.1).

Template Removal.

Figure IV.10 shows the X-ray powder diffraction patterns of as-synthesized PCH-fluorohectorite, ethanol extracted, ethanol-extracted, calcined PCH-fluorohectorite prepared by using $HDTMA^+$/decylamine as template and TEOS as neutral silica precursor, at a reaction stoichiometry of 1 : 20 : 150 with $HDTMA^+$-Fluorohectorite : decylamine : TEOS respectively.

The XRD data for the as-synthesized PCH-fluorohectorite shows multiple (00l) reflection which are preserved even after ethanol extraction of the material, indicating that the structure is preserved. However after calcination of the ethanol-extracted sample, a significant broadening of the corresponding X-ray powder diffraction pattern was observed. It is very important to note that calcination resulted in almost complete decomposition of the structure. This indicates that prior to calcination, partial removal of the template by ethanol extraction results in incomplete crosslinking of the gallery nanostructure; leading to collapse of the gallery.

Figure IV.11 shows the thermo gravimetric analysis of the as-synthesized, ethanol-extracted, and ethanol-extracted, calcined PCH-fluorohectorite prepared from $HDTMA^+$/decylamine and TEOS. Several weight loss features for the as-synthesized PCH-fluorohectorite materials

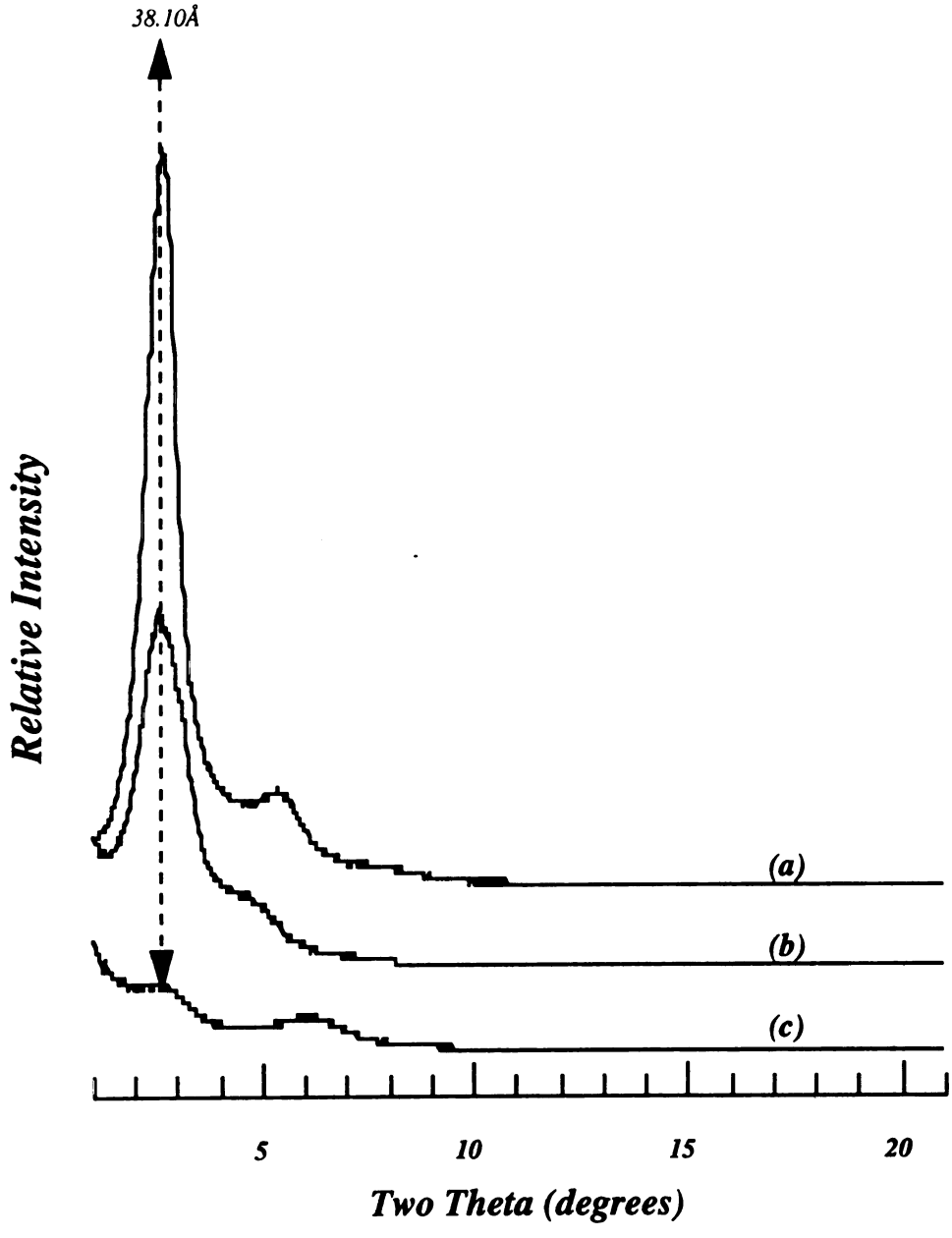

Figure IV.10 : X-ray diffraction pattern of PCH-Fluorohectorite prepared using $HDTMA^+$/decylamine template and TEOS at a molar ratio of 1 : 20 : 150.

(a) As-synthesized PCH-fluorohectorite.
(b) Ethanol-extracted PCH-fluorohectorite.
(c) Ethanol-extracted and calcined PCH-fluorohectorite.

can be observed. The TGA curve shows a five step weight loss for the as-synthesized PCH. The first step of 1.5% from 25°C to 140°C corresponds to loss of physisorbed water, the weight loss of 16.5% that occurs until 360°C and the weight loss of 14% up to 460°C are due the decomposition of the organic templates.

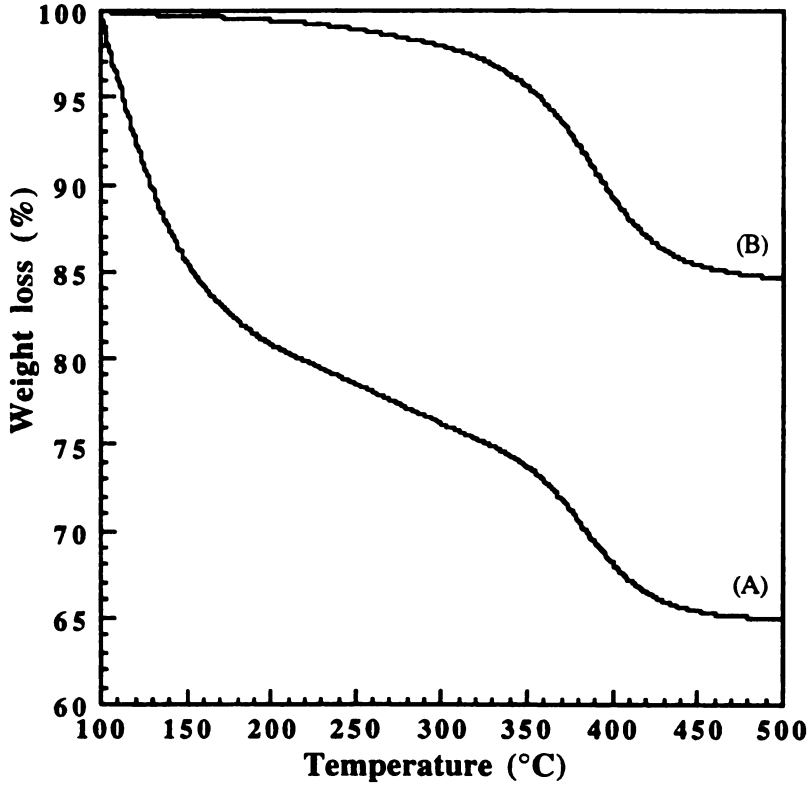

Figure IV.11 : Thermal gravimetric analysis of PCH-fluorohectorite prepared from decylamine-solvated $HDTMA^+$-Fluorohectorite/TEOS.
(A) As-synthesized PCH-fluorohectorite
(B) Ethanol-extracted PCH-fluorohectorite.

However, in contrast the TGA curve of the ethanol-extracted PCH-fluorohectorite (as shown in figure IV.11 b) clearly differs from that of the as-synthesized material in the temperature region between 160°C to 500°C. The final weight loss of 1.9% between 460-600°C is related to water losses via condensation of silanol groups to form siloxane bonds. The similar kind of weight loss curve has been observed in MCM-41. The weight loss curve for the as-synthesized PCH-fluorohectorite shows a two step weight loss for the decomposition of the organic template between 160°C to 500°C. The first step is most probably due to decomposition of the neutral amine co-template from the structure and the second weight loss at ~360°C is due to decomposition of the cationic surfactants. The TGA profile for the ethanol-extracted PCH shows a plateau up to a temperature of ~350°C, which indicates the absence of any neutral amine in the structure. However due to the presence of the charge balancing surfactant the second weight loss arises at ~ 360°C due to the thermal decomposition of the cationic surfactants in the clay galleries. Figure IV.12 illustrates the N_2 adsorption/desorption isotherms and the corresponding H-K pore size distribution curves for the as-synthesized, calcined PCH-fluorohectorite and the ethanol-extracted, calcined material. Both, isotherm and pore size distribution curves differ markedly from each other. The calcined PCH-fluorohectorite adsorption isotherm shows an adsorption behaviour characteristic for a nanoporous adsorbent, with a linear portion in the adsorption curve at a partial pressure region of 0.02-0.25, also indicating the presence of nanopores. Indeed, the H-K pore analysis with a pore size maxima at ~21Å confirms the presence of these pores.

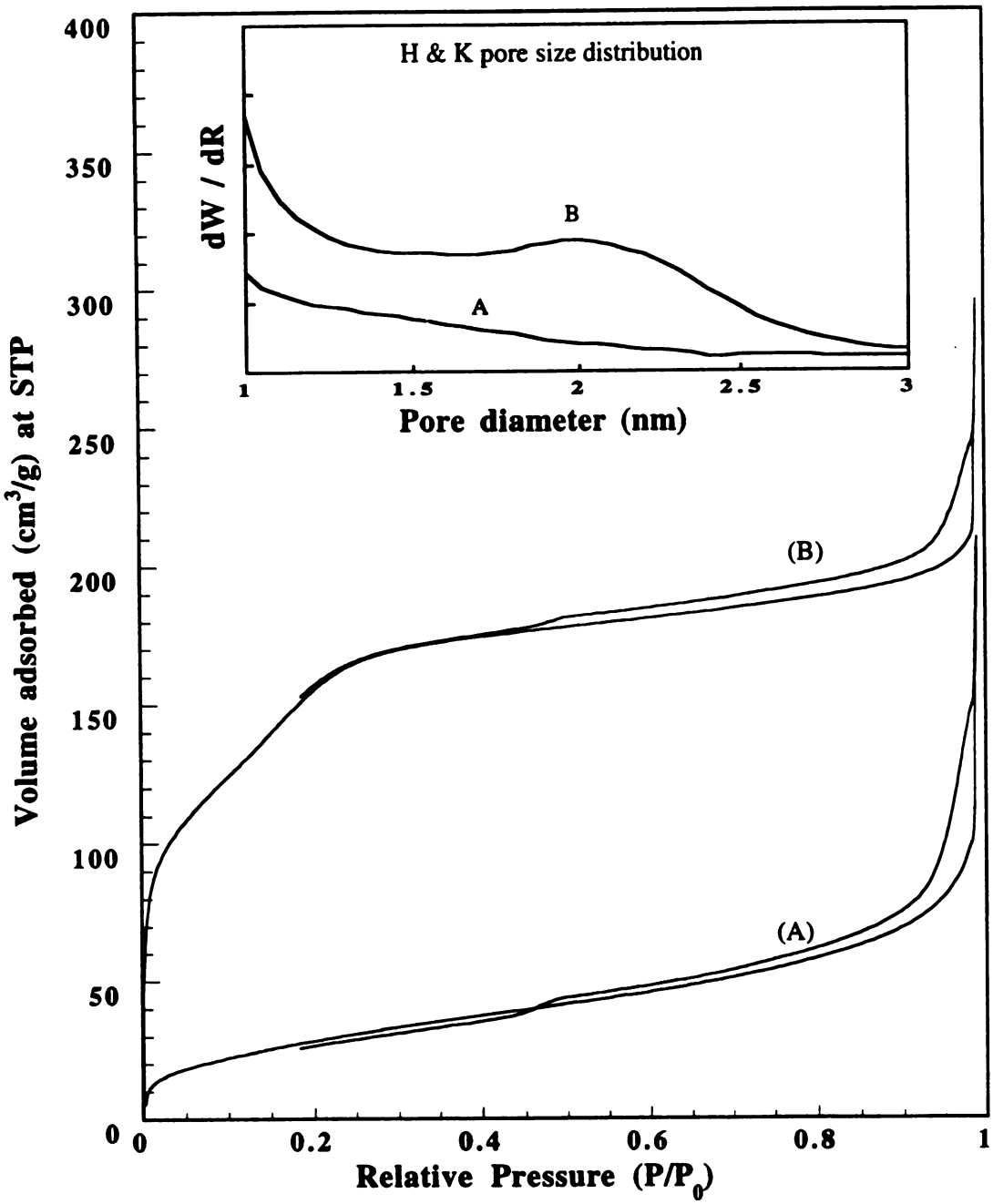

Figure IV.12 : Nitrogen adsorption/desorption isotherm for PCH-Fluorohectorite (a) calcined at 650°C and (b) Ethanol-extracted and calcined at 650°C **Insert** : The correspoding Horvath- Kawazoe pore size distribution curves of PCH-Fluorohectorite.

The ethanol-extracted PCH-fluorohectorite shows a type II isotherm where the majority of the porosity is due to the presence of textural pores and not due to uniform crystallographic intra-gallery pores. The H-K pore size distribution confirms the absence of gallery nanopores.

In conclusion it can be stated that calcination is probably the best approach to template removal for PCH materials. The partial removal of template prior to calcination results in the decomposition of the gallery structure. The X-ray diffraction data and TGA analyses clearly show that ethanol extraction for PCH materials does not lead to highly ordered and thermally stable heterostructures. In other words; the presence of the template during calcination helps in the cross-linking of the gallery nanostructure.

B. Hydrothermal stability of PCH-rectorites.

The mineral rectorite has been known to be a good cracking catalyst; it exhibits high hydrothermal stability. Hence our rationale in using rectorite for the synthesis of porous clay hetrostructures was to obtain a nanoporous cracking catalyst with high hydrothermal stability that would enable shape-selective processing of heavy crude oils.

X-ray powder diffraction.

Figure IV.13 illustrates the X-ray powder diffraction patterns of PCH-rectorite exposed to steam at different tempeartures. It is observed that PCH-rectorite shows high steam stability by maintaining its initial

gallery height up to 650°C. However, the structure collapses at 700°C hydrothermal temperature.

BET surface area measurement and pore size distribution.

Nitrogen adsorption-desorption experiments were performed on PCH-rectorite exposed to steam at different temperatures (see figure IV.14). The surface areas were calculated by using the BET equation for multilayer surface coverage by the adsorbate molecules. The method of Horvath Kawazoe was adopted to determine the pore size distribution of the products after hydrothermal treatments. The surface areas and pore size distribution for the samples are summarized in table IV.2. The BET surface area and H-K pore size for the PCH-rectorite is unaltered up to a temperature of 600°C, however steam treatment of the sample beyond 600°C results in the decrease of the BET surface area and loss of the uniformly stable pore size of 21Å. These results are consistent with the X-ray diffraction results.

Table IV.2 : BET surface area, Horvath and Kawazoe pore sizes of PCH-rectorite after hydrothermal treatment at different temperatures.

Hydrothermal Temperature (°C)	Gallery Heights (Å)	S_{BET} (m^2 / g)	H&K pore size (Å)
400	21	410	21
500	20	400	20
600	20	400	20
700	11	130	-

*Gallery height is defined as the observed X-ray basal spacing minus the 19.0Å thickness of the rectorite clay layers.

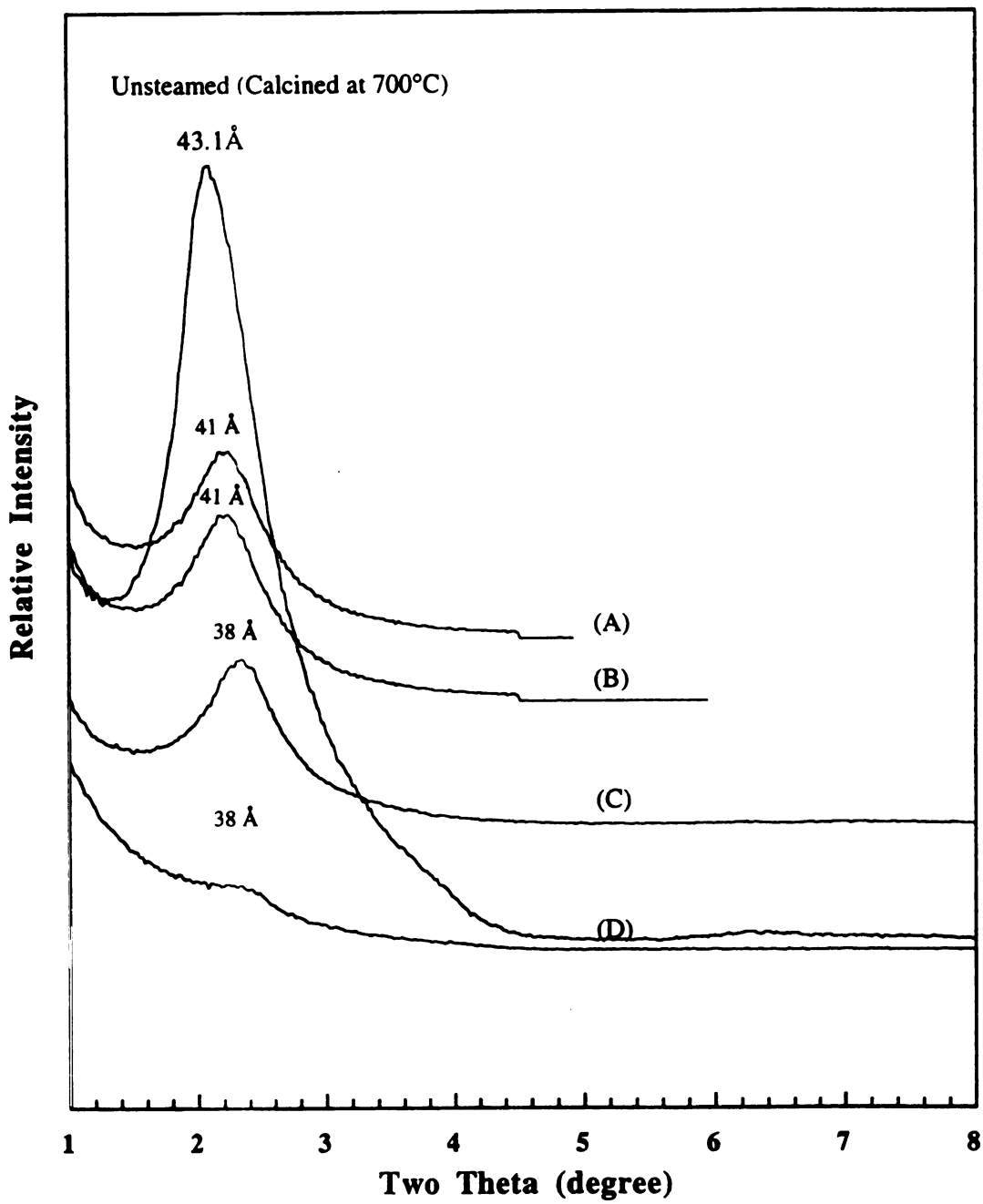

Figure IV.13 : X-ray diffraction pattern of PCH-rectorite prepared using $HDTMA^+$/decylamine template and TEOS at a molar ratio of 1 : 20 : 150, calcined at 700°C prior to hydrothermal treatment at different temperatures. (A) 400°C steaming, (B) 500°C steaming, (C) 600°C steaming and (D) 700°C steaming.

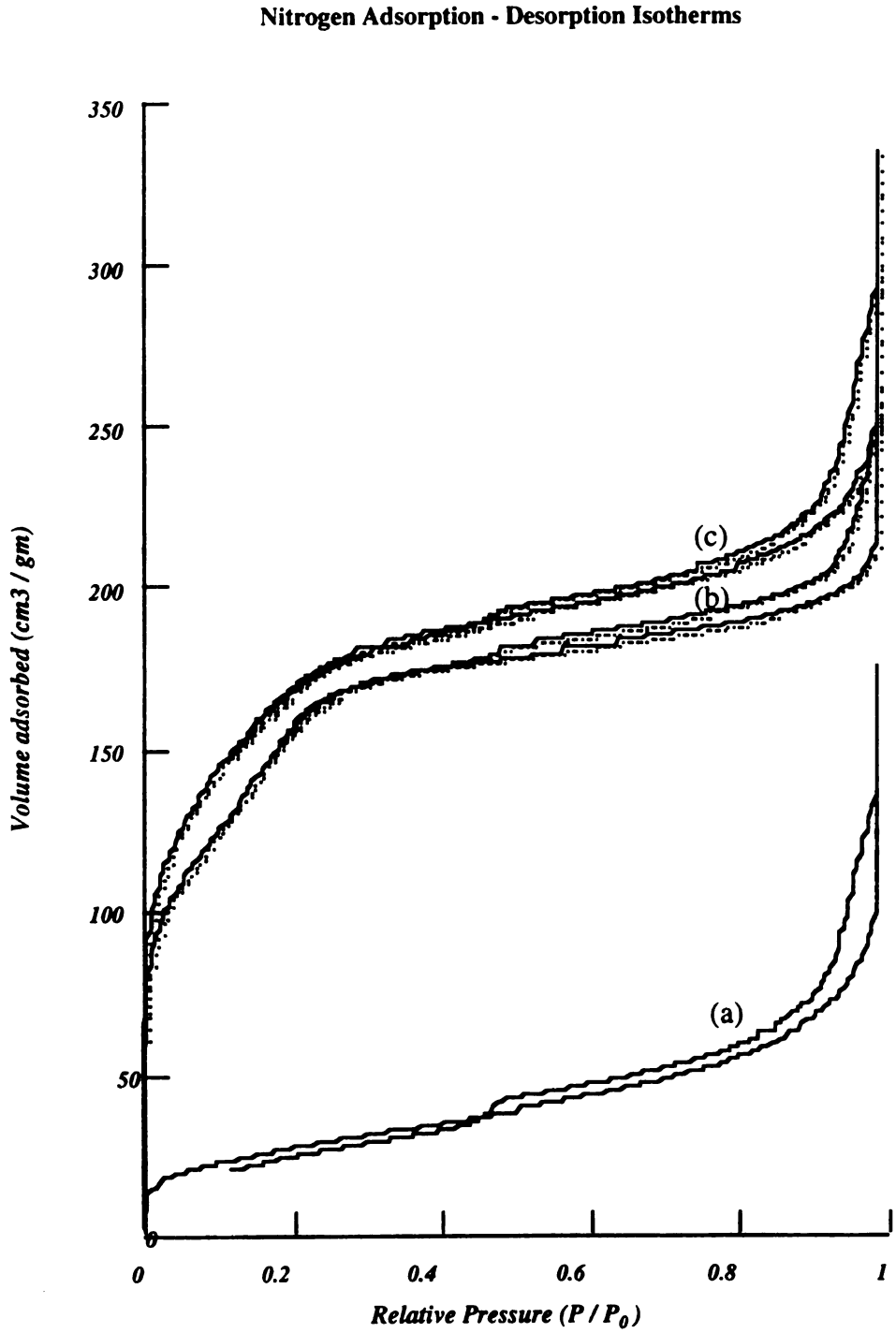

Figure IV.14 : Nitrogen adsorption/desorption isotherm for PCH-rectorite (A) calcined at 700°C and (B) Calcined at 700°C and steamed treated at 600°C and (C) calcined at 700°C and steam treated at 700°C **Insert** : The corresponding Horvath-Kawazoe pore size distribution curves of PCH-rectorite at different hydrothermal temperatures.

C. Enhanced acidity of porous clay heterostructures.

In order to more cogently demonstrate the acidity of calcined PCH compositions; we investigated the pyridine chemisorption properties of these materials. The chemisorption of pyridine at 150°C as monitored by FTIR is shown in figure IV.15. PCH-vermiculite calcined at 650°C in air for 4 hrs and then outgassed at 350°C under vaccum overnight reveals two new hydroxyl vibrations at 3627 and 3573 cm^{-1} in addition to a strong 3740 cm^{-1} band due to isolated Si-OH stretching vibrations from the gallery silica mesostructure. After exposure several pyridine ring stretching vibrations in the mid infrared region were observed at 1447, 1491, 1547, 1614 and 1639 cm-1 for PCH-vermiculite. These bands revealed the presence of both Bronsted bound pyridine and Lewis and hydrogen bonded pyridine. However in the silica MCM-41, sample the two main bands of pyridine ring stretching observed were at 1445 cm^{-1} and 1597 cm^{-1}, which corresponds to hydrogen bonded pyridine only. There was no evidence for a band at 1540 cm^{-1} which would indicate Bronsted acidity and the 1440 cm^{-1} band shift is not large enough to indicate appreciable Lewis acidity. In the silica MCM-41 the decrease in the intensity of the 3740 cm^{-1} Si-OH vibration upon pyridine adsorption confirm the presence of hydrogen bonded pyridine and the disappearance of almost all the pyridine stretch bands by 150°C degassing temperature indicates that the pure silica mesostructure posesses virtually little or no acidity. In PCH-vermiculite, the presence of several pyridine stretching vibrations in the 1400-1700 cm^{-1} region confirms the presence of both Bronsted and Lewis acidity, and also after degassing at 300°C, the retention of the pyridine stretches indicates the strength of these acid sites.

Figure IV.15 : Infrared spectra of pyridine adsorbed on PCH-vermiculite calcined at 650°C and silica MCM-41 calcined at 650°C.pyridine-adsorbed sample was evacuated at 150°C.

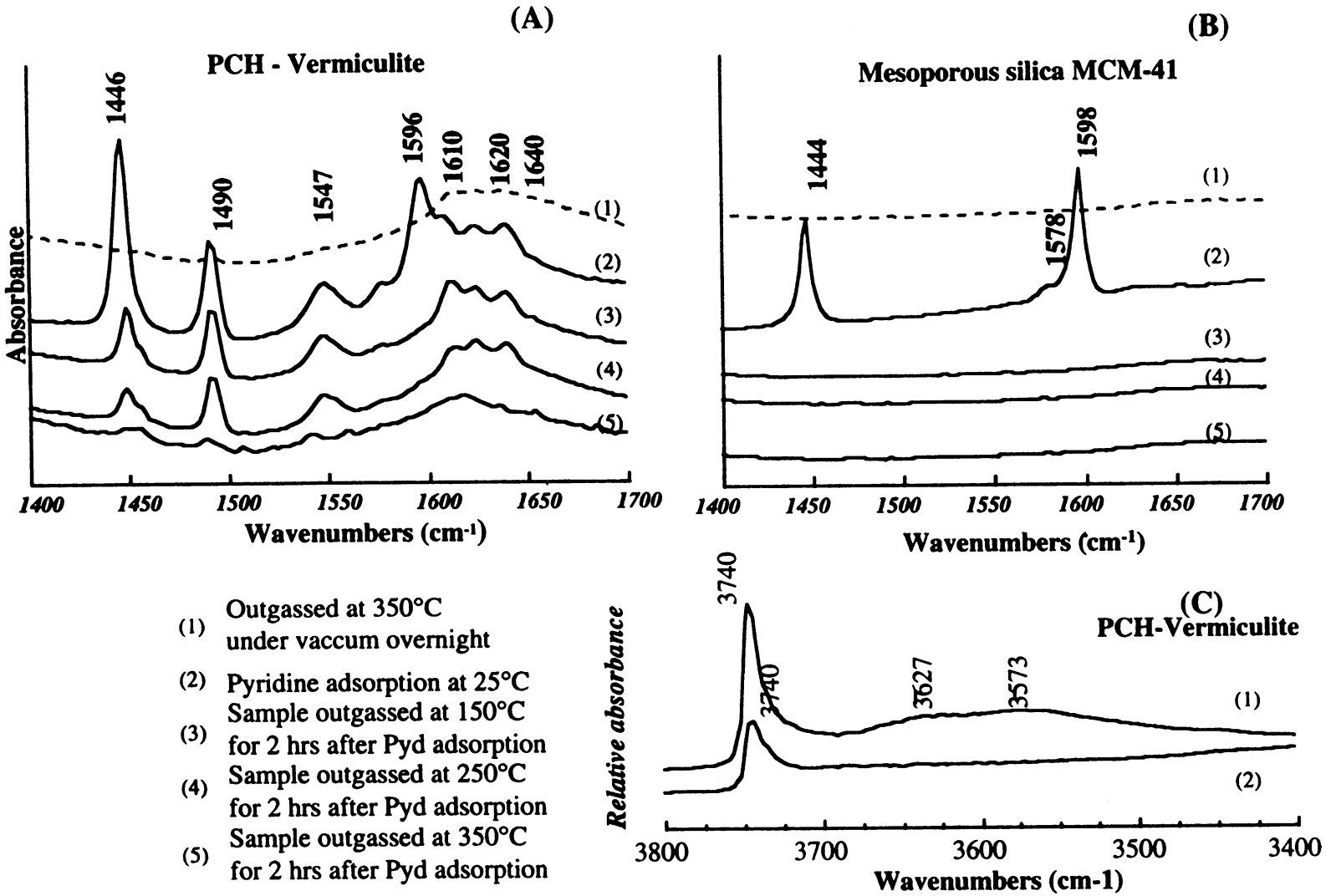
(A)
PCH - Vermiculite
1446
1490
1547
1596
1610
1620
1640
(1)
(2)
(3)
(4)
(5)
Absorbance
1400
1450
1500
1550
1600
1650
1700
Wavenumbers (cm-1)
(B)
Mesoporous silica MCM-41
1444
1578
1598
(1)
(2)
(3)
(4)
(5)
1400
1450
1500
1550
1600
1650
1700
Wavenumbers (cm-1)
(1) Outgassed at 350°C under vaccum overnight
(2) Pyridine adsorption at 25°C
(3) Sample outgassed at 150°C for 2 hrs after Pyd adsorption
(4) Sample outgassed at 250°C for 2 hrs after Pyd adsorption
(5) Sample outgassed at 350°C for 2 hrs after Pyd adsorption
(C)
PCH-Vermiculite
3740
3740
3627
3573
(1)
(2)
Relative absorbance
3800
3700
3600
3500
3400
Wavenumbers (cm-1)

Metal ion substitution during synthesis of PCH materials

The isomorphous substitution of Si by Ti during the synthesis of zeolites with MFI and MEL structures has generated a new family of titanium containing zeolites named as TS-1 and TS-2, respectively. These zeolites are able to perform the selective oxidation of organic compounds such as alkanes, alkenes, and alcohols by H_2O_2. The range of organic compounds that can be oxidized is greatly limited, however by the relatively small pore size (about 6 nm) of the host framework. The recent discovery of large pore silica-based molecular sieves by Kresge et al. has broken the previous pore size barrier of zeolites and opened up new avenues for selective catalysis. There have been recent reports in the literature on the synthesis of silica-based molecular sieves, partly substituted by titanium, aluminum, chromium etc. and a range of other metal ions. Here we report initial attempts at forming a silica-templated nanostructure partly substituted with aluminum, and/or titanium metal ions inside the galleries of a 2:1 layered silicate. While the results obtained do not support significant metal ion substitution, even at low metal ion concentration some interesting structural changes are observed.

Ti-ion substitution.

To a 1 wt % suspension of Li^+-Fluorohectorite was added a 0.3 M aqueous solution of $[(C_{16}H_{33})(CH_3)_3N]Br$ in two-fold excess of the CEC value of the clay. The suspension was stirred for 24 h at 50°C to ensure complete ion exchange. Next, the resulting solid was centrifuged, washed repeatedly with ethanol to remove the excess surfactant and then

resuspended and washed with water until free of halide ions. The pure product was collected by centrifugation and air-dried at room temperature. The resulting $[(C_{16}H_{33})(CH_3)_3N]^+$-fluorohectorite henceforth is noted HDTMA$^+$-Fluorohectorite.

Decylamine was added to HDTMA$^+$-fluorohectorite in the molar proportion HDTMA$^+$-Fluorohectorite : decylamine = 1 : 20, and the resulting suspension was stirred for 30 minutes. In a separate reaction vessel, a mixture of tetraethylorthosilicate and titanium iso-propoxide was mixed at Ti/Si molar ratios that ranged from 0.001 to 0.1. These mixtures were stirred for 10 minutes in a closed container and then added to the amine-solvated HDTMA$^+$-fluorohectorite to achieve a final molar ratio of HDTMA$^+$-fluorohectorite : decylamine : mixed metal alkoxide = 1 : 20 : 150, respectively. The mixture was stirred for 30 minutes at room temperature in a closed container. The reaction products were recovered by centrifugation and air-dried. The as-synthesized Ti substituted PCH derivatives were then ramped to 650°C for 4 h, ata ramp rate of 2°C/min and heated at that temperature for 4 h.

Figure IV.16 illustrates the X-ray powder diffraction patterns for both the as-synthesized and calcined PCH-fluorohectorite prepared using different Ti/Si molar ratios. The as-synthesized materials exhibits multiple (00l) reflections indicating the presence of a layered structure, however the gallery heights for the as-synthesized Ti substituted derivatives are substantially smaller than the initial pure silica-templated PCH-fluorohectorites. It must be noted here that all the Ti substituted materials require at least 14 days of drying time and the materials obtained after drying were hard and difficult to grind.

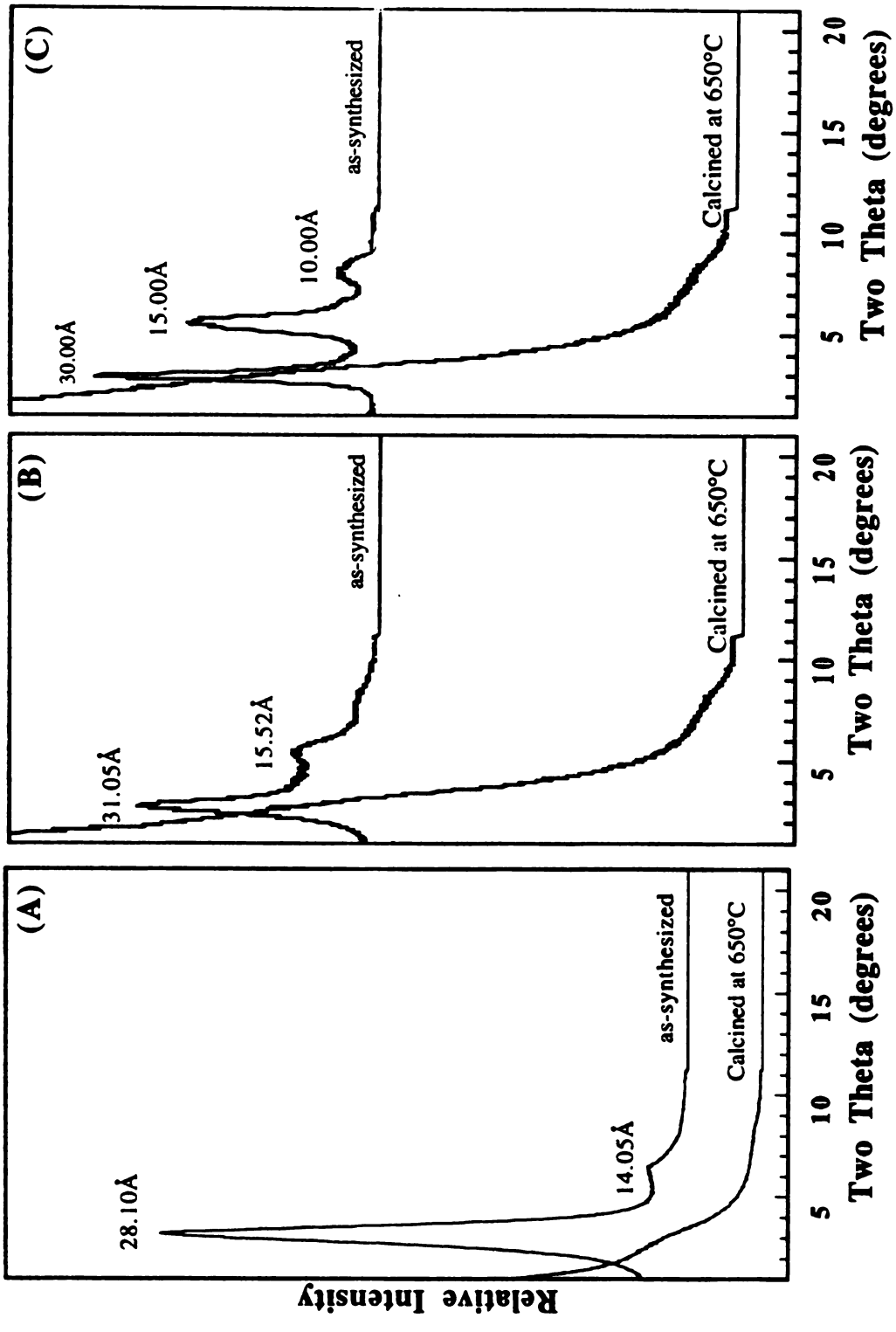

Figure IV.16 : X-ray diffraction powder patterns for as-synthesized and calcined PCH-fluorohectorite prepared using different Ti/Si molar ratios. (A) Ti/Si molar ratio = 0.001, (B) Ti/Si molar ratio = 0.01, (C) Ti/Si molar ratio = 0.1.

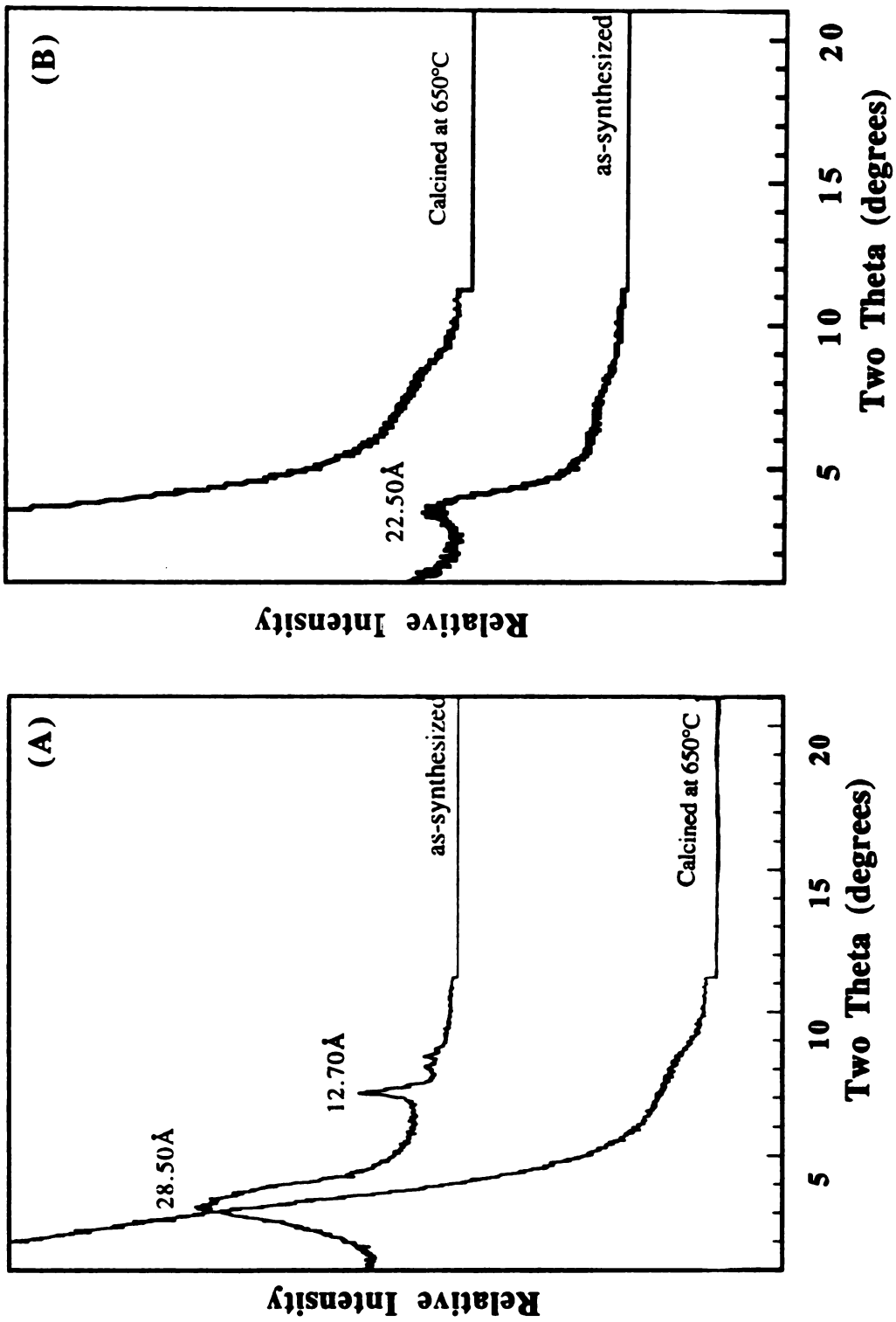

Figure IV.17 : X-ray diffraction powder patterns for as-synthesized and calcined PCH-fluorohectorite prepared using different Al/Si molar ratios. (A) Al/Si molar ratio = 0.1, (B) Al/Si molar ratio = 0.01.

Covalent grafting of Ti on the hydroxyl groups lining the pore walls of PCH-fluorohectorite.

The recent advances in mesoporous molecular sieves [8-12] have been at the forefront of research in the field of nanoporous materials design. The high surface areas (ranging from 600 m^2/g to 1200 m^2/g) and uniform pore structures (pore diameters ranging from 20 to 100Å) associated with them, have made these materials promising catalysts or catalyst supports. They are highly suitable for reactions involving molecules with large kinetic diameters. One route to obtaining such catalysts has been through the grafting of organic units on to the walls of MCM-41. Recently, heavy metal-ion adsorbents have been developed based on the covalent grafting of chelating functionalities to the pore wall hydroxyls of a mesoporous molecular sieve.

Here we report the covalent grafting of Ti on the inner lining of the intra-gallery nanostructure of porous PCH-fluorohectorite. We hoped that such a synthetic approach could allow for isomorphous grafting of Ti metal-ions in the structure of PCH and thereby generate a highly efficient bifunctional catalyst.

Synthesis.

To a 1 wt % suspension of Li^+-Fluorohectorite was added a 0.3 M aqueous solution of $[(C_{16}H_{33})(CH_3)_3N]Br$ in two-fold excess of the CEC value of the clay. The suspension was stirred for 24 h at 50°C to ensure complete ion exchange. Next, the resulting solid was centrifuged, washed repeatedly with ethanol to remove the excess surfactant and then

resuspended and washed with water until free of halide ions. The pure product was collected by centrifugation and air-dried at room temperature. The resulting $[(C_{16}H_{33})(CH_3)_3N]^+$-fluorohectorite henceforth is noted HDTMA$^+$-Fluorohectorite.

Decylamine was added to HDTMA$^+$-fluorohectorite in the molar proportion HDTMA$^+$-Fluorohectorite : decylamine = 1 : 20, and the resulting suspension was stirred for 30 minutes. Tetraethylorthosilicate was then added to achieve a final molar ratio of HDTMA$^+$-FH : decylamine : TEOS = 1 : 20 : 150. The mixture was vigorously stirred for 4 hours at room temperature in a closed container. The reaction products were recovered by centrifugation and air-dried in the open atmosphere. As-synthesized PCH-fluorohectorite was then calcined at 650°C for 4 hours using a ramp rate of 2°C/min. 1.0 g of freshly calcined material was then dried at 110°C under 10^{-3} torr vaccum and refluxed with titanium iso-propoxide (ranging from 0.45 g to 1.0 g of Ti-alkoxide / 1.0.g of PCH-fluorohectorite) in 25 ml of dry toluene for 24 hrs. The resulting material has covalently grafted titanium on the hydroxyl groups that line the PCH pore walls. The functionalized product (hereafter denoted as Ti-PCH) was filtered, washed several times with toluene followed by ethanol and then dried at 75°C for 1 h.

Figure IV.18 illustrates the X-ray powder diffraction patterns for the freshly calcined PCH-fluorohectorite, and shows multiple (00l) reflections and a gallery height of ~22.0Å. Upon Ti grafting the basal spacing of the material changes by <2.0Å; a slight decrease in the intensity of the (00l) peaks is observed. This decrease in crystallinity is probably due to some perturbation of the structure by the grafting reaction, however the intra-gallery nanostructure remains intact

Calcination of the as-synthesized materials at 650°C for 4 h gave powder diffraction patterns with a weak reflection corresponding to a basal spacing of ~12.7Å. This reflection is characteristic of a silica-intercalated derivative with no intra-gallery nanostructure. BET surface areas for the materials ranged between 100 to 150 m^2/gm.

Al-ion substitution.

To a 1 wt % suspension of Li^+-Fluorohectorite was added a 0.3 M aqueous solution of $[(C_{16}H_{33})(CH_3)_3N]Br$ in two-fold excess of the CEC value of the clay. The suspension was stirred for 24 h at 50°C to ensure complete ion exchange. Next, the resulting solid was centrifuged, washed repeatedly with ethanol to remove the excess surfactant and then resuspended and washed with water until free of halide ions. The pure product was collected by centrifugation and air-dried at room temperature. The resulting $[(C_{16}H_{33})(CH_3)_3N]^+$-fluorohectorite henceforth is noted $HDTMA^+$-Fluorohectorite.

Decylamine was added to $HDTMA^+$-fluorohectorite in the molar proportion $HDTMA^+$-Fluorohectorite : decylamine = 1 : 20, and the resulting suspension was stirred for 30 minutes. In a separate reaction vessel, mixture of tetraethylorhosilicate and aluminum tributoxide was mixed at Al/Si molar ratios that ranged from 0.01 to 0.1. These mixtures were stirred for 10 minutes in a closed container and then added to the amine-solvated $HDTMA^+$-fluorohectorite to achieve a final molar ratio of $HDTMA^+$-fluorohectorite : decylamine : mixed metal alkoxide = 1 : 20 : 150, respectively. The mixture was stirred for 30 minutes at room temperature in a closed container. The reaction products were recovered

by centrifugation and air-dried. The as-synthesized Al substituted PCH derivatives were then ramped to 650°C for 4 h, at a ramp rate of 2°C/min and heated at that temperature for 4 h.

Figure IV.17 illustrates the X-ray powder diffraction patterns for both the as-synthesized and calcined PCH-fluorohectorite prepared using different Al/Si molar ratios. The as-synthesized materials exhibit multiple (00l) reflections indicating the presence of a layered structure, however the gallery heights for the as-synthesized Al substituted derivatives are substantially smaller than the initial pure silica-templated PCH-fluorohectorites. It must be noted here that all the Al substituted materials require at least 10 to 14 days of drying time and the materials obtained after drying were hard and difficult to grind.

Calcination of the as-synthesized materials at 650°C for 4 h gave powder diffraction patterns with a weak reflection corresponding to a basal spacing of ~12.7Å. This reflection is characteristic of a silica-intercalated derivative with no intra-gallery nanostructure. BET surface areas for the materials ranged between 100 to 150 m^2/gm.

The above results suggest that the direct incorporation of metal ions inside the gallery framework structure leads to the formation of a collapsed mixed metal oxide derivative with no intra-gallery porosity. This can be explain due to the difference in the rate of hydrolysis of TEOS and Ti-iso propoxide or Al-tributoxide or some kind of chemical reaction with the basic alkylamines.

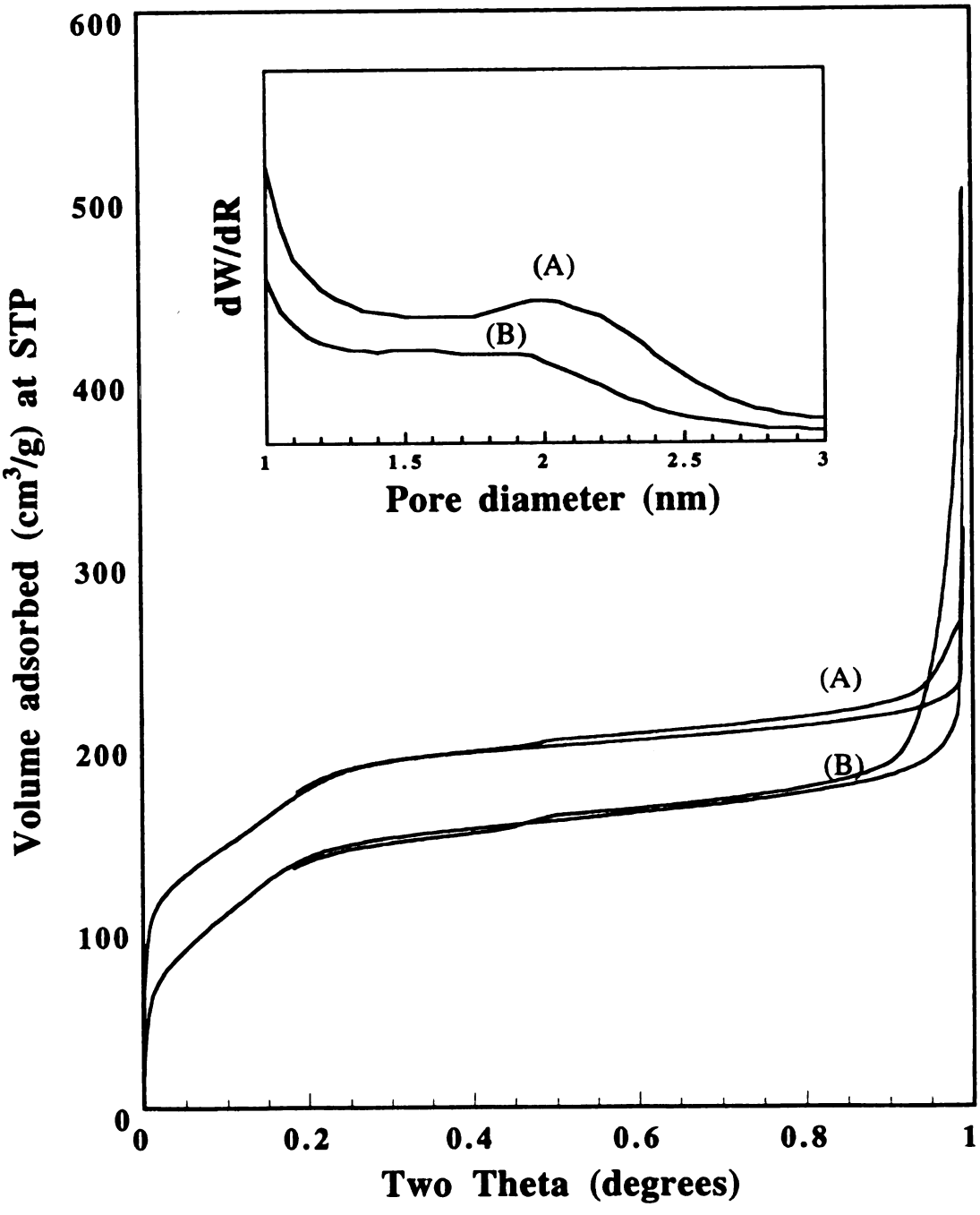

Figure IV.19 : N2 adsorption/desorption isotherms and the corresponding H-K pore size distribution for (A) PCH-fluorohectorite, calcined at 650°C. (B) Ti-PCH with Ti-alkoxide conc of ~0.45g/g of PCH-fluorohectorite.

It is important to note that the diffraction patterns of Ti-PCH at higher Ti-alkoxide concentration are similar to those prepared at Ti-alkoxide=0.45g/g of PCH-fluorohectorite.

Figure IV.19 illustrates the N_2 adsorption/desorption and the corresponding H-K pore size distributions for the calcined PCH-fluorohectorite and Ti-PCH prepared at a Ti loading of 0.45g/1 g of PCH-fluorohectorite. The BET surface area for PCH-fluorohectorite was 850 m^2/g and decreased to 790 m^2/g for Ti-PCH. Here again the BET surface areas remained constant at higher Ti loadings. The H-K pore size distribution gave pore diameters of 21Å and 18Å for the calcined PCH-fluorohectorite and Ti-PCH, respectively. These observations suggests the presence of a significant amount of grafted titanium species attached to the pore walls of PCH, causing constriction of the intra-gallery pore channels, yet conserving the porosity of the grafted materials.

Catalytic evaluation of Ti-grafted PCH materials could be one an areas for future investigation.

Porous clay heterostructure formation using low charge density smectites.

Attempts were made to effect PCH syntheses with low charge density smectites such as Wyoming Montmorillonite, Chinese Beidellite and Arizona Montmorillonite.

Figure IV.20 illustrates the X-ray powder diffraction patterns for the alkali metal-ion, and the corresponding quaternary ammonium exchanged (Q^+-clay). The XRD patterns for all Na^+-clays show a diffraction peak with a basal spacing of ~12.1Å, which on exchanging with the $HDTMA^+$ ion increases to a higher value depending on the exchange capacity of the clay. Mixtures of hydrated $HDTMA^+$-clay, decylamine and TEOS at the molar ratio of 1 : 20 : 150, respectively, were allowed to react for 4 h at ambient temperature. The resultant intercalates were then centrifuged, and dried in open air to give the as-synthesized products. Removal of the organics by calcination at 500°C in air for 4 h gave the final calcined material. Figure IV.21 illustrates the X-ray diffraction patterns for the air dried and the calcined materials synthesized from Wyoming montmorillonite, Chinese beidellite and Arizona montmorillonite. The diffraction patterns for the air dried PCH-beidellite showed a broad (001) reflection with a gallery height of ~20Å. Both PCH-montmorillonite samples exhibited gallery heights of ~9Å, significantly smaller than observed for the beidellite system. The gallery heights of the as-synthesized PCH materials from low charge density smectites was found to be significantly smaller than those of the corresponding high charge density smectite such as fluorohectorite. Calcination of the air dried sample at 650°C yields materials with a collapsed structure and a basal spacing of ~12.7Å.

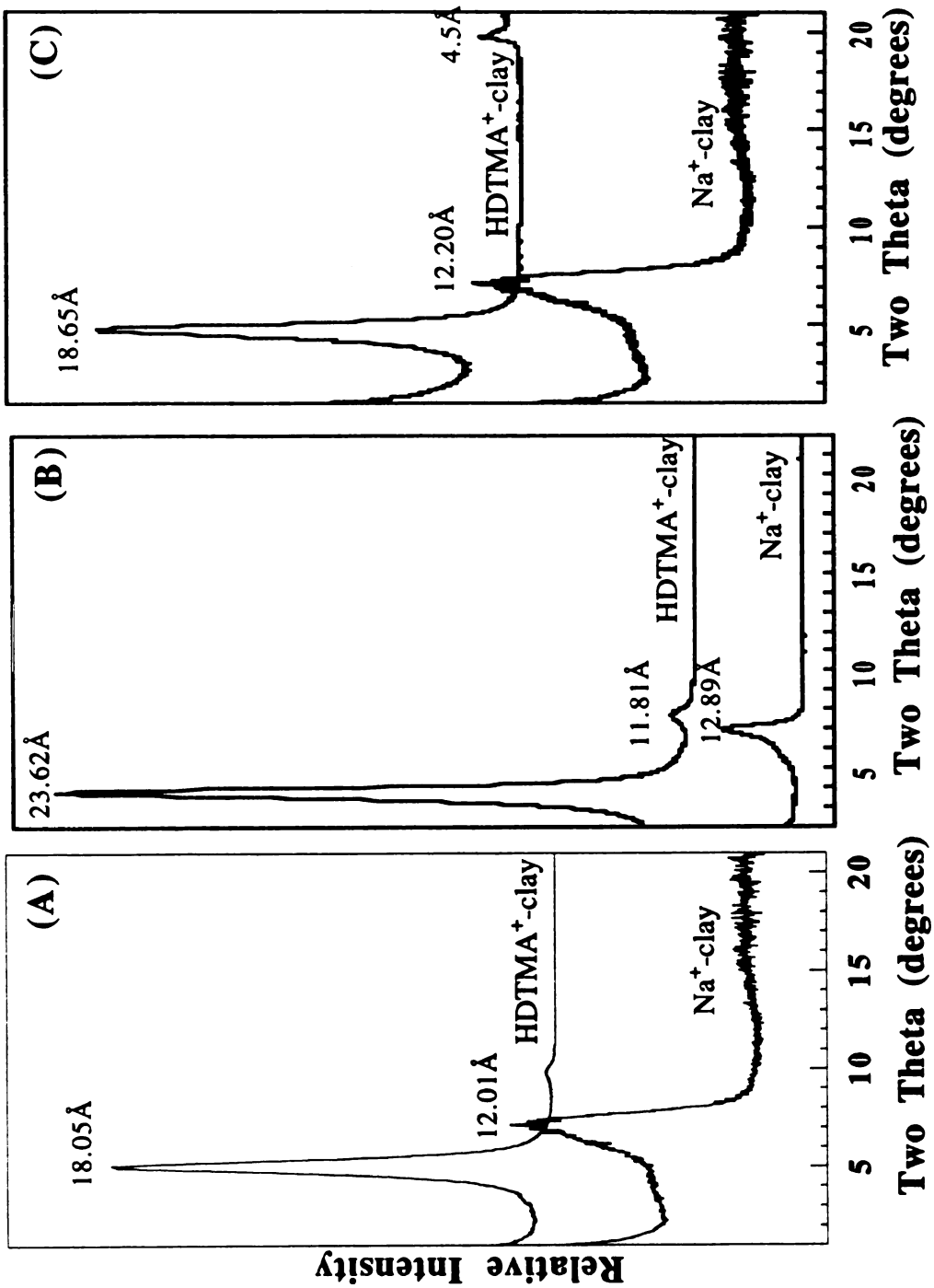

Figure IV.20 : X-ray diffraction powder patterns for alkali metal-ion exchanged and their corresponding quaternary ammonium exchanged Q+-clay.(A) montmorillonite (Arizona). (B) beidellite(Chinese). (C) montmorillonite (Wyoming).

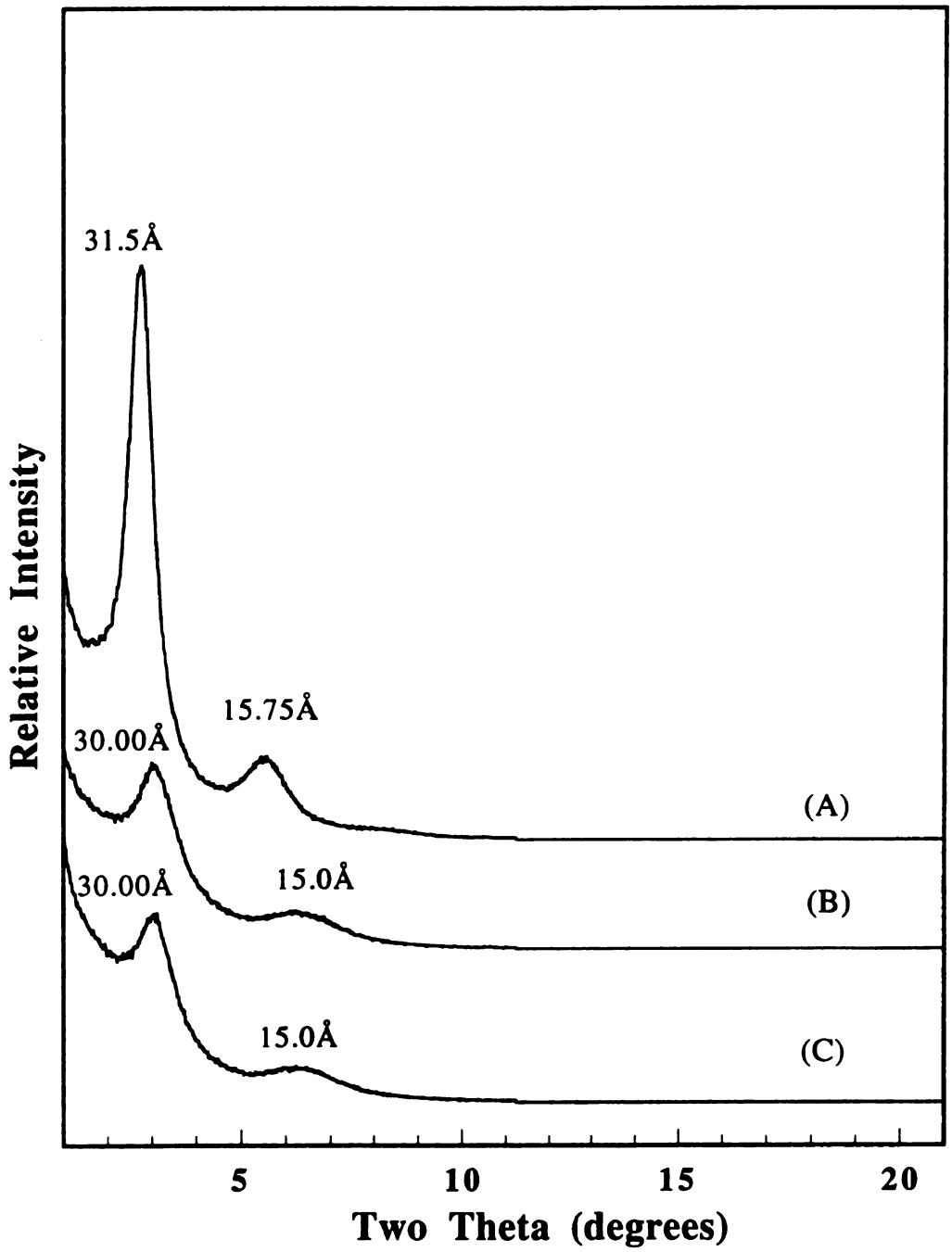

Figure IV.18 : X-ray diffraction powder patterns for freshly calcined and Ti grafted PCH-fluorohectorite prepared using different Ti loadings. (A) Freshly calcined PCH-fluorohectorite. (B) Ti-PCH with Ti-alkoxide conc of ~0.9g/g of PCH-fluorohectorite. (C) Ti-PCH with Ti-alkoxide loading of ~0.45g/g of PCH-fluorohectorite.

These results suggests that an appropriate layer charge-compensating ratio is critical for the successful formation of a gallery nanostructure. In montmorillonites and beidellites, due to the low cation exchange capacity, the amount of quaternary ammonium ions intercalated inside the smectite is lower than that in the high charge density fluorohectorite system. In addition, natural clays exhibit charge heterogeneity which results in a non-uniform distribution of the intercalated ions. Thus the template concentration per cross-sectional area fluctuates across the layers, hindering formation of the co-operative micellar assembly process.

We attempted to overcome the shortcomings of low charge density smectites by using the dialkyl quaternary ammonium ion and neutral decylamine co-surfactants. We assumed that the dialkyl long chains would occupy more space in the clay galleries and thereby stabilize the organic nanotemplate, which would then enhance gallery nanostructure formation. However the results clearly suggest an absence of any gallery structure.

Two dialkylchain lengths were used for PCH synthesis, namely Didecyldimethylammonium (denoted as $DDDMA^+$) and dioctadecyldimethylammonium (denoted as $DODDMA^+$). Decylamine was used as co-template and TEOS as the source of a neutral inorganic precursor. To a 1 wt % suspension of Na^+-clay was added a 0.3 M ethanolic solution of dialkyldimethylammonium bromide in two-fold excess of the CEC value of the clay. The suspension was stirred for 24 h at 50°C to ensure complete ion exchange. Next, the resulting solid was centrifuged, washed repeatedly with ethanol to remove the excess surfactant and then resuspended and washed with water until free of halide ions. The pure product was collected by centrifugation and air-dried at room temperature. The resulting organo$^+$-clay henceforth is noted Q^+-clay. Figure IV.22

illustrates the X-ray powder diffraction pattern for the dialkyl quaternary ammonium exchanged (Q^+-clay) product. Both the $DDDMA^+$ and $DODDMA^+$-montmorillonite exhibit multiple (00l) reflections, indicative of a well-ordered structure along the c-axis. The gallery heights for the $DDDMA^+$-montmorillonite is ~10.0Å, indicating a paraffin type of orientation of the quaternary ammonium cations. In $DODDMA^+$-montmorillonite, a gallery height of ~18Å is obtained with an simiar orientation of the $DODDMA^+$ onium cations. In $DDDMA^+$-beidellite the gallery height of ~15Å, indicates a paraffin type of orientaion, but with a much larger tilt angle of the alkyl chains from the silicate layers. In $DODDMA^+$-beidellite the gallery height of ~28Å obtained indicates a lipid-like structure of the organic quaternary ammonium ions inside the clay galleries. Figure IV.22 b displays the relationship between basal spacing and cation exchange capacity per 100 g of these materials. The neutral decylamine/Q^+-clay powder patterns in excess amine suspension are displayed in Figure IV.23. The narrow peaks at 30.0Å for the decylamine samples is indicative of the presence of alkylammonium salts, formed by the reaction of the amine with atmospheric CO_2, to form an alkylammonium carbonate. The relatively broad XRD peaks at 42Å for the decylamine solvated organoclay is assigned to Q^+-clay swollen by decylamine. This reflection results from intercalation of amine into the organoclay galleries. Notice that similar gallery heights are obtained for both montmorillonite and beidellite inspite of the different orientation of the intercalated quaternary ammonium cations prior to amine solvation.

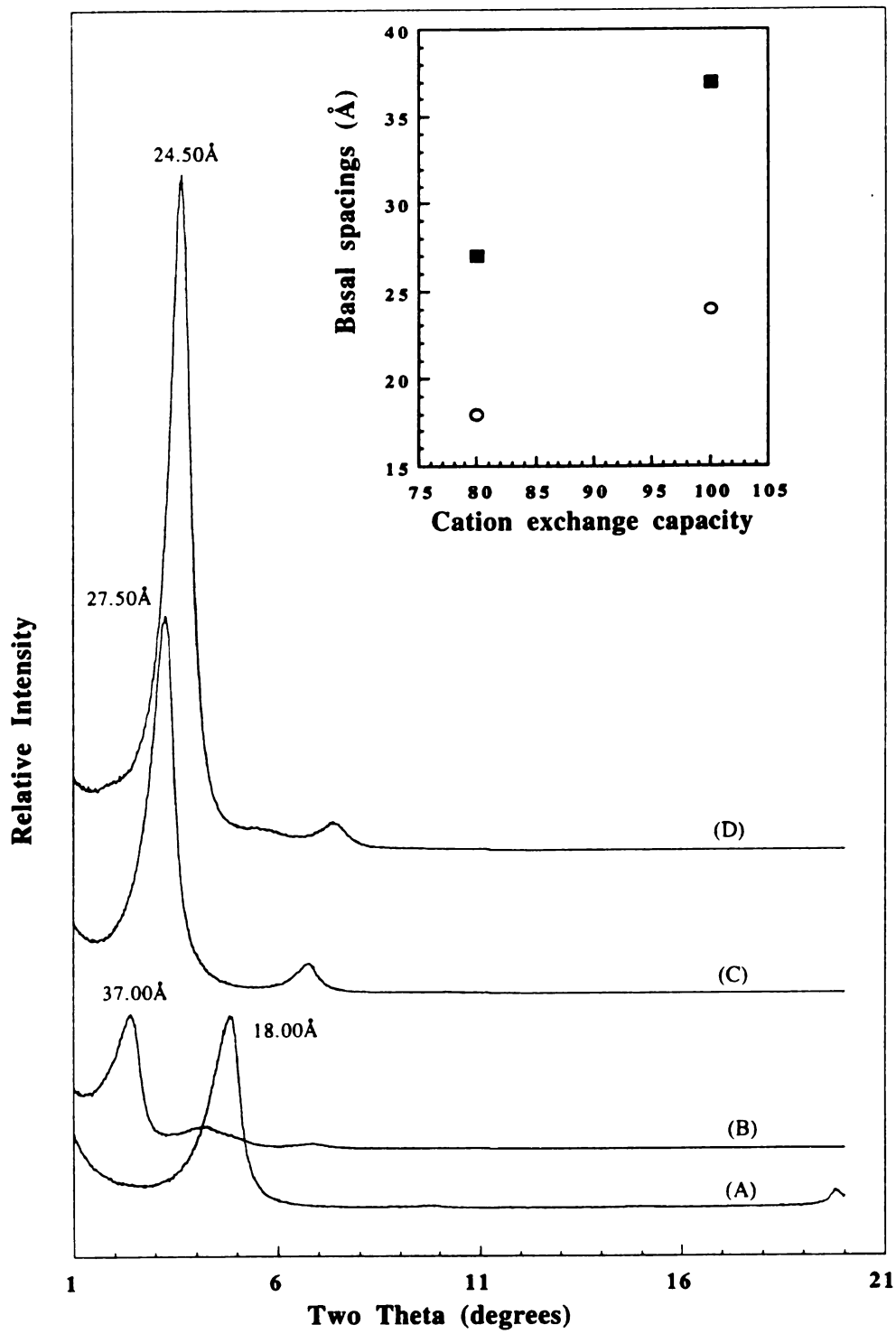

Figure IV.22 : X-ray diffraction powder patterns for the dialkyl quaternary ammonium exchanged clays (Q^+-clays). (A)$DDDMA^+$-montmorillonite(Wyoming). (B) $DODDMA^+$-beidellite (Chinese). (C) $DODDMA^+$-montmorillonite (Wyoming). (D) $DDDMA^+$-beidellite (Chinese).**(Insert)** A plot of the basal spacings to cation exchange capacity/100g of clay.

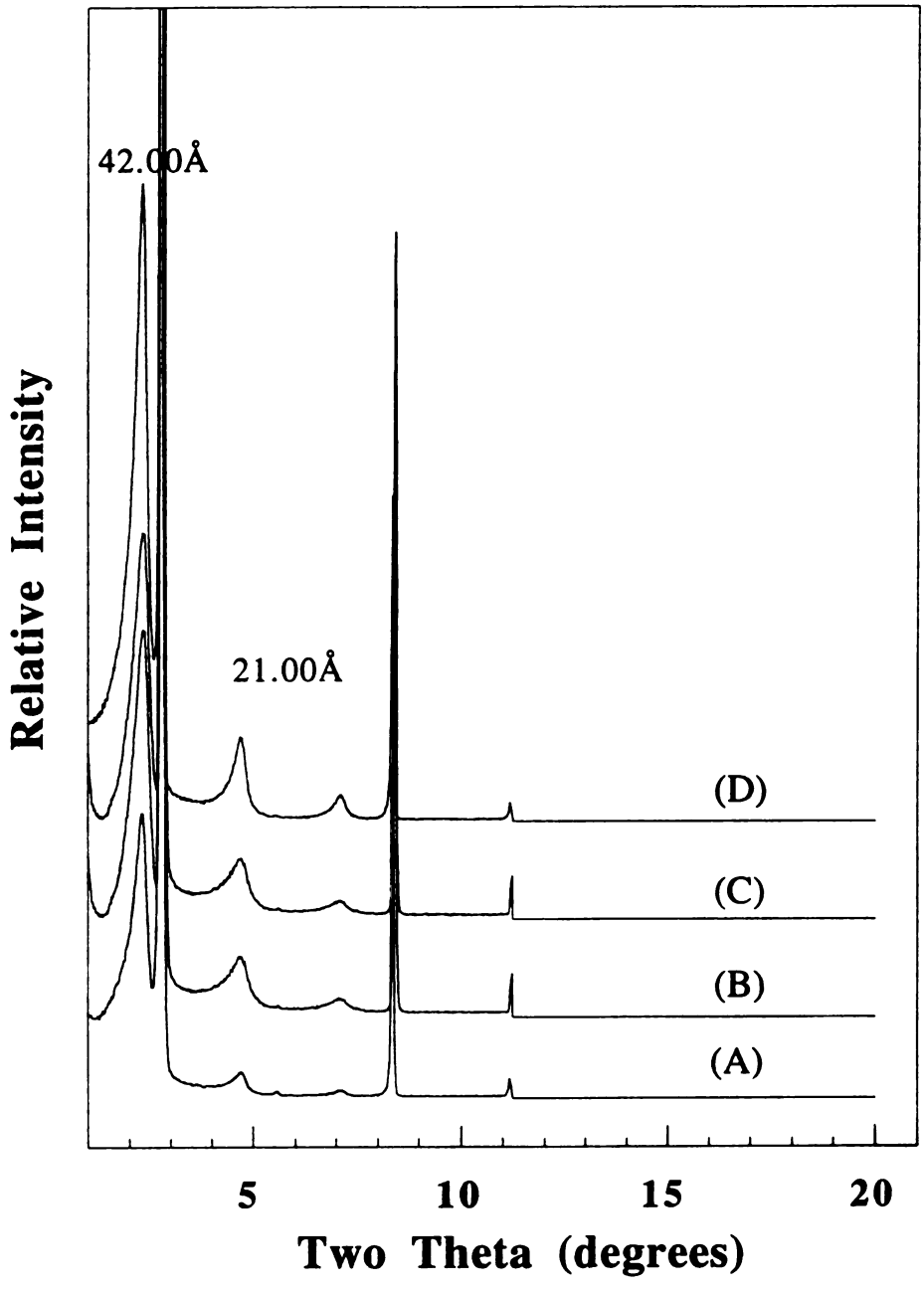

Figure IV.23 : X-ray diffraction powder patterns for the dialkyl quaternary ammonium exchanged clays (Q^+-clays) in excess amine suspension with a molar ratio of 1 : 20 between Q^+-clay and amine. A)$DDDMA^+$-montmorillonite(Wyoming). (B) $DDDMA^+$-beidellite (Chinese). (C) $DODDMA^+$-beidellite (Chinese). (D) $DODDMA^+$-montmorillonite (Wyoming).

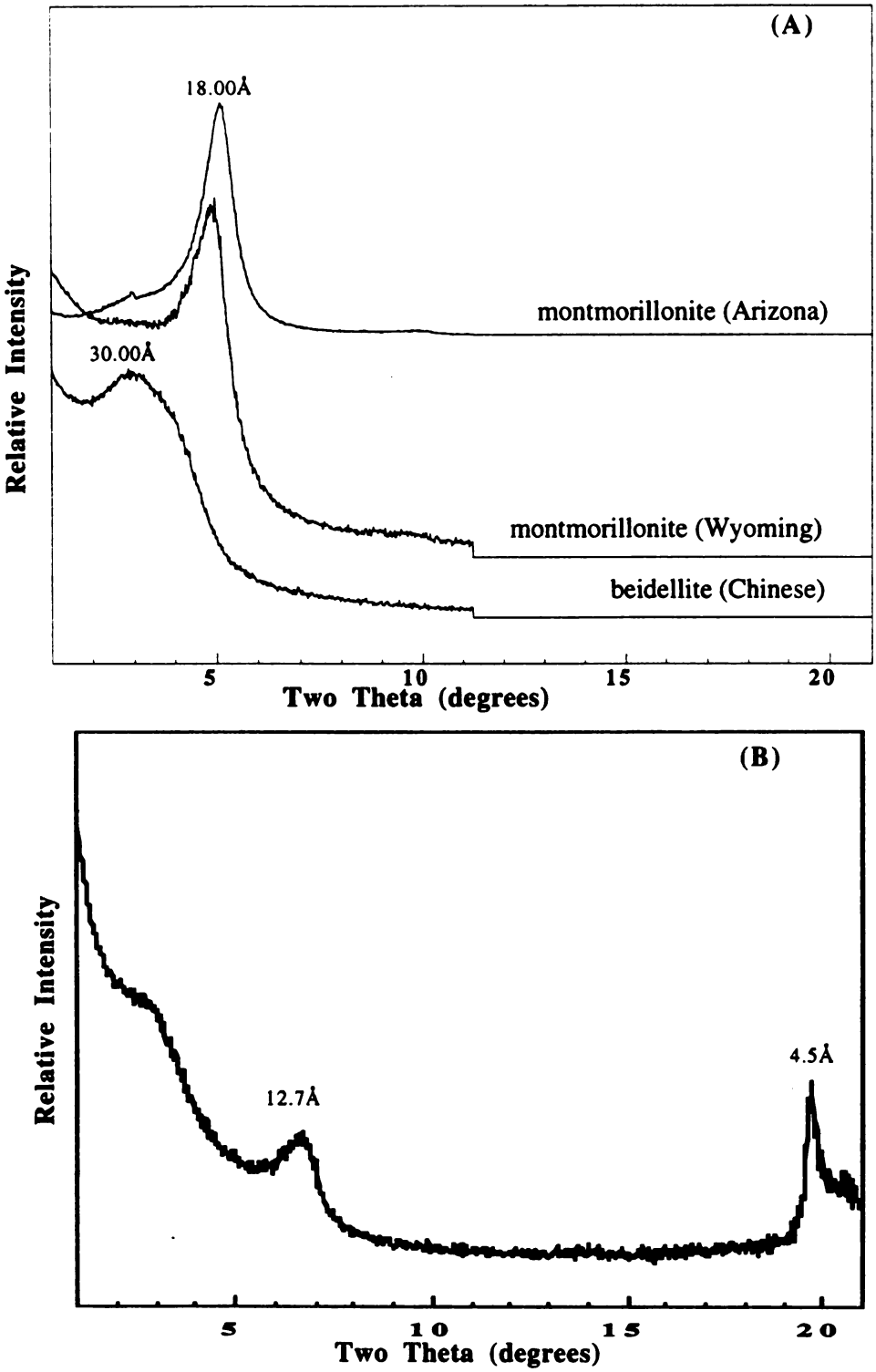

Figure IV.21 : X-ray diffraction powder patterns for PCH prepared using decylamine/$HDTMA^+$ as templates and different low charge density smectites with a Q^+-clay : amine : TEOS of 1 : 20 : 150 respectively. (A) as-synthesized. (B) calcined at 500°C for 4 h.

Mixtures of Q^+-clay : decylamine : TEOS at molar ratio of 1 : 20 : 150, respectively, were allowed to react for 4 h at ambient tempearture. The resultant intercalates were then centrifuged, dried in open air to give the as-synthesized products. Removal of the organics by calcination at 500°C in air for 4 h gave the final calcined material.

Figure IV.24 illustrates the X-ray powder diffraction patterns for the as-synthesized and freshly calcined materials obtained by using montmorillonite(Wyoming) and beidellite(Chinese) as layered host and dialkyldimethylammonium$^+$/decylamine for templating. The diffraction pattern for the air dried PCH-montmorillonite (DDDMA$^+$/decylamine as templates) exhibits a single broad diffraction peak with a gallery height of ~9.0Å. With DODDMA$^+$/decylamine as template a gallery height of ~21Å is obtained. Significantly higher gallery heights for the corresponding quaternary ammonium chain lengths are obtained with beidellite as the layered host. For instance, in PCH-beidellite synthesized by using DODDMA$^+$/decylamine as templates a gallery height of ~29Å is obtained.

The X-ray powder diffraction pattern for the corresponding materials calcined at 500°C is displayed in Figure V.24 b. All the XRD patterns show a single weak diffraction peak at 12.7Å, corresponding to a collapsed silica-intercalated phase. These results do not support an intra-gallery templated nanostructure.

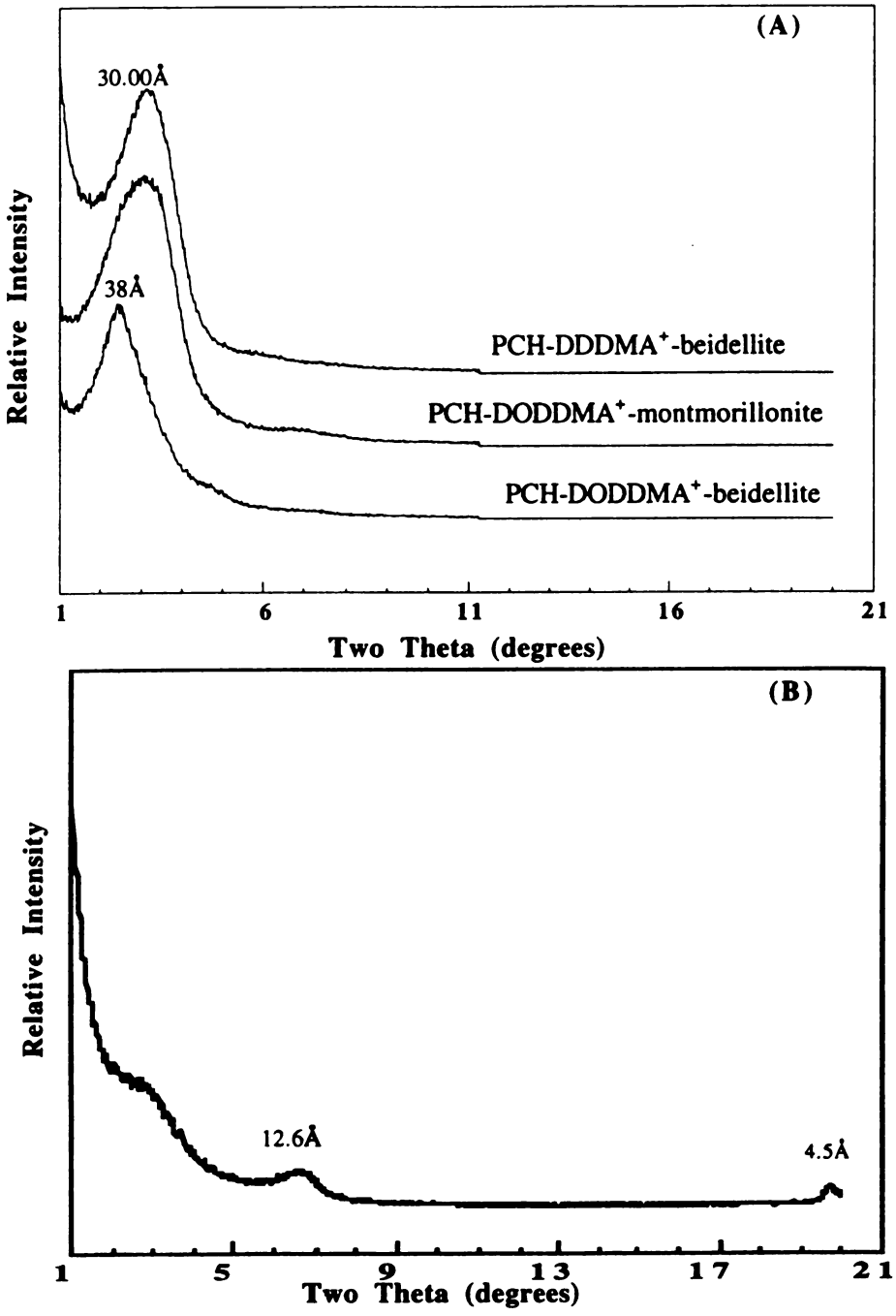

Figure IV.24 : X-ray diffraction powder patterns for PCH prepared using decylamine/dialkyl quaternary ammonium as templates and different low charge density smectites with a Q^+-clay : amine : TEOS of 1 : 20 : 150 respectively. (A) as-synthesized. (B) calcined at 500°C for 4 h.

References :

1. Figueras, F., *Catal. Rev.-Sci. Eng.* **1988** *30 (3)*, 457.
2. Izumi, Y.; Urabe, K.; Onaka, M., *Zeolite, Clay, and Heteropoly Acid in Organic Reactions* VCH Publishers, **1992**, 49-98.
3. Butruille, J.-R. and Pinnavaia, T. J., *Catal. Today* , **1989**, *62*, 3221.
4. Butruille, J.-R.; Michot L. J. and Pinnavaia, T. J. *J. Catal.* **1993**,*139*, 664.
5. Galarneau, A.; Barodawalla, A. and Pinnavaia, T. J., *Nature* **1995**, *374*, 529.
6. Brunauer, S. ; Emmett, P.; Teller, E., *J. Am. Chem. Soc.* **1938**, *60*, 309.
7. Horvath, G.; Kawazoe, K.J., *J. Chem. Engng Jap.* **1983**, *16*, 470.
8. Farmer, V. C., *"The Infrared Spectra Minerals"* **1974** *Ed. V. C. Farmer*, mineralogical society (London).
9. Chen, C-Y; Li, H-X and Davis, M. E., *Microp. Mater.*, **1993**, *2*, 17.
10. "*The Sadtler infrared spectra Handbook of minerals and clays*" ed. John Ferraro, **1982**, Sadtler Research laboratories.
11. Makarova, M. A.; Garforth, A.; Zholobenko, V. L.; Dwyer, J.; Earl, G. J. and Rawlence, D., *Stud. Surf. Sci. Catal.*, **1994**, *84*, 365.
12. (a) Connell, G. and Dumesic, J. A. *Journal of Catal.*, **1987**, *105*, 285-298. (b) Parry, E. P. *Journal of Catal.* **1963**, *2*, 371-379.
13. Khabtou, S.; Chevreau, T.; Lavalley, J. C., *Microp. Mat.*, **1994** *3*, 133.
14. Engelhardt, G.; Michel, D., *"High resolution solid-state NMR of silicates and zeolites"* **1987** Ed. John Wiley & sons.
15. Plee, D.; Borg, F.; Gatineau, L.; Fripiat, J. J., *J. Am. Chem. Soc.*

1985, *107*, 2362.

16. Pinnavaia, T. J.; Landau, S. D.; Tzou, M-S and Johnson I. D., *J. Am. Chem. Soc.* ,**1985**, *107*, 7222.